TÉCNICO LISBOA

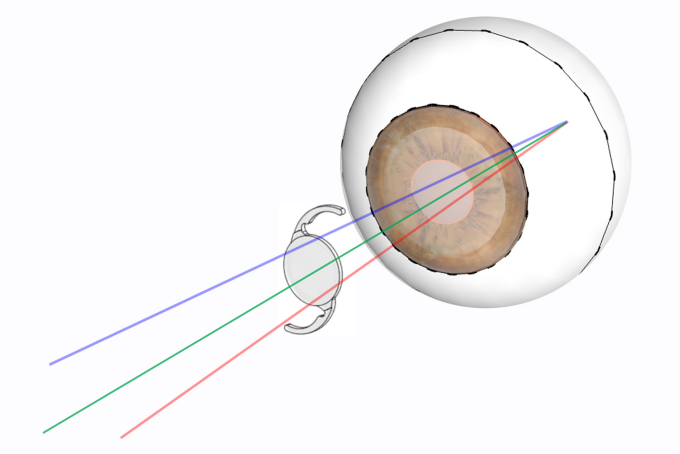

Residual astigmatism prediction in cataract surgery: improvement strategies

Catarina Isabel Praefke Aires Coutinho

Thesis to obtain the Master of Science Degree in

Biomedical Engineering

Supervisors: Prof. Dr. João Alberto dos Santos Mendanha Dias
Prof. Dr. Maria Filomena Jorge Ribeiro

Examination Committee

Chairperson: Prof. Dr. João Miguel Raposo Sanches
Supervisor: Prof. Dr. João Alberto dos Santos Mendanha Dias
Member of the Committee: Prof. Dr. Carlos Alberto Matinho Marques Neves

December 2021

I declare that this document is an original work of my own authorship and that it fulfills all the requirements of the Code of Conduct and Good Practices of the Universidade de Lisboa.

Preface

The work presented in this thesis was performed at the Institute for Plasmas and Nuclear Fusion of Instituto Superior Técnico (Lisbon, Portugal), during the period February-November 2021, under the supervision of Prof. Dr. João Mendanha Dias, and co-supervision of Prof. Dr. Filomena Ribeiro (Hospital da Luz Lisboa, Lisbon, Portugal), continuing the research work started in July 2019. In addition, during the period May-July 2021, an internship was performed at the Studio Oculistico D'Azeglio (Bologna, Italy), under the supervision of Dr. Giacomo Savini, and co-supervised at Instituto Superior Técnico by Prof. Dr. João Mendanha Dias.

Acknowledgments

First, I would like to thank specially Prof. Dr. João Mendanha Dias for his tutorship and guidance, sharpening my critical sense and giving me kind support. A special thank you goes as well to Prof. Dr. Filomena Ribeiro for her enthusiastic guidance and encouragement. A small internship at Group of Lasers and Plasmas, IPFN, supervised by both, turned out a great project, that challenged me and increased continuously my interest in this subject. Besides, both showed me in first-hand how it is possible to bridge Engineering and Medicine.

I would also like to thank Dr. Tiago Ferreira for his encouraging words and his keenness, besides the medical contributions along this path.

My cordial thanks to Dr. Giacomo Savini and Dr. Piero Barboni for receiving me with open doors at their *Studio Oculistico D'Azeglio*, and integrating me since the first day. I am specially grateful to Dr. Giacomo Savini for the close guidance and constant encouragement, giving me daily opportunities to expand my horizons and experience the clinical perspective. I also would like to thank Dr. Kristian Næser with whom I had the pleasure to hold enriching discussions about issues related to my thesis, and who rendered me promptly advice and support.

I thank as well Dr. Francisco Castro Alonso and Dr. Hannah Chiu for the kind support and readiness in providing me valuable information.

To all GoLP members for the nice time we spent together, specially in the challenging times of pandemic lockdown for the weekly online meetings.

A particular thank you to my friends who walked with me in this journey, and will do so in what comes next, for their constant support and cheering, for their presence and making this path colorful and rich in good memories. Here I include the staff from *Studio Oculistico D'Azeglio* for their warm welcome and for introducing me into the best of Italian way of life.

Last, but not least, to my family, to three Praefke women, in particular my mother and sister, for their constant support and encouragement, for always believing in me, without them I would not have achieved what I have. And to my dear grandmother, whom I deeply miss, and who showed me the importance of strength and kindness in life.

Resumo

A cirurgia da catarata é atualmente uma das intervenções mais comuns para restituir a acuidade visual onde o prevalente astigmatismo associado pode ser corrigido através da implantação de uma lente intra-ocular (LIO) tórica. Melhorar os resultados refrativos por cálculos exatos e precisos da potência da LIO é crucial para alcançar resultados pós-operatórios ótimos, satisfazendo as expetativas dos pacientes.

Procurando minimizar o astigmatismo residual foram desenvolvidos nomogramas baseados em regressões lineares entre o astigmatismo queratométrico medido pelo Lenstar® e o astigmatismo corneano total medido pelo Cassini®, considerando o efeito do astigmatismo da córnea posterior e reduzindo o erro de previsão. Ademais, foram observadas variações de astigmatismo entre as zonas central e periférica, com decréscimo para a periferia da potência da LIO determinada para implantação. Números distintos de medições efetuadas em diferentes fases relativas ao processo cirúrgico para várias modalidades não evidenciaram diferenças de erro refrativo no astigmatismo.

A optimização do astigmatismo queratométrico e corneano total foi avaliada para estimadores lineares e não-lineares de aprendizagem automática numa análise exploratória, incluindo vários parâmetros biométricos. Modelos lineares e baseados em árvores mostraram resultados promissores na redução do erro refrativo no astigmatismo, requerendo mais dados para teste.

O modelo de um olho pseudofáquico astigmático com uma LIO tórica genérica simulada criada, adequado à inclusão de dados específicos dos pacientes, possibilitou cálculos da potência LIO apropriada por traçado de raios, para diversos cenários, evidenciando a sensibilidade da potência esférica para as estimativas da posição da LIO e a relação entre potência cilíndrica e córnea posterior.

Palavras-chave: Cirurgia da Catarata, Lentre Intra-Ocular Tórica, Astigmatismo Queratométrico, Astigmatismo Corneano Total, Astigmatismo Residual, Erro de Previsão

Abstract

Cataract surgery is currently one of the most common interventions to restore visual acuity, where the associated astigmatism can be corrected by toric intraocular lens (IOL) implantation. Improving refractive outcomes by accurate and precise IOL power calculations is crucial to achieve optimal post-operative results matching the patients' expectations.

For the minimization of residual astigmatism, linear regression-based nomograms between the Lenstar® keratometric astigmatism and the Cassini® total corneal astigmatism were developed, considering the posterior corneal effect and reducing the prediction error. Also, astigmatism variations were observed between center and peripheric zones, with a decrease of the toric IOL power determined to be implanted towards the periphery. Distinct numbers of measurements at different surgery-related stages for diverse measurement modalities evidenced no differences regarding the error in refractive astigmatism.

Keratometric and total corneal astigmatism optimization was evaluated for linear and non-linear machine learning estimators in a three-step exploratory analysis, encountering several biometric parameters. Linear and tree-based models showed promising results for the reduction of the error in refractive astigmatism, requiring more testing data.

Tailored IOL power calculations via ray-tracing, in diverse scenarios, were enabled by the implementation of an astigmatic pseudophakic eye model with a created generic simulated toric IOL, suitable for patient-specific data incorporation, highlighting the spherical power tenderness to the IOL position estimations and the cylindrical power relation with the posterior cornea.

Keywords: Cataract Surgery, Toric Intraocular Lens, Keratometric Astigmatism, Total Corneal Astigmatism, Residual Astigmatism, Prediction Error

Contents

List of Tables

List of Figures

Abbreviations

σ	Standard deviation.
H_0	Null hypothesis.
H_a	Alternative hypothesis.
n	Refractive index.
R	Radius of curvature.
R^2	Coefficient of determination.
C	Cylindrical power.
Q	Asphericity.
S	Spherical power.
A/Z	Apex zone.
ACD	Anterior chamber depth.
AG	Anterior chamber diameter.
AI	Artifical intelligence.
AL	Axial length.
ANOVA	Analysis of variance.
AS-OCT	Anterior segment optical coherence tomography.
ATR	Against-the-Rule.
b.f.l.	Back focal length.
CCT	Central corneal thickness.
CI	Confidence interval.
CoV	Coefficient of variation.
CSF	Contrast Sensitivity Function.

D Diopters.

ELP Effective lens position.

EPA Error in predicted residual astigmatism.

ERA Error in refractive astigmatism.

ER Expected refraction.

EVO Emmetropia Verifying Optical.

f.f.l. Frontal focal length.

f Effective focal length/focal length.

GB Gradient Boosting.

HOA High-order aberration.

IA Intraocular lens astigmatism.

ICC Intraclass correlation coefficient.

IOL Intraocular lens.

KA Keratometric astigmatism.

KNN K-Nearest Neighbors.

LASIK Laser-assisted in situ Keratomileusis.

LCI Low-coherence interferometry.

LED Light-emitting diode.

LOA Low-order aberration.

LoA Limit of agreement.

LT Lens thickness.

MAE Mean Absolute Error.

MedAE Median Absolute Error.

MF Merit function.

ML Machine learning.

MSE Mean Squared Error.

MTFA Average Modulation Transfer Function.

MTF Modulation Transfer Function.

OCT Optical coherence tomography.

OLCR Optical low-coherence reflectometry.

OPD Optical path difference.

OTF Optical Transfer Function.

P/Z Pupil zone.

PCA Posterior corneal astigmatism.

PCI Partial coherence interferometry.

PD Pupil diameter.

PPMA Polymethyl methacrylate.

PPM Personalized Pseudophakic Eye Model.

PRA Predicted residual astigmatism.

PSF Point Spread Function.

PTF Phase Transfer Function.

RA Refractive satigmatism.

RF Random Forest.

SD-OCT Spectral-domain optical coherence tomography.

SD Standard deviation.

SF Surgeon Factor.

SIA/SICA Surgical induced astigmatism/Surgical induced corneal astigmatism.

SIRC Surgical induced refractive change.

SS-OCT Swept-source optical coherence tomography.

SVR Support Vector Regression.

TCAst Target corneal astigmatism.

TCA Total corneal astigmatism.

TCRP Total corneal refractive power.

TD-OCT Time-domain optical coherence tomography.

TNP True net power.

TRA Target refractive astigmatism.

TRT Test-retest repeatability.

VA Visual acuity.

V Vertex distance.

WFE Wavefront error.

WHO World Health Organization.

WTR With-the-Rule.

WTW White-to-white.

Chapter 1

Introduction

1.1 Motivation

Vision, one of the human five senses, is of upmost importance for the perception of the surrounding environment, through complex and not yet fully understood mechanisms carried out by the articulation of eye and brain: the incoming light reaching the retina is converted into electric pulses and interpreted by the brain. As any other organ, the eye is subjected to defects, as cataracts, the opacification of the natural lens. Cataracts are considered the leading cause of blindness and the second major cause of vision impairment, affecting about 94 million people worldwide according to the World Health Organization (WHO)[1].

The opaque natural lens can be removed and replaced by an artificial intraocular lens (IOL) in cataract surgery. Since the implantation of the first IOL over 60 years ago [1], a remarkable progression has taken place. Different IOL types, with different geometries and materials have emerged throughout time, offering the possibility of tailored refractive error correction, along with an increasing post-operative stability and biocompatibility. Also, the precision of the measuring instruments increased, providing a wider range of optical biometric measurements for eye parameters and clinical aberrometry. Accordingly, formulas for the IOL power determination and corresponding refractive outcome prediction have been developed, considering patient-specific measured data, such as corneal power and axial length (AL), along with IOL features. These are either regression formulas, vergence formulas[2], artificial intelligence-based calculations or ray-tracing[3]. While the first three formulas are based on population characteristics for future predictions, the latter one uses patient specific characteristics.

Currently, with the increase of life expectancy, along with the continuous improvement of surgical techniques, cataract surgery is a common procedure in developed countries and regarded as one of the most effective and successful interventions to restore visual quality [2]. A key step for the success in post-operative vision regain is the adequate IOL dioptric power determination, superseding the dioptric

[1] World Health Organization. https://www.who.int/news-room/fact-sheets/detail/blindness-and-visual-impairment. Accessed: 2021-08-04.

[2] Vergence formulas are based on geometric optics, in which distances are converted into dioptric power.

[3] M. Mott. Navigating IOL Power Formulas. https://www.aao.org/eyenet/article/navigating-iol-power-formulas. Accessed: 2021-09-26.

power of the crystalline lens along with the necessary power for the correction of inherent refractive errors and achievement of the targeted post-operative refraction, whereby a zero refractive outcome corresponds to emmetropia. In recent years, more attention has been drawn to the importance of accurate pre-operative planning to attain spectacle independence after surgery, highlighting the relevance of astigmatism inclusion [3]. Astigmatism is highly prevalent in cataract patients, as found in a study with 23 239 eyes where: more than 60.0% of the cases had a power within 1.00 diopters (D), and more than 25.0% between 1.00 and 2.00 D [4]. According to another study with 4 540 eyes, more than 34.0% had an astigmatism power of more than 1.00 D [5]. Moreover, a correction of 0.50 D or more of corneal astigmatism was pointed out as potentially beneficial to improve visual outcomes [6]. For the spherical refractive error, through the combination of precise pre-operative optical biometric measurements with accurate IOL power calculations, prediction errors[4] equal or lower than 0.50 D have been reported to range between 72.0% to 80.0% [7] and 80.0% to 88.5% of the eyes [8]. As regards refractive astigmatism a prediction error equal or lower than 0.50 D, with toric IOL power calculations, has been shown to vary between 53.9% and 65.6% [9], and 35.0% to 75.0% [10]. Therefore and along with the increasing rate of performed cataract surgeries and patients' demand of perfect refractive outcome, the improvement in precision of toric IOL power calculations is essential.

1.2 Objectives

The overall goal of this thesis was to explore refractive astigmatism prediction error improvement strategies in the ophthalmology context of cataract surgery. This goal was cross-sectional and analyzed over the three different approaches, employing different astigmatism analysis methods with several eye data parameters from various devices with different underlying technologies. First, construct generic and astigmatism-group specific nomograms,[5] relating keratometric and total corneal astigmatism, from data provided by *Hospital da Luz Lisboa* (Lisbon, Portugal). Second, analyze the variation of corneal astigmatism within a 3.0- and a 4.0 mm zone and its influence on the predicted residual refractive astigmatism, using data provided by *Hospital da Luz Lisboa*, and further a two-folded analysis related to the internship performed at *Studio Oculistico D'Azeglio* (Bologna, Italy): compare the error in refractive astigmatism considering a different number of measurements and different modalities, keratometric and total corneal astigmatism; assess the influence of several biometric parameters in an exploratory study of linear and non-linear methods for keratometry and total corneal astigmatism optimization, comparing the respective prediction errors. Finally, with an astigmatic pseudophakic[6] eye model, adapted from the Personalized Pseudophakic Eye Model (PPM) developed by Ribeiro *et al.* [11, 12], ray-tracing simulations were performed to test a created generic simulated toric IOL in different scenarios with different parameters based on data collected during the internship performed at *Studio Oculistico D'Azeglio*.

[4] Prediction errors are calculated as the difference between the post-operative and the predicted refractive outcome.
[5] A nomogram is a graphical representation of a mathematical formulation.
[6] Pseudophakic refers to an eye where the natural crystalline lens was replaced by an artificial lens.

1.3 Thesis outline

This thesis starts with a description, in Chapter 2, about the background of the eye's anatomy and physiology along with the bridging physical concepts when regarding the eye as an optical system, including the optical performance and associated vision defects. Also presented in this Chapter is the standard cataract surgery technique with the main IOL types. Chapter 3 gives a description of the used measuring devices and the highlighted parameters of influence and methods for toric IOL power calculations. The development and implementation of the nomograms and the analysis of the prediction error are covered in Chapter 4. In the first section of Chapter 5, the corneal astigmatism variation within center and peripheric zones is analyzed, while in the subsequent section are detailed methods and outcomes of the influence of different measurement modalities and types. At the end of Chapter 5, linear and non-linear machine learning estimators are implemented and compared in terms of the error in refractive astigmatism in order to test if they are suitable as optimization methods. At the same time, different sets of biometric parameters are studied regarding their possible influence on the optimization process. The ray-tracing simulation steps and outcomes with the astigmatic pseudophakic eye model and generic simulated toric IOL are described in Chapter 6. At last, Chapter 7 gives a summary of the main conclusions and improvement pathways for future studies.

Chapter 2

Medical and physical views on the eye

The eye along with the optic nerve and visual cortex comprises the complex visual system, enabling the recognition of the surrounding environment. Hence, in the first part of this chapter, a description of the eye from an anatomical and physiological point of view is given, followed by a physical description where the eye is regarded as an optical system.

2.1 Human eye

The human eye is a sensory structure that plays a major role in the perception of the external environment [13], contributing to the total sensory input into the human brain through the conversion process of light rays of the visible frequency range (400 to 750 nm) into electrical impulses, that further lead to the creation of the perceptual image.

The adult eye's shape is a slightly asymmetrical sphere, as depicted in Figure 2.1, with a typical antero-posterior diameter of 24 mm.

The eye is composed of the outer, middle, and inner layers. The outer layer includes the posterior sclera, that covers the eye, and the anterior cornea, which is convex and transparent with a radius of curvature of about 8 mm and 40 D of refractive power, being responsible for most of the refraction of the eye. The middle layer is composed of the pupil, the iris, the choroid, and the ciliary body. The aperture of the pupil, which can vary between 2 and 8 mm and is adjusted by the surrounding iris that contains the sphincter and dilator muscles, acts as a diaphragm, determining thereby the amount of light that reaches the retina. The choroid mainly provides oxygen and nutrients to the retina, while the ciliary muscles connected to the suspensory ligaments of the ciliary body hold the crystalline lens in place and are related to the accommodative ability of the crystalline lens to change the curvature and hence the eye's ability to focus objects at different distances ensuring the proper focus of the image on the retina. The crystalline lens located posteriorly to the iris is mainly composed of water and proteins, and accounts for the remaining dioptric power that, overall, is roughly 60 D. The inner layer, the retina, which is located posteriorly to the vitreous body and is light-sensitive, contains the photoreceptors: the cones, color sensitive and mainly located in the fovea that is associated to sharp vision and, in turn, placed on

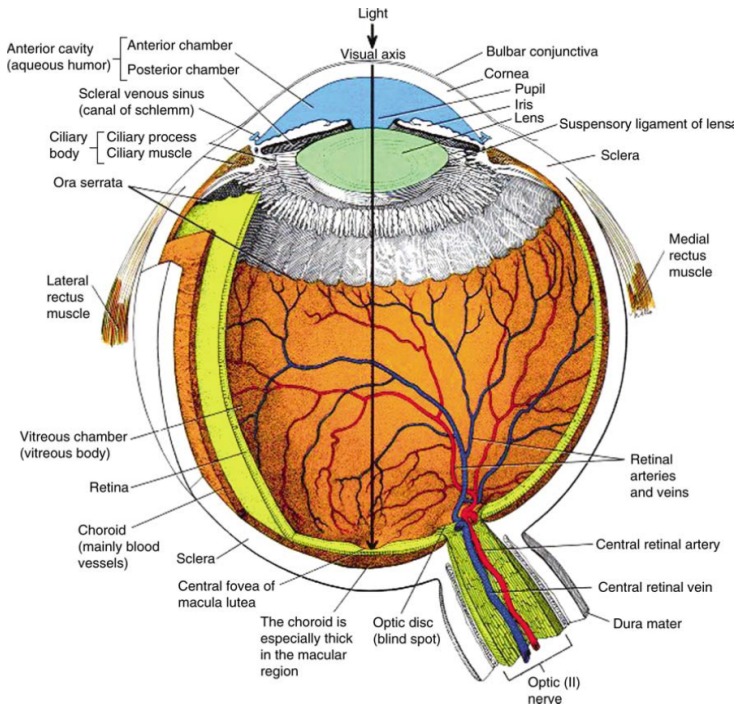

Figure 2.1: Schematic representation of the human eye and its major components and layers [13].

the central part of the macula (shifted about 5° from the optical axis[1]); and the rods, color insensitive and located in the fovea's periphery. The retina passes the information to the brain through the optic nerve that is constituted of around one million nerve fibers and receives the information from the axons of the ganglionic cells.

Inside the eye there are three different compartments: the anterior chamber, between the cornea and the iris and containing the aqueous humor; the posterior chamber, between the ciliary body and the crystalline lens, which also contains aqueous humor; and the vitreous chamber, between the crystalline lens and the retina and containing the vitreous humor. The aqueous humor is responsible for the maintenance of the intraocular pressure that ensures the transparency and shape of the eye, and provide nutrients, mainly, to the cornea and lens. Both, aqueous and vitreous humor have a refractive index of 1.336 [14, 15].

2.1.1 Eye modeling

Several eye models have been developed aiming the study and replication of optical characteristics of the human eye. Paraxial schematic eye models, such as the Gullstrand-Emsley model, considered as one of the first exact eye models, are the simplest and only accurate without considerable error in the paraxial region, which lies close to the optical axis. This model type solely works for optical systems with small apertures and assuming that refraction surfaces are spherical and centered on the optical axis, and that the refractive indices remain unchanged in each medium [14, 16]. More sophisticated and real models are termed finite or wide-angle models. These incorporate aspheric surfaces and chromatic

[1] The optical axis goes through the center of the cornea and crystalline lens, whereas the visual axis is relative to the fovea and displaced to the optical axis by an angle α.

dispersion, consider the gradient refractive index of the lens, and enable predictions for on- and off-axis aberrations. Further, accommodation and age-dependent changes can be included, and even serve as basis for personalized eye models [11, 16]. Currently, the Liou-Brennan finite model is considered the most accurate and realistic one in terms of anatomic resemblance and real-world performance of the human eye [16]. It intends to predict spherical and chromatic aberrations as close as possible to real data, enabling vision modeling for different scenarios, such as refractive surgery. Developed, when possible, based on empirical biometric data of in average 45-years-old patients with healthy emmetropic eyes and, alternatively, from data of previous studies, this model encounters the four refractive surfaces and models an eye with an equivalent power of 60.35 D and an AL of 23.95 mm [17].

Since in this work the Liou-Brennan schematic eye model [17] was used, two eye elements will next be described in more detail.

Cornea

The cornea is covered by the tear film and composed of five layers, three cellular, namely epithelium, stroma, and endothelium, and two interface layers, the Bowman and the Descemet membranes [18]. Although each layer has a characteristic refractive index, the dominant is the stroma's one, the thickest layer (90%), and thus a refractive index of 1.376 is associated to the cornea [14]. With a horizontal diameter of about 11.5 to 12.0 mm and a vertical diameter slightly smaller by around 1 mm, a central thickness of 0.5 mm and a larger peripheral thickness ranging between 0.6 and 0.8 mm, the shape of the cornea is not completely spherical, becoming flatter from the apex to the periphery (prolate shape) [17, 18]. Furthermore, the cornea can present toricity due to differences of the radius of curvature along the horizontal and vertical meridians. Thus, it is considered as an aspheric surface and can be described as a conicoid by equation (2.1):

$$x^2 + y^2 + (1+Q)z^2 - 2zR = 0 \tag{2.1}$$

where x and y are the horizontal and vertical meridians, respectively, z is the axis of revolution, R is the vertex radius of curvature, in this case the surfaces' apex, and Q is the asphericity parameter (that can take the values presented in Figure 2.2) [14, 17].

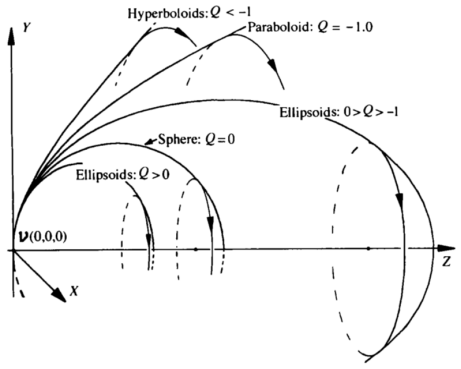

Asphericity Parameter, Q	Conicoid Type
$Q < -1$	Hyperboloid
$Q = -1$	Paraboloid
$-1 < Q < 0$	Prolate Ellipsoid
$Q = 0$	Sphere
$Q > 0$	Oblate Ellipsoid

Figure 2.2: Conicoid types and corresponding asphericity values [14].

In the Liou-Brennan model, based on equation (2.1), the cornea is described as a rotationally symmetric ellipsoid ($Q < 0$), with $R = 7.77$ mm and $Q = -0.18$ for the anterior curvature, and $R = 6.40$ mm and $Q = -0.60$ for the posterior surface. Surface radii are averaged from biometric empirical data, while asphericities are modeled such that spherical aberration values are similar to experimental ones. These surfaces are two of the four refractive surfaces of the eye considered in this model [17].

Crystalline lens

Enclosed in an elastic capsule and connected to the zonules of the ciliary body, the crystalline lens has on its bulk, mass of cellular tissue, a non-uniform gradient refractive index that is higher and more constant in the center than in the periphery. In the relaxed state, the thickness of the lens is about 3.6 mm with an equatorial diameter ranging between 8.5 and 10.0 mm. The anterior and posterior lens curvature are the other two refractive surfaces of the eye, however with a lower refractive power than the cornea [14].

Regarded in the Liou-Brennan model as rotationally symmetric conicoid, the lens has curvature radii of $R = 12.4$ mm for the anterior surface and $R = -8.1$ mm for the posterior surface, based on *in vivo* measuring results of other studies. On the other hand, the asphericity values are obtained through equation (2.1), and take distinct values for the anterior and posterior lens surfaces: $Q = -0.94$, corresponds to a prolate ellipsoid, and $Q = +0.96$, corresponds to an oblate ellipsoid, according to Figure 2.2 [17].

2.2 Eye as an optical system

Since the eye can be regarded as an optical structure, a parallelism to optic concepts follows with the proper context.

The propagation of light coming from a point source can be represented by successive arcs centered on the point source, termed wavefronts and defined as the locus of points with equal optical distance to the light source [19]. A ray light describes the path of a given point on the wavefront. Light, a type of electromagnetic radiation, can suffer phenomena as refraction, reflection, diffraction, and interference. Particularly, light in the visible range can be detected by the human eye, itself an optical system.

An optical system can be regarded as comprised by reflective or refractive surfaces with a common axis, the optical axis. These surfaces bend the incoming light rays changing their direction, or reshape part of the incident wavefront, in a way such that an image is created from an object. In other words, the object space can be considered as the space lying before or to the left of the interface (optical system), and the image space the space lying after or to the right of the interface, as represented in Figure 2.3 [15]. In the ideal case, also termed stigmatic [20], the emanating rays from a point source, S, in the object space, converge to one single point in the image space, P, creating a perfect point image, and the wavefronts assume a spherical form — Figure 2.3 [15].

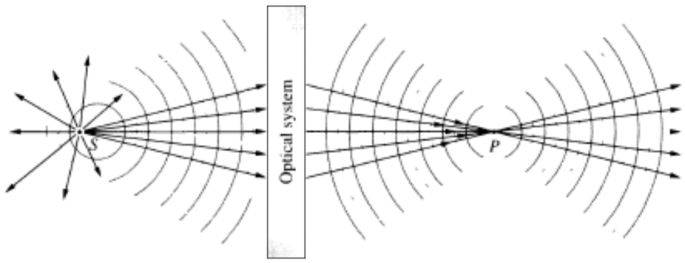

Figure 2.3: Relation between wavefronts and rays coming from the point source, S, passing through the optical system, and converging in the image space, P. If not stopped at P, the propagation of the rays continues. (Adapted from [15].)

Geometrical optics is an optics domain where the light propagation in homogeneous media is described in a rectilinear form, only considering reflection and refraction phenomena. In this context, light is represented by rays moving in straight lines that are perpendicular to wavefronts that, in turn, can bend. Refraction can be defined as the bending of a wave upon a medium change and the consequent change in velocity due to the difference of the medias' refractive indices (n). Snell-Descartes or simply Snell's Law[2] translates the relation of these indices as well as the directions of propagation between the two transparent media, through equation (2.2), where I refers to incident and R to refracted [15, 20]:

$$n_I \times sin\theta_I = n_R \times sin\theta_R \Leftrightarrow \frac{n_I}{n_R} = \frac{sin\theta_R}{sin\theta_I} \tag{2.2}$$

First-order, Paraxial or Gaussian[3] Optics, assumes parallel rays that form small angles with the optical axis, thus enabling the paraxial approximation of $sin\theta \approx \theta$ and leading to the simplification of the Snell's Law ($n_I\theta_I = n_R\theta_R$) [15].

Lenses are refractive elements where discontinuities are induced in the originating wave medium, being responsible for the formation of the image by reshaping the transmitted wave independently of the light frequency. Spherical lenses feature spherical curvatures with a single radius of curvature across the lens, while aspheric lenses have a non-spherical curvature with distinct radii in the center and lens' edge, namely being flatter in the periphery than in the center, taking one of the forms of Figure 2.2. Lenses are usually composed of two or more refracting interfaces and can be classified as:

- Convex, converging, or positive: thicker at the center, where the second lens surface leads to the ray's convergence, usually, to a point (principal focal point) by decreasing the wavefront's radius of curvature.
- Concave, diverging, or negative: thinner at the center, making the incoming wavefronts more divergent [15].

[2]Defined after the Dutch scientist Willebrørd Snellius (1580?–1626) and the French philosopher René Descartes (1596–1650).
[3]Called after the German mathematician, astronomer, and physicist Carl Friedrich Gauss (1777-1855).

An optical system can be characterized by cardinal points (Figure 2.4) — two focal points, the first or object focal point where the light rays emerge and the second or image focal point where the respective image is formed; two principal points, corresponding to the intersection of the optical axis by two different principal planes, one where the extended rays entering the optical system intersect and the other where the rays emerging from the optical system intersect; and two nodal points, one axial point to which a ray is directed, then passing through the system and emerging with a parallel direction in the second axial point. Thereby, the frontal focal length ($f.f.l.$) can be defined as the distance from the vertex of the first surface of the optical system to the object focal point, and the back focal length ($b.f.l.$) as the distance from the last surface of the optical system to the image focal point. The effective focal length or focal length (f) is the distance from the principal point to the focal point, related to the object distance (o) and the image distance (i) by the Gaussian Form (2.3).

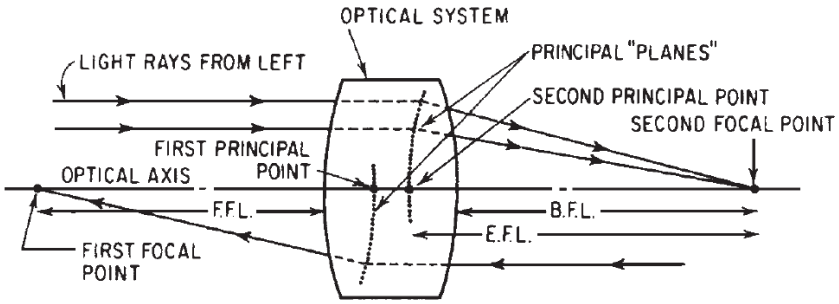

Figure 2.4: General representation of the cardinal points of an optical system [19].

Considering the object and image distances measured from the respective principal planes, the focal length of a lens regarded as a set of two refractive surfaces separated by a distance or thickness can be described by equation (2.4), called thick lens equation:

$$\frac{1}{f} = \frac{1}{o} + \frac{1}{i} \tag{2.3}$$

$$\frac{1}{f} = \frac{n_l - n_m}{n_m}\left(\frac{1}{R_1} - \frac{1}{R_2} + \frac{n_l - n_m}{n_m}\frac{t}{R_1 R_2}\right) \tag{2.4}$$

where n_l and n_m are the lens and surrounding medium refractive indices, R_1 and R_2 are the surface radii, and t is the thickness of the lens. For a thin lens, where the thickness is neglected, the principal points coincide with the lens location and the thin lens equation (2.5), which is usually employed in first-order optics, can be derived from the thick lens equation (2.4).

$$\frac{1}{f} = \frac{n_l - n_m}{n_m}\left(\frac{1}{R_1} - \frac{1}{R_2}\right) \tag{2.5}$$

The dioptric power ($\mathcal{D}$), in D, is the inverse of the focal length, in meters (m) — equation (2.6).

$$\mathcal{D} = \frac{1}{f} \tag{2.6}$$

The finite lens' diameter restricts the amount of transmitted light originated from a point source. Thereby, the clear diameter of a lens can be termed as aperture stop, defining the amount of light that reaches the imaging area from an axial point of the object [15, 19].

In ray-tracing the propagation of meridional (in the plane of the optical axis), as well as skew light rays (not intersecting the optical axis) from a starting point through a given optical system until the image surface can be modulated. The various angles of the ray's direction changing relatively to the system's optical axis can be calculated adapting the Snell's Law to a vector form and applying it to the successive refractive systems' surfaces, according to equation (2.7):

$$n_i(\widehat{k}_i \times \widehat{u}_n) = n_t(\widehat{k}_t \times \widehat{u}_n) \tag{2.7}$$

where n_i and n_t are the refractive indices, $\widehat{k}_i$ and $\widehat{k}_t$ the unitary vectors defining the ray's coordinates at the surface, and $\widehat{u}_n$ the unitary vectors normal to the surface at the intersection point [15].

Transposing these concepts to the eye structure: first, the entering light from an infinite distance object reaches the cornea, the primary refractive surface. Then, the iris acts as an aperture that regulates the amount of light that passes the pupil to the crystalline lens. This focusing lens element turns the image upside down before it is detected by the retina. And finally, the brain processes the image turning it such that a correct interpretation is possible.

Optical performance

A real optical system is limited by diffraction, which occurs when a wavefront changes by encountering an obstacle. For circular apertures this phenomenon limits the image produced by a point source. A diffusive ring-like area appears, the Airy Pattern[4]. It represents the diffraction pattern with a pronounced peak in the center (maximum intensity), being surrounded by concentric rings of decreasing intensity with local maxima and minima. The Rayleigh Criterion[5] establishes a limit of resolution for an optical system. Particularly, for the diffraction patterns of two close point sources of light, these are distinguishable when the minimum of one pattern overlaps the maximum of the other [15, 19].

Regarding the human eye, which is not a perfect optical system, the Point Spread Function (PSF) characterizes the light intensity distribution across the retina from a point light source. The shape and width of this function are not only limited by diffraction due to the pupil, the circular aperture of the eye, but also by the eye aberrations.

The Optical Transfer Function (OTF) is the Fourier Transform (FT) of the PSF and measures the quality of the image projected by an optical system from different frequencies of the object when compared to the original one. This is a complex function with a magnitude component, the Modulation Transfer Function (MTF), and a phase component, the Phase Transfer Function (PTF). Considering a one-dimensional pattern with a sinusoidal-like light level variation, equation (2.8) describes this variation

[4]Named after the English mathematician and astronomer Sir George Biddell Airy (1801-1892).

[5]Termed after the English mathematician, physicist, and Nobel Prize winner John William Strutt (1842-1919), also known as Lord Rayleigh.

along the distance x in the object space, while equation (2.9) describes it in the image space:

$$Light\ level(x) = A_o + Asin(2\pi xf + \delta) \tag{2.8}$$

$$Light\ level(x') = A'_o + A'sin(2\pi x'f' + \delta') \tag{2.9}$$

where A and A' are the variation amplitudes in the object and image spaces, respectively, while δ and δ' are the phase factors and f and f' the spatial frequencies.

The MTF describes the optical system's ability to reproduce contrast over a wide frequency range through a contrast magnitude ratio between image and object, i.e., by the ratio A/A'. The PTF assess the phase shift, $\delta - \delta'$, with spatial frequency. When there is no shift, the OTF becomes the MTF [14].

The Contrast Sensitivity Function (CSF) quantifies the capability of a subject to differentiate gray shades through sinusoidal gratings across a range of spatial frequencies and contrast. Contrast sensitivity patterns can be plotted with the spatial frequencies in the horizontal axis and the (decreasing) contrast in the vertical axis, corresponding the CSF curve to the ensemble of spatial frequencies for a contrast threshold at which a grating is visible, as represented in Figure 2.5. For the human eye, the cut-off at high frequencies is related to the photoreceptors packing on the retina, while the drop-off at low frequencies is related to neuronal inhibition within the ganglion cells, leading to the CSF band-pass-filter-like profile [11, 21].

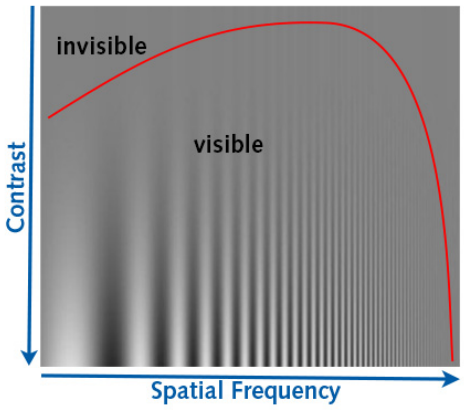

Figure 2.5: Typical contrast sensitivity function curve (in red) for a human eye[6].

Optical aberrations

Image errors, known as aberrations, occur in a real optical system degrading the image quality. They arise when incoming marginal or non-paraxial rays of light do not focus on one single point, thereby first-order optics are no longer applicable. Aberrations can be classified into chromatic and monochromatic. The first can be termed transversal when the direction is vertical to the optical axis or longitudinal if along the optical axial direction. These kinds of aberrations arise due to distinct light refraction for different wavelengths. Namely the refractive index is a function of the frequency, thus a light wave with a shorter

[6]Spatial Contrast Sensitivity. `https://www.psychophysics.uk/spatial-contrast-sensitivity/`. Accessed: 2021-11-2.

wavelength will suffer a bigger refraction than one with a longer wavelength. Monochromatic aberrations are only related to one wavelength and can be further described according to the shift between the measured and the reference aberration free wavefronts. Monochromatic low-order aberrations (LOAs) include myopia, hyperopia and astigmatism, the most common refractive errors, while the high-order aberrations (HOAs) comprehend spherical aberration and coma, among others [15, 22]. A common mathematical approach to describe optical aberrations is the Zernike polynomial expansion[7].

2.3 Vision defects

The eye, an optical system, is entitled as normal or emmetropic when in a relaxed state the parallel incoming rays from a very far object will converge to the focal point located on the retina, creating a sharp and focused image. On the other hand, it is termed as ametropic eye when the incoming light rays deviate from the desired path due to changes in the eye's shape, such as the distance between the crystalline lens and the retina, or in the cornea or lens refraction mechanisms, namely corneal curvature and, thus, its power. Presbyopia is an age-related condition that can be described as a gradual loss of the lens accommodation capacity to focus close objects. A commonly known anomaly is myopia or nearsightedness: due to an abnormal long eye, a steeper corneal curvature, or an imbalance between both, the eye has a higher refractive power and the parallel incoming light rays from distant objects focus anterior to the retina. Therefore, close objects appear sharp while with increasing distance these become more blurred. Correction can be achieved by placing a negative spectacle lens in front of the eye, reducing the power, leading to the divergence of the incoming rays and so bringing the focus point to the retina. In contrast, hyperopia also termed hypermetropia or farsightedness, is related to a shorter axial length or a flatter corneal curvature, leading to an insufficient light refraction and, therefore, the rays will not be focused on but posterior to the retina. Consequently, distant objects appear focused and near objects blurred. For this condition, a positive spectacle lens can be placed in front of the eye, increasing the power and, thus, leading to the convergence of the entering light rays and movement of the focus point to the retina [15]. For a slight hyperopic eye, accommodation by the crystalline lens may be sufficient to bring the distant objects to focus [23]. Another current correction alternative for both myopia and hyperopia besides the use of contact lens and IOL implantation, is the alteration of the corneal surface by Laser-Assisted in Situ Keratomileusis (LASIK) surgery. These last two conditions are considered as spherical refractive errors. Astigmatism, a common vision defect, in turn is considered a cylindrical error.

As astigmatism is the subject of this work, it will be described in more detail. An optical system is denominated astigmatic when it is non-point-like, i.e. no focal point is formed for the incoming parallel rays from a point source [20]. Astigmatism in the eye is due to asymmetries in the refractive surfaces, leading to power differences along meridians. Therefore, two principal meridians passing through the eye and perpendicularly to the optic axis are considered: one for the maximal curvature/power and another for the minimal curvature/power. When these power directions are perpendicular, the astigmatism

[7] Developed by the Dutch physicist and Nobel Prize winner Frits Zernike (1888-1966).

is termed regular and, thus, a low-order aberration, otherwise it is defined as irregular arising from highly irregular corneal shapes, as in the keratoconus condition [14, 15].

In this work only regular astigmatism is addressed, which is mainly due to anterior corneal toricity, however the posterior corneal surface also contributes to the total astigmatism of the optical system, as well as the crystalline lens, and with a minor contribution the retina [24]. Due to the existing power difference, the horizontal and vertical light rays from a distant object are focused as two perpendicular lines forming a three-dimensional structure termed Sturm's Conoid[8]. Along this interval, the blurred image assumes different shapes and directions. For a circular lens aperture, as present in the eye, the first emergent cross-section has an elliptic format, further narrowing down to a line. In the Conoid's center is located the circle of least confusion, with a diameter proportional to the astigmatism magnitude. Its position is determined by the dioptric average between the focal lines and given by the spherical equivalent power. Afterwards the image attains again linear and elliptic formats, perpendicular to the previous ones [20]. The line and the ellipse orientations depend on the axis direction of the astigmatic eye: it is considered With-the-Rule (WTR) with a steeper vertical meridian between 60° and 120°; Against-the-Rule (ATR) with a horizontal steeper meridian between 0 and 30° or 150° and 180°; or Oblique with the steepest meridian between 31° and 59° or 121° and 149° — Figure 2.6. Further, if regular astigmatism occurs simultaneously with myopia, the Sturm's Conoid falls in front of the retina, while in the case of hyperopia it can fall behind the retina. In an astigmatic eye the image projected on the retina appears blurred with the best possible visual acuity for the case where the circle of least confusion is located at the retina [25].

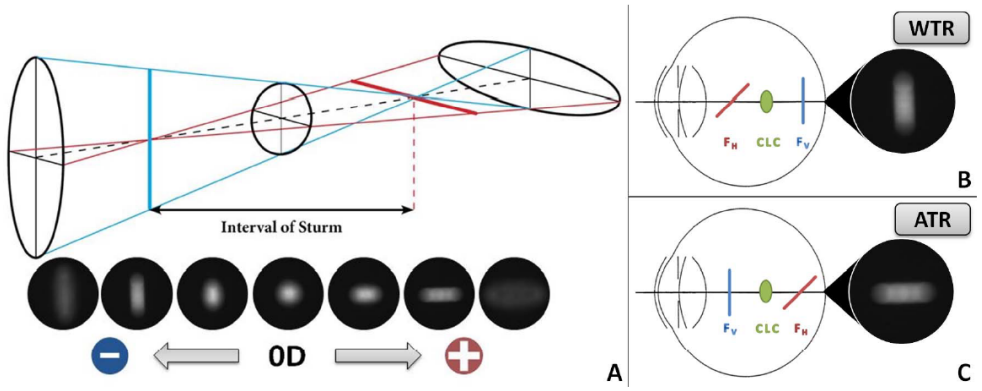

Figure 2.6: (A) Astigmatism related Sturm's Conoid, with the circle of least confusion and the different shapes and directions of the retinal blurred images. (B) and (C) represent the astigmatism foci for a WTR and ATR eye, respectively. F_V stands for vertical focus, CLC for circle of least confusion and H_V for horizontal focus [25].

Visual acuity

Visual acuity (VA) is the ability of an optical system to recognize details [26]. Therefore, it is related to the visual function and sensitive to refractive errors as well as to retinal or neural disorders [27]. In clinical practice, the evaluation of visual acuity is subjective and can be assessed through different tests,

[8]Named after the French mathematician Jacques Sturm (1803-1855).

as the Log MAR (Logarithm of the Minimum Angle of Resolution) and the Snellen Chart[9], considered as the most common one, and represented in Figure 2.7 [26]. In this case the optotypes (targets) are black letters tailored from a 5x5 grid, shown progressively in smaller sizes from the top to the bottom of the chart, with a strong contrast to the projected white background, read at a distance of 20 ft or 6 m. For this test, the visual acuity's scoring is made through the Snellen Fraction, where the numerator corresponds to the subject's distance to the chart, while the denominator to the correspondent distance at which a subject with normal visual acuity can perceive the same letter[10]. Normal acuity is defined as 20/20 (ft) or 6/6 (m), which corresponds to the ability to recognize a letter that vertically subtends 5 arcminutes, and 1/5 of them (1 arcminute = 1/60°) for the gap between the letter's limbs [28].

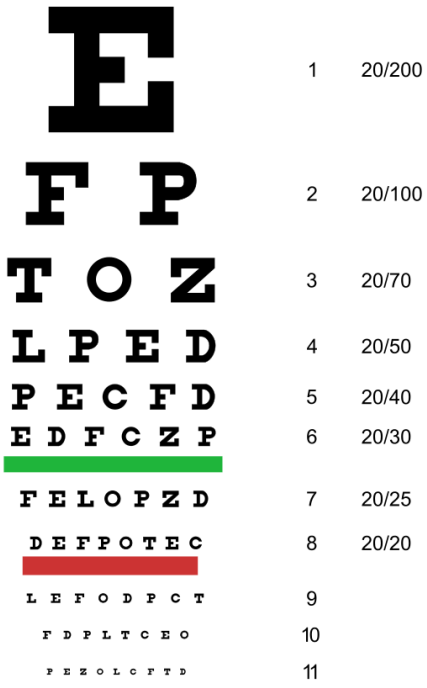

Figure 2.7: Common Snellen Chart for visual acuity assessment[11].

2.4 Cataract surgery

Cataract is described as the opacification of the natural crystalline lens due to the loss of transparency and increasing thickness of the lens, hindering the passage of light. Cataracts are mostly related to aging, and less commonly congenital [2]. Through surgical intervention the associated vision loss can be restored. Phacoemulsification is a conventionally used minimally invasive technique. A 2 to 3 mm long incision is made at the cornea, through which an ultrasonic probe is inserted. The cataract is then safely removed by a gradual destruction of the opacified lens using ultrasonic energy, and particle aspiration from the intervened eye. Thereafter, across the incision, a folded artificial IOL is inserted in

[9] Called after the Dutch ophthalmologist Herman Snellen (1834-1908).
[10] Oxford Reference. `https://www.oxfordreference.com`. Accessed: 2021-08-19.
[11] Snellen Chart. `https://commons.wikimedia.org/wiki/File:Snellen_chart.svg`. Accessed: 2021-11-2.

the capsular bag, that will replace the natural lens and correct the existing refractive errors, whenever necessary — Figure 2.8 [29].

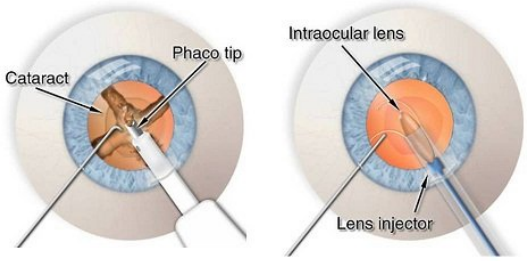

Figure 2.8: Schematic representation of the phacoemulsification procedure used in cataract surgery [12].

Intraocular lens

Since the first IOL implantation in 1949, structure and constitution of IOLs have evolved. Polymethyl methacrylate (PMMA) and silicone IOLs are more and more rarely used, being replaced by foldable IOLs, mainly composed of soft biocompatible materials like hydrophobic or hydrophilic acrylic. With an overall length ranging between 10 and 13 mm, with a thickness around 1 mm [30], usually IOLs are constituted by a small optical piece, the central part, with a biconvex or plano-convex shape and a 5 to 7 mm diameter, and two haptics, the side structures, for the support of the lens in the capsule bag after implantation inside the eye. According to their design, haptics can be classified as plate- or loop-haptics. In a single-piece IOL the haptics and optical are one structure, being the most common choice for in capsular bag implantation, while the more seldom three-piece IOLs, where the haptics and optical structure are separated, are used for sulcus implantation.

To be suitable for phacoemulsification through small, 2 mm long, incisions as well as guarantying a high degree of biocompatibility and post-operative stability with no rotation, most IOLs employed in cataract surgeries with in-capsular bag implantation are foldable, single-pieced, and made of hydrophilic acrylic material. In addition, the lens often features an aspheric surface to compensate the average positive spherical aberration of the cornea [31].

Classifying the vision into near (approximately 40 cm), intermediate (approximately 80 cm) and far (beyond 100 cm) distances, the suitable IOL needs to be selected:

- Monofocal: only one focal point for near, medium or distance vision; commonly used in cataract surgery.
- Multifocal: comprise more than one focal point within different segments in the same lens, namely bifocal IOLs that restore clear vision at near and far distances, and trifocal IOLs that restore clear vision at all three distances, leading to a higher spectacle independence.
- Toric: astigmatism correction with a stronger curvature along one lens' meridian than in the orthogonal one[13].

[12] Vision and Eye Health. https://www.vision-and-eye-health.com/cataractsurgery-steps.html. Accessed: 2021-11-2.
[13] Zeiss. https://www.zeiss.com/corporate/int/home.html?vaURL=www.zeiss.de/en. Accessed: 2021-08-09.

Chapter 3

Astigmatism and toric intraocular lenses

In developed countries, the rate of performed cataract surgery has increased in the past years, as it is one of the most effective and successful interventions to restore visual acuity [2]. Although HOAs as coma and spherical aberration have an impact on vision quality, these only represent approximately 10% of the total eye's aberrations and cannot be corrected by sphero-cylindrical lenses [32], while LOAs are predominant comprehending roughly 90% of all optical aberrations, in turn correctable by sphero-cylindrical lenses [33]. Therefore, the latter are considered the primarily correction target in cataract surgery to improve post-operative outcomes and achieve spectacle independence [6].

Corneal astigmatism is a predominant LOA that significantly deteriorates vision quality. In a study including 4 540 eyes of patients candidate to cataract surgery, in 64.4% astigmatism between 0.25 and 1.25 D was prevalent, and in 22.2% of the patients with astigmatism of 1.50 D or more [5]. A common option proven to be safe and effective is the implantation of toric IOLs during cataract surgery for the correction of pre-operative astigmatism [34], namely of 0.50 D or more, since this was pointed out as potentially beneficial to improve visual outcomes. However, to achieve the best possible post-operative outcomes and to meet the patients' expectations, accurate biometric measurements are essential, as well as precise IOL calculations for both spherical and cylindrical powers [6].

3.1 Measuring devices

In the present work, different measuring devices with different techniques were used to acquire the data for the studies, hence in the following subsections the instruments used are briefly described. Comparisons of their accuracy and repeatability are also mentioned. The technologies correspondent to each instrument are described in Appendix A.

Keratometry measurements are confined to an approximately 3.0 mm diameter central area of the cornea, assuming that the cornea is symmetric with two main meridians 90° apart. Furthermore, only the anterior corneal curvature is measured and the standard keratometric index, a fictitious index of usually

1.3375, is used to include the effect of the posterior corneal surface in the conversion to total corneal power [35]. Corneal topography and tomography consider a larger corneal zone for the measurement acquirement. Topography only measures the anterior corneal surface, while tomography analyses the whole cornea, providing information of the anterior and posterior surfaces [36].

Aladdin®

The Aladdin (Topcon, Tokyo, Japan) is an optical biometry and topography large-cone Placido disc-based system (technology detailed in section A.1 in Appendix A). Low-coherence interferometry (LCI), which is described in section A.4 in Appendix A, is employed for anterior chamber depth (ACD), lens thickness (LT) and central corneal thickness (CCT) measurements, and along with an 850 nm super luminescent diode for AL measurements. White-to-white (WTW) is measured in a 8.0 mm to 14.0 mm range. Pupillometry is also displayed. Corneal topography is acquired through the reflection on 24 Placido disc rings with an 8.0 mm diameter, analyzing more than 100 000 points. Color-coded axial maps are displayed for topography, where cold colors (green, blue) represent low-power zones and warm colors (red, orange) the high-power zones. In particular, keratometry is acquired from light reflection on 4 Placido disc rings with a 2.4 mm to 3.4 mm diameter, analyzing 1 024 points. Aberrometry analysis of the topographic data is available for pupil sizes between 2.5 mm and 7.0 mm[1] [37].

Lenstar®

The Lenstar LS 900 (Haag-Streit AG, Köniz, Switzerland) is an optical low-coherence reflectometry (OLCR) biometer (technology detailed in section A.4 in Appendix A). Measurements of AL, ACD, LT and CCT are calculated from reflected light based on the different reflection properties, namely refractive indices, of the different eye layers. Pupil diameter (PD) and WTW parameters use the diameter of an ideal circle, thus provided along with pupillometry[2].

Dual-zone keratometry readings are derived from the anterior corneal curvature, which is measured from the reflection of 32 closely spaced points separated along two concentric rings, the inner with a 1.65-mm diameter, and the outer with a 2.30-mm diameter. Each measurement is the mean of four measurements, thus by performing the five recommended scans, keratometry arises from information of 640 reference points. Then, the equivalent of an ideal sphere is calculated for each point and the steep and the flat radii come from the best data ellipsoid fit. Total corneal power is estimated using the standard keratometric index[3] [38].

Cassini®

The Cassini (i-Optics, Den Haag, The Netherlands) is a topographer employing multi-colored light-emitting diode (LED) point-to-point forward ray-tracing (technology detailed in section A.2 in Appendix A).

[1] *Aladdin Optical Biometry and Topography System.* Topcon, Tokyo, Japan, 2018.

[2] Haag-Streit UK: Lenstar LS 900. `https://www.haag-streit.com/haag-streit-uk/products/haag-streit-diagnostics/biometry/lenstar-ls-900/`. Accessed: 2021-09-04.

[3] *Instruction Manual Biometer Lenstar LS 900®.* Haag-Streit AG, Koeniz, Switzerland, 6 edition, 2013. Section 4.4.

Through this technology and from 679 LEDs, a reconstruction of the anterior corneal surface is made from red, green, and yellow points, while for the posterior corneal surface, the reflection of second-Purkinje[4] images from 7 monochromatic infrared LEDs, organized in a circular shape, is evaluated.

Keratometry values are obtained from a 3.0 mm zone and the standard refractive index is used to convert curvature measurements of the anterior corneal surface to total corneal power. Also provided are anterior, posterior, and total corneal astigmatism values, considering a CCT of 550 μm. WTW, pupil size, and decentration (angle kappa), and topographic indices, such as corneal Q, are displayed. Axial and refractive maps with quality parameters, as well as high order aberrations analysis of the anterior corneal surface are displayed[5].

Pentacam®

The Pentacam (Oculus Optikgeräte GmbH, Wetzlar, Germany) is a tomographer, composed of a Scheimpflug camera — the respective principle is described in section A.3 in Appendix A — that rotates around a central axis capturing anterior segment eye images illuminated by a 475 nm blue LED source. In approximately two seconds the Scheimpflug camera takes, in a single scan, 50 images from which a maximum of 25 000 distinct elevation points are extracted to create complete images of the anterior and posterior corneal surfaces. A three-dimensional image of the whole anterior segment eye is constructed and calculated by the ray-tracing software incorporated in the Pentacam, using the provided data and relying on the Snell's Law to track the light[6] [39]. However, a poor image quality and low resolution are associated to the anterior segment images [40]. Three reference shapes are considered by this device, a best-fit sphere, a best-fit ellipse for the real corneal shape, and a best-fit toric ellipse for the astigmatism case [39].

Along with biometrical measurements, as corneal curvatures and ACD, the pachymetry (corneal thickness) is measured and the lens density evaluated by quantifying the amount of transmitted light. For the special case of the Pentacam AXL, the AL is measured by partial coherence interferometry (PCI). Corneal topography for astigmatism calculations include: sagittal or axial curvature maps with keratometry values using the standard keratometric index (1.3375); the true net power (TNP) map, where the power is calculated by adding the sagittal power of the anterior and the posterior corneal surfaces using refractive indices of 1.376 for the cornea and 1.336 for the aqueous humor; and the total corneal refractive power (TCRP) map, where the power is calculated by ray-tracing, employing the Snell's Law, considering both corneal surfaces, corneal thickness and true refractive indices[7] [39].

MS-39®

The MS-39 (Costruzione Strumenti Oftalmici, Florence, Italy) is an anterior segment optical coherence tomographer (AS-OCT), that combines spectral-domain OCT (SD-OCT) with an 845 nm LED

[4] Purkinje figures are patterns of shadows of the projected retinal blood vessels, visible when light is projected on the eye.

[5] *Brochure Cassini color led topography.* Cassini Technologies BV, Anna BV Buerenplein, The Hague, The Netherlands, 2019.

[6] *Interpretation Guide Pentacam® /Pentacam® HR.* Oculus Optikgeräte GmbH, Wetzlar, Germany, 3 edition.
Oculus: The measurement principle. https://www.pentacam.com/int/opticianoptometrist-without-pentacamr/technology/measurement-principle-licences-network.html. Accessed: 2021-09-04.

[7] Oculus: Topography Maps. https://www.pentacam.com/us/technology/topography-maps.html. Accessed: 2021-09-04.

source and Placido disc technology with a 635 nm LED illumination source — technologies described in sections A.1 and A.4 in Appendix A. From 22 Placido disc rings and 31 232 points on the anterior corneal surface and 25 600 on the posterior corneal surface over a 10.0 mm coverage, corneal topography is obtained. Corneal and epithelial thickness, corneal Q, and ACD, as well as pupillometry are provided. Profiles of both anterior and posterior cornea, and anterior lens and iris are displayed from 25 SD-OCT scans.

Simulated keratometry is obtained from the Placido discs between 2.5 and 4.0 mm, using the mean curvature radii of the steep and flat meridians of the anterior corneal surface and the standard keratometric index. It incorporates ray-tracing technology, using the Snell's Law and real refractive indices, for the total corneal power calculation from both, anterior and posterior, surfaces in a 3.0 mm pupil diameter zone. Corneal aberrometry is displayed in wavefront error (WFE) and optical path difference (OPD) maps along with visual simulations, as PSF and MTF[8] [40].

Summary

In Table 3.1 are summarized for each measurement device the underlying techniques, and the measurements performed with it.

Table 3.1: Techniques for each measuring device and the respective measurements.

Device	Technologies	Measurements								
		K	Posterior	Total	AL	ACD	CCT	LT	PD	WTW
Aladdin (Topcon)	Placido disc LCI	x			x	x	x	x	x	x
Lenstar (Haag-Streit)	OLCR	x			x	x	x	x	x	x
Cassini (i-Optics)	Multi-colored LED point-to-point forward ray-tracing	x	x	x						x
Pentacam (Oculus)	Scheimpflug	x	x	x	x*	x	x	x	x	x
MS-39 (CSO)	Placido disc SD-OCT	x	x	x		x	x	x	x	

K = Keratometry; LCI = Low-coherence interferometry; $OLCR$ = Optical low-coherence reflectometry; $SD-OCT$ = Spectral-domain optical coherence tomography; * = Only with Pentacam AXL

3.1.1 Devices repeatability and agreement

Repeatability of a measuring device is based on the variation between measurements performed under the same conditions in a short period of time. Whereas agreement is assessed between devices, quantifying their similarity and interchangeability for a same subject [36].

In Table 3.2 are summarized, for each device, based on the literature, the values for three parameters used for the analysis of the repeatability, namely: the test-retest repeatability (TRT), related to the

[8] *HighTech Diagnostics, MS-39 Anterior Segment OCT*. CSO®, Florence, Italy.

variability of two measurements with respect to a subject; the coefficient of variation (CoV), related to the measurements dispersion or variation; and the intraclass correlation coefficient (ICC), which relates the between-subject and within-subject variances in a region, in this case in a 95% confidence interval (CI) [40]. High repeatability was found for all devices, confirmed by the TRT values below or around 0.20 D, CoV percentages below 1%, and ICC values higher than 0.900.

Table 3.2: Repeatability analysis for each device with respect to the simulated (anterior) keratometry, posterior keratometry, and total cornea.

	TRT (D)	CoV (%)	ICC (95% CI)
Simulated (Anterior) K			
Aladdin (Topcon) [41]	0.25	0.21	0.996
Lenstar (Haag-Streit) [42]	0.22	0.14	0.998
Cassini (i-Optics) [43]	-	0.29	0.988
Pentacam (Oculus) [44]	0.17	0.14	0.996
MS-39 (CSO) [40]	0.20	0.16	0.999
Posterior K			
Cassini (i-Optics) [43]	-	0.85	0.936
Pentacam (Oculus) [44]	0.06	0.34	0.992
MS-39 (CSO) [40]	0.07	0.39	0.997
Total Cornea			
Cassini (i-Optics) [43]	-	0.29	0.989
Pentacam (Oculus) [44]	0.14	0.11	0.998
MS-39 (CSO) [40]	0.27	0.22	0.999

CoV = Coefficient of variation; ICC = Intraclass correlation coefficients; TRT = Test-retest repeatability

Comparing Total Cassini (anterior and posterior surfaces) to Cassini, a high agreement was found for the astigmatism magnitude, with a reported 95% limit of agreement (LoA) of 0.86 D, while when comparing Cassini to Lenstar a 2.40 D LoA value was found, with an ICC value of 0.798 [45]. A lower LoA value (1.59 D) was reported in another study for the comparison of astigmatism magnitude with Lenstar and Cassini [42]. In both studies, no conclusion was redrawn for their interchangeability due to the wide data spread [42, 45]. Likewise, for Pentacam and Cassini the interchangeability was discouraged, with a LoA value of 0.74 D for anterior astigmatism and of 2.22 D for total astigmatism when comparing the devices [46]. Statistically lower total corneal power measurements were reported with the Pentacam when compared to the MS-39, with a LoA value of 0.98 D. Although the overall moderate agreement between the measurements of these devices, they were not considered to be interchangeable [40].

3.2 Parameters of influence

Neglecting the contribution of the posterior corneal surface for toric IOL calculations was pointed out as one of the major error sources [47] and investigated by several authors. A study performed by Ho *et al.* showed that both anterior and posterior corneal surfaces contribute to the total corneal astigmatism (TCA). In 28.8% of the eyes, a difference of at least 0.50 D or 10° between keratometric astigmatism (KA) and TCA was found. An average reduction of anterior corneal astigmatism by the posterior

corneal astigmatism (PCA) of 0.21 D was reported [48]. For a sample of eyes with only moderate to high astigmatism, Savini *et al.* reported a significant correlation between the KA and PCA magnitudes. Individual analysis of keratometric WTR, ATR and Oblique astigmatism with reference to the steeper anterior corneal meridian revealed a higher power effect of the posterior cornea on the WTR subgroup, -0.61 D, than in the ATR and the Oblique subgroups, -0.05 and -0.40 D, respectively [49].

Koch *et al.* found an average negative power of -0.30 D and a steep vertical meridian alignment in 86.6% of the cases for the posterior cornea. When comparing KA and TCA, they observed an average underestimation of the first by 0.22 D at 180°, related to the increase of the ATR astigmatism in TCA measurements created by the compensation of the negative power along the steep posterior corneal meridian [50]. Savini and Næser pointed out a mean cylinder over-correction of -0.59 D in WTR eyes and a mean under-correction of 0.32 D in ATR eyes, when using KA, in contrast to mean values of -0.13 D and 0.07 D for WTR and ATR eyes, respectively, when considering TCA [47].

Furthermore, Koch *et al.* suggested an age-related decreasing tendency of the compensatory effect of the posterior cornea, linked to the observed shift of the anterior corneal steepest meridian from vertical to horizontal with increasing age, and only a minimal change for the steep meridian of the posterior cornea [50]. Age-related corneal changes were also found by Hayashi *et al.*, namely a shift to ATR astigmatism of both anterior and total corneal astigmatism, with a significant correlation to age, and a slight change towards WTR astigmatism of the posterior cornea, only weakly correlated to age [51].

The importance of considering the variable distance between the cornea and the IOL plane, i.e., the corneal thickness and ACD, rather than a fixed ratio, was pointed out by Goggin *et al.* for the case of IOL calculations to correct astigmatism at the corneal plane [52]. In a theoretical study performed by Savini *et al.* for eyes with long AL and high corneal power, the ratio for IOL toricity and corneal astigmatism could be as high as 1.82 for a 30.0 mm long eye with 48.00 D, while for eyes with short AL and low corneal power, this ratio decreased to 1.29 for a 20.0 mm short eye with 38.00 D. When compared to the 1.46 fixed ratio provided by the manufactures “based on the average pseudophakic eye”, an under-correction of corneal astigmatism can occur for the first case (eyes with deep ACDs), while over-correction for the latter case (eyes with shallow ACDs) [53]. In addition, Goggin *et al.* showed that even if the ACD and cylindrical power at the IOL plane are kept constant, a change of the IOL spherical power leads to a different cylindrical power at the corneal plane. This dependence is more pronounced for IOLs with high cylindrical power, where the underestimation of the cylindrical power can be of 1.00 D or more, when spherical power is left out of consideration [52]. The effective lens position (ELP), usually defined as the estimated distance between the anterior corneal surface and the IOL plane, and more related to the spherical power, was pointed out by Ribeiro *et al.* as one of the impacting error sources on refractive outcomes, being almost 0.50 D, by the analysis of the post-operative ACD [54].

Different factors were analyzed by Zheng *et al.* regarding their impact on astigmatism estimation errors. Through multiple regression, a significant association was observed between the absolute error in magnitude and the difference between the anterior and posterior corneal astigmatism axis, AL, and magnitude of both keratometric and posterior astigmatism. On the other hand, for the absolute error in the angle, a significant influence was found for the difference between the anterior and posterior corneal

astigmatism axis, magnitude of keratometric astigmatism, magnitude of posterior astigmatism, as well as age. In particular, univariate analysis of the AL predictor showed an influence on the estimation error magnitude, namely for shorter eyes (20.0 to 24.0 mm) [55]. Moreover, Ribeiro *et al.* found that for a short eye with an AL of 19.5 mm, a 0.31 D refractive error was associated, while for a long eye, 28.5 mm, a 0.28 D error [54].

Only some studies analyzed the variation of central and peripheric corneal astigmatism. Read *et al.* performed a study with young adults, focused on the corneal topography variation from the center to the periphery, up to a zone of 9.0 mm. A reduction of astigmatism power towards the periphery was observed and a slightly higher flattening rate of the steeper corneal meridian [56]. Further, Kawamorita *et al.* investigated the astigmatism variation between the 2.0- and 6.0-mm diameter zones of the cornea in elderly patients. With an increasing diameter a decrease of corneal astigmatism was observed, namely for each zone, 1.0 mm apart, the obtained astigmatism mean values were 2.16, 2.00, 1.79, 1.60 and 1.44 D. The difference of astigmatism was analyzed by setting the 3.0 mm diameter zone as reference zone, and an increasing difference was noticed with the corneal astigmatism increase [57].

The variation in optical biometric parameters and their relation to IOL power calculations were also documented. Hoffer and Savini compared the results for AL, ACD, LT and corneal power measurements according to gender. They found that, in average, male eyes had longer ALs (23.75 mm), deeper ACDs (3.15 mm), and flatter corneas (43.60 D) when compared to female eyes with average values of 23.23 mm, 2.99 mm and 44.26 D for AL, ACD and corneal power parameters, respectively. An identical average value of 4.48 mm for the LT parameter was found for both genders [58]. Also, Ferreira *et al.* observed a gender dependence for AL, ACD and corneal power parameters for a Portuguese population, denoting a significant correlation between AL, ACD, LT and corneal diameter parameters [59].

Surgically induced (corneal) astigmatism (SIA/SICA) produce an impact on the magnitude and axis of the resultant corneal cylindrical power. The SICA amount depends on factors, such as incision location, due to the associated meridian flattening along the incision with the respective steepening in the orthogonal meridian, and also incision size, since smaller incisions are associated to less SICA. Therefore, the estimation of this factor should be personalized, and the expected amount considered in toric IOL calculations for the appropriate choice of the cylindrical power and alignment axis. IOL rotation was shown to play a role in refractive outcomes, since a rotation error of 10° is associated to a 35.0% residual error in astigmatism magnitude [60]. In a study of Weikert *et al.*, it was shown that tilting toric IOLs aligned at 180° resulted in a decrease of WTR astigmatism [61].

3.3 Toric intraocular lens power calculation

Aiming to address the raised matter of the influence of PCA in toric IOL calculations, several calculation methods have been developed for total corneal power estimation supported solely by anterior cornea-based measurements. The Baylor Toric IOL Nomogram developed by Koch *et al.* gathers guidelines for the calculation of the best toric IOL power. The pre-operative corneal measurements are adjusted by mean population values of the PCA, so that post-operative eyes have small amounts of

WTR astigmatism [62]. For cases with cylindrical power up to 2.0 D, Goggin *et al.* developed distinct adjustment coefficients for WTR and ATR eyes, used for anterior keratometric power in IOL calculation, encountering the IOL spherical power [63].

The Abulafia-Koch Formula [64] (incorporated in the PhysIOL Toric Calculator[9]) is based on a linear regression that adjusts standard keratometric measurements for TCA estimation. Derived from the difference of the post-operative astigmatism refraction and the toricity of the implanted IOL, the formula considers astigmatism as a vector, having an x and a y component, and encompassing only the measured astigmatism power [64]. The Næser-Savini Toric Calculator[10] optimizes the measured corneal astigmatism through one linear regression formula reducing the corneal astigmatism magnitude for WTR eyes and increasing it for ATR eyes. The optimized pre-operative values for the formula development were obtained by back-calculations, subtracting the IOL toricity and SICA from the post-operative refraction. The calculator incorporates AL and ACD parameters, as well as the measured astigmatism power and steep meridian derived from keratometric Scheimpflug or Placido disc measurements, or from Scheimpflug total corneal measurements. Further, it enables the introduction of three different measurements that are then averaged and optimized [65]. Both calculators can be used for IOL toricity calculation, requiring additional independent spherical IOL power calculation.

The Barrett Toric Calculator[11] predicts both spherical and cylindrical powers and axis orientation for toric IOL at the corneal plane, predicting, respectively, a lower and a higher astigmatism for WTR and ATR eyes. One keratometric measurement or the set of up to three different measurements from different Scheimpflug- or swept-source-OCT (SS-OCT)-based devices can be introduced, while the posterior corneal surface can be based on real introduced measurements or, otherwise, predicted by an incorporated theoretical model. Through the Barrett Universal Formula II, the ELP is calculated. The desired IOL must be selected, while the AL and ACD biometric parameters must be introduced, along with the SICA and incision location and, optionally, also LT and WTW measurements. The Kane Toric Calculator[12] uses the Kane Formula, based on an algorithm with regression, theoretical optics, and artificial intelligence (AI) for IOL spherical equivalent and cylindrical power predictions, as well as ELP calculation. It requires the same parameters as the Barrett Toric Calculator, aside from the CCT instead of the WTW parameter. Other toric calculators that require the above mentioned patient data are the Holladay Toric Calculator[13] and the EVO Toric Calculator 2.0. The latter is derived from the Emmetropia Verifying Optical (EVO) thick lens formula, that covers different geometries and powers for toric IOLs, and predicts theoretically the PCA for the total corneal estimation power[14].

Some manufactures have particular IOL toric calculators, such as Alcon that includes the Barrett Toric Calculator[15], or Johnson & Johnson's that owns the Tecnis® Calculator[16], which includes a PCA algorithm that by vector summation to anterior corneal astigmatism enables TCA estimation [66].

[9] PhysIOL Toric Calculator. `https://www.physioltoric.eu/`. Accessed: 2021-10-25.
[10] Næser/Savini Toric Calculator Version 1.2.4. `https://www.sedesoi.com/toric-2021/`. Accessed: 2021-10-26.
[11] Barrett Toric Calculator (Version 2.0). `https://ascrs.org/tools/barrett-toric-calculator`. Accessed: 2021-10-25.
[12] Kane Formula. `https://www.iolformula.com/`. Accessed: 2021-09-10.
[13] Holladay Consulting. `http://www.hicsoap.com/`. Accessed: 2021-09-10.
[14] EVO Formula Toric IOL Calculator v2.0. `https://www.evoiolcalculator.com/toric.aspx`. Accessed: 2021-09-10.
[15] Alcon Online Toric IOL Calculator. `https://www.myalcon-toriccalc.com/#/calculator`. Accessed: 2021-09-20.
[16] Tecnis Toric IOL Calculator. `https://tecnistoriccalc.com/calculator/`. Accessed: 2021-09-10.

An alternative approach for IOL power calculations is ray-tracing. Real and patient-specific topographic and biometric measurements can be used in addition to the real refractive indices, namely for the corneal refractive index instead of the keratometric index. As regards the IOL, it is described by the correspondent anterior and posterior central curvature radii, asphericity, thickness and refractive index values. The post-operative IOL position is a geometrically true position, reflecting the ACD, that pre-operatively can only be predicted [67]. Ribeiro *et al.* implemented a Personalized Pseudophakic Eye Model with patient-specific data, using a formula for the estimation of the post-operative IOL position based on the Liou-Brennan eye model with pre-operative ACD and LT. A strong correlation to the standard SRK-T formula was found, and with ray-tracing implementation it was shown to be adequate for IOL power calculation, even for post-LASIK eyes [11, 12]. Also the C Constant by Olsen and Hoffmann, a concept for the estimation of the IOL position that incorporates pre-operative ACD and LT, was shown to be adequate for IOL power calculations with ray-tracing [68]. Numerical ray-tracing implementation for IOL power calculation has been suggested by Preussner *et al.*, showing the possibility to find the appropriate IOL for an individual eye characteristics along with IOL design [69], and also by Olsen and Funding, that changed the anterior and posterior IOL curvatures of a known IOL design to measure the effective IOL power for a pseudophakic eye with a fixed 3.0 mm pupil diameter and biometric measurements [70]. In a study performed by Savini *et al.*, in which the author of this work participated, the prediction error for IOL power calculation using the MS-39 (CSO) AS-OCT device ray-tracing with different AL adjustment formulas (associated to the ELP) was evaluated for long eyes that underwent previous corneal refractive surgery. It was shown that ray-tracing with AL adjustments for both toric and non-toric IOLs permits accurate calculations, since, namely, the lowest obtained prediction error was as low as 0.08 D with the Holladay 2 Formula [71].

In a study performed by Ferreira *et al.*, the impact of the Baylor nomogram, the Abulafia-Koch Formula, the Goggin nomogram, when combined with the Holladay Toric Calculator, and via ray-tracing with the PhacoOptics software were assessed regarding the prediction error. The prediction error centroid decreased with the Baylor nomogram from 0.40 D @ 168° to 0.35 D @ 169°, with the Abulafia-Koch Formula to 0.25 D @ 158°, and with the Goggin nomogram to 0.38 D @ 170°. Via ray-tracing the prediction error centroid was 0.32 @ 171° [72]. A recent study by Kane and Connell, where toric IOL formulas were compared, showed that with the Kane Calculator a percentage of 65.6% eyes had a prediction error within 0.50 D, while with the Barrett Toric Calculator a percentage of 59.9%, with the Abulafia-Koch formula of 59.5%, with the EVO Toric Calculator 2.0 of 58.9%, and the Næser-Savini Toric Calculator a percentage of 56.7% [9].

Chapter 4

Nomograms for total corneal estimation power

Based on pre-operative astigmatism data collected with Lenstar and Cassini of patients candidate for cataract surgery, four nomograms were developed aiming to adjust Lenstar's KA by considering the Cassini's TCA, i.e., astigmatism from both anterior and posterior corneal surfaces. These nomograms are described in the first part of this chapter, being in a second step applied to a separate dataset with pre- and post-operative data as well as with information about the implanted toric IOL. The respective error in predicted residual astigmatism was assessed, as detailed in the second part of this chapter.

4.1 Nomogram construction

4.1.1 Patients and methods

A database was set up with pre-operative measurements of patients undergoing cataract surgery, provided by *Hospital da Luz Lisboa*. Measurements of 3 245 patients made with Lenstar and of 462 patients with Cassini were provided. Only patients with measurements taken with both devices were considered. Further on, were established all possible combinations of the measurements made with these devices: this means that, if for a given patient two measurements were taken with each instrument, four combinations were established. KA was calculated as the difference between the power of the steepest and the flattest meridians for Lenstar, while for Cassini anterior, posterior, and total corneal (from both surfaces) astigmatisms were considered. A minimum value of 80 was set for Cassini's quality factor of the posterior corneal surface, this criterion being met by 637 cases (334 right eyes). According to the astigmatism steepest meridian of Lenstar's measurements, these cases were then divided into subgroups: WTR (60° to 120°), ATR (0° to 30° and 150° to 180°) and Oblique (31° to 59° and 121° to 149°). From the total number of cases, 273 (42.86%) were WTR, 255 (40.03%) ATR and 109 (17.11%) Oblique.

Astigmatism vector analysis

Through the method of Holladay *et al.* [73] for analysis of surgically induced refractive change (SIRC) and calculation of the prediction error, astigmatism can be transformed from polar coordinates (magnitude and direction) into cartesian coordinates (xy components), using equations (4.1) and (4.2). Since astigmatism has a 180° rather than a 360° period, the cartesian form considers a double-angle and enables a mathematical analysis, as the components are orthogonal.

$$x = Cylinder \times \cos(2 \times Axis) \tag{4.1}$$

$$y = Cylinder \times \sin(2 \times Axis) \tag{4.2}$$

To transform the cartesian values back into polar values, the standard notation for astigmatism, termed net astigmatism, equation (4.3) can be used for the magnitude calculation, the $Cylinder$, and equation (4.4) for the direction, $Axis$, according to the x and y conditions.

$$Cylinder = \sqrt{x^2 + y^2} \tag{4.3}$$

$$Axis = \begin{cases} \frac{1}{2} \times \arctan(\frac{y}{x}), & if\ x\ and\ y > 0 \\ \frac{1}{2} \times \arctan(\frac{y}{x}) + 90°, & if\ x < 0 \\ \frac{1}{2} \times \arctan(\frac{y}{x}) + 180°, & if\ x > 0\ and\ y < 0 \end{cases} \tag{4.4}$$

Based on (4.1) and (4.2), Lenstar's KA and Cassini's TCA were decomposed into xy components. The x vectors represent the horizontal components, namely x_L for the KA of Lenstar and $x_{C_{TCA}}$ for the TCA of Cassini. In turn, the y vectors represent the vertical components, y_L and $y_{C_{TCA}}$. These vectors were then used to construct the nomograms, by modeling the relation between the horizontal components of Lenstar and Cassini through a linear regression, and the same for the vertical components. These regressions are of the type $y = Bx + A$, where y represents the dependent variable, in this case the TCA horizontal/vertical component that will be estimated, x or the independent variable, representing the measured KA, and B and A the slope and intercept coefficients, respectively. Equations (4.5) translate the used correspondence between the astigmatism components and the linear regression parameters, while equations (4.6) and (4.7) represent the uncertainties associated to the dependent variable (σ_y), and slope (σ_B) and intercept (σ_A) regression coefficients, respectively, according to [74].

$$\begin{gathered} Horizontal\ component:\ x_{C_{TCA}} = B \times\ x_L + A \\ Vertical\ component: y_{C_{TCA}} = B \times\ y_L + A \end{gathered} \tag{4.5}$$

$$\sigma_y = \sqrt{\frac{1}{N-2} \sum_{i=1}^{N} (y_i - A - Bx_i)^2} \tag{4.6}$$

$$\sigma_B = \sigma_y \sqrt{\frac{N}{N \sum x^2 - (\sum x)^2}} \qquad \sigma_A = \sigma_y \sqrt{\frac{\sum x^2}{N \sum x^2 - (\sum x)^2}} \tag{4.7}$$

Statistical analysis

For several measurements of the same quantity, there is an associated distribution, termed normal or Gaussian for the case where the respective errors do not have a large impact, and, if present, systematic errors are negligible. In a normal distribution, the center is the mean value corresponding to the curve's maximum, while the width parameter of the curve is set by the standard deviation (SD). To determine whether a sample follows a normal distribution or not, statistical tests can be performed, such as the Shapiro-Wilk test. The null hypothesis (H_0) states that the sample comes from a normal distributed population, while the alternative hypothesis (H_a) states that the data does not come from a normal distributed population. H_0 is rejected for p-values lower than the defined significance level, α, usually 0.05 [75]. Using the scipy.stats module of Python 3.7 (Anaconda), the Shapiro-Wilk test was performed to assess the distribution of the horizontal and vertical components of Lenstar's KA and Cassini's TCA.

4.1.2 Nomograms

In Table 4.1 are presented, separately, for the whole sample and the subgroups, the mean$\pm$SD values for Lenstar's KA and Cassini's anterior and posterior astigmatism, and also the TCA when both corneal surfaces are considered. For the whole sample, the mean$\pm$SD Lenstar's AL, in mm, were 23.81$\pm$1.56, and the range values, in mm, were 20.60 and 30.95.

Table 4.1: Mean$\pm$SD corneal astigmatism values, in D, for Lenstar and Cassini.

Group	L_{KA}	C_{Ant}	C_{PCA}	C_{TCA}
Total (637 eyes)	1.09$\pm$0.85	1.31$\pm$1.03	-0.33$\pm$0.20	1.24$\pm$0.95
WTR (273 eyes)	1.20$\pm$0.91	1.41$\pm$1.12	-0.39$\pm$0.22	1.20$\pm$1.01
ATR (255 eyes)	1.08$\pm$0.82	1.31$\pm$1.00	-0.28$\pm$0.18	1.35$\pm$0.95
Oblique (109 eyes)	0.84$\pm$0.71	1.08$\pm$0.84	-0.31$\pm$0.16	1.05$\pm$0.75

C_{Ant} = Cassini anterior corneal astigmatism; C_{PCA} = Cassini posterior corneal astigmatism; C_{TCA} = Cassini total corneal astigmatism; L_{KA} = Lenstar keratometric astigmatism

The mean astigmatism values for WTR eyes are similar for Lenstar's KA and Cassini's TCA, while for ATR and Oblique eyes Lenstar's KA is 0.27 D and 0.21 D, respectively, lower than Cassini's TCA. Also, for the whole sample Cassini's TCA power is higher than Lenstar's KA by 0.15 D. Cassini's anterior corneal astigmatism mean values are for all groups higher than the KA of Lenstar, while Cassini's PCA has an average value of -0.30 D. Cassini measurements including both corneal surfaces have a lower mean astigmatism when compared to the anterior corneal astigmatism, except for the ATR subgroup. These tendencies have already been appointed by several authors, who linked them to the mentioned posterior cornea compensation effect regarding WTR eyes and adding effect in ATR eyes (see Chapter 3 — 3.2) [47–50].

The mean$\pm$SD values and the range for the cartesian components of Lenstar's KA and Cassini's TCA are presented in Tables 4.2 and 4.3, respectively. For each component, the Shapiro-Wilk test was performed considering α=0.05, and the p-values were determined. Also presented is the net astigmatism, that is calculated based on equations (4.3) and (4.4) for the magnitude and direction, respectively.

Table 4.2: Lenstar's KA for each group, with mean±SD, range, in D, and p-value for the Shapiro-Wilk test, regarding the horizontal and vertical components, and net astigmatism, in D and °.

Group	x_L	y_L	Net astigmatism (D±SD @ °)
Total			
Mean ± SD	-0.09*±1.14	0.02*±0.78	0.10±0.94 @ 82.8
Range	-5.01, 4.07	-4.72, 4.19	
WTR			
Mean ± SD	-1.06*±0.81	-0.01*±0.69	1.06±0.75 @ 90.2
Range	-5.01, -0.05	-3.77, 1.94	
ATR			
Mean ± SD	0.92*±0.69	0.06*±0.72	0.92±0.71 @ 1.8
Range	0.08, 4.07	-4.72, 4.19	
OBL			
Mean ± SD	-0.05*±0.29	0.03*±1.07	0.06±0.56 @ 73.1
Range	-0.96, 0.76	-2.52, 3.66	

x_L = Lenstar horizontal component; y_L = Lenstar vertical component; *Shapiro-Wilk test with $p < 0.05$ (Non normal distribution)

Table 4.3: Cassini's TCA for each group, with mean±SD, range, in D, and p-value for the Shapiro-Wilk test, regarding the horizontal and vertical components, and net astigmatism, in D and °.

Group	$x_{C_{TCA}}$	$y_{C_{TCA}}$	Net astigmatism (D±SD @ °)
Total			
Mean ± SD	0.13*±1.28	0.04*±0.87	0.13±1.06 @ 8.5
Range	-6.49, 4.30	-7.54, 4.98	
WTR			
Mean ± SD	-0.72*±1.17	-0.01*±0.76	0.72±0.94 @ 90.5
Range	-6.49, 3.20	-3.05, 2.13	
ATR			
Mean ± SD	1.03*±0.96	0.03*±0.86	1.03±0.91 @ 0.8
Range	-2.18, 4.30	-7.54, 4.98	
OBL			
Mean ± SD	0.15*±0.58	0.19*±1.13	0.24±0.81 @ 26.1
Range	-1.44, 1.36	-2.52, 4.42	

$x_{C_{TCA}}$ = Total Cassini horizontal component; $y_{C_{TCA}}$ = Total Cassini vertical component; *Shapiro-Wilk test with $p < 0.05$ (Non normal distribution)

In both Lenstar and Cassini cases the horizontal components have higher mean values when compared to the vertical components, where the mean values close to zero. However, for both, high SD and range values are observed. The mean values for the horizontal components are higher compared to the total case, namely for the WTR and the ATR subgroups. Regarding the net astigmatism magnitude, it is highest for the WTR subgroup in the Lenstar case, and highest for the ATR in the Cassini case. For the Oblique subgroup, in the Lenstar case, the net astigmatism angle is rather characteristic of the WTR subgroup, while for the Cassini case it is rather characteristic of the ATR subgroup.

Four nomograms were constructed by modeling linear correlations based on Lenstar's KA and Cassini's TCA: a generic nomogram considering all eyes, and astigmatism subgroup specific nomograms. These suggest a tendency to turn the horizontal WTR component less negative, while turning more positive the ATR one.

4.2 Prediction error analysis

4.2.1 Calculation methods

An independent dataset with 175 eyes from 150 patients submitted to cataract surgery with toric IOL implantation was used for the test of the nomogram, containing the following parameters:

- Pre-operative: AL, ACD and keratometry (K1, K2 and axis) measured with Lenstar.
- Post-operative: subjective refraction, including spherical and cylindrical powers, and axis.
- Implanted toric IOL: spherical and cylindrical powers, and axis of implantation.

The KA was, once more, calculated as the difference between the power of the steepest and the flattest meridians, and classified into subgroups according to the steepest meridian. Then, the KA was decomposed by equations (4.1) and (4.2) into cartesian values and adjusted using, in one case, the generic nomogram and, in the other, the specific nomograms, WTR, ATR or Oblique, for each horizontal and vertical component. The same procedure was performed using the Abulafia-Koch regression formulas to adjust Lenstar's KA [64]. Afterwards, the adjusted horizontal and vertical components were converted back into magnitude and direction values, using equations (4.3) and (4.4), respectively.

Predicted residual astigmatism

The predicted residual astigmatism (PRA) calculation was based on and adapted mainly from three methods: the Holladay *et al.* method, published in 2001 [73], hereinafter indicated by I; the Holladay *et al.* method, published in 1988 [76], indicated by II; and the meridional analysis by Fam and Lim [77], indicated by III.

A spherocylindrical format, $S/C \times A$, is used, where S refers to the spherical power, in D, C to the cylindrical power in a minus cylinder notation, also in D, and is related to the astigmatism magnitude, and A to the astigmatism axis, in $^\circ$. The following steps were taken for the PRA calculations:

1. The adjusted astigmatism magnitude, or cylinder (C_{adj}), was combined with the corneal power by the set of equations (4.8), based on III:

$$\begin{aligned} S &= Max_K + C_{adj} \\ C &= -C_{adj} \\ A_{flat} &= A_{adj} + \theta \end{aligned} \tag{4.8}$$

   where Max_K is the maximum keratometry of the cornea, A_{adj} the axis of the adjusted astigmatism, and A_{flat} the combined flat axis for which θ is either 90°, if $0^\circ < A_{adj} < 90^\circ$, or -90° if $90^\circ < A_{adj} < 180^\circ$.

2. The correspondent steep and flat radii of curvature, in mm, were calculated by (4.9) and (4.10), respectively, based on III and I:

$$r_{steep} = \frac{0.3375}{S} \tag{4.9}$$

$$r_{flat} = \frac{0.3375}{S + C} \tag{4.10}$$

where the value of 0.3375 corresponds to the difference between the standard keratometric index (1.3375) and the refractive index of the air (1.00).

3. The ACD is calculated following III by (4.11) as the sum of the ELP (4.12), and the Surgeon Factor (SF), a constant representing the distance between the "anterior iris plane to the effective optical plane of the IOL" [76], based on II and here considered 1.67 — Figure 4.1. For the ELP estimation, the anterior chamber diameter (AG) had to be calculated using (4.13) in accordance to II:

$$ACD = ELP + SF \tag{4.11}$$

$$ELP = 0.56 + \frac{r_{steep} + r_{flat}}{2} - \sqrt{\left(\frac{r_{steep} + r_{flat}}{2}\right)^2 - \frac{AG^2}{4}} \tag{4.12}$$

$$AG = \frac{12.5 \times AL}{23.45},\ if\ AG > 13.5\ mm,\ then\ AG = 13.5\ mm \tag{4.13}$$

For eyes with an AL longer than 25.0 mm the Wang-Koch adjustment was performed [78].

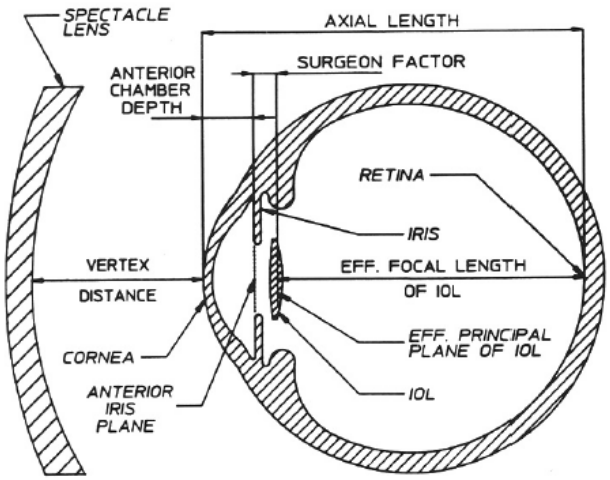

Figure 4.1: Eye cross-sectional representation with the identified parameters, in particular AL, ACD, and SF, and spectacle (lens) plane, according to II [76].

4. Based on III, from (4.14) and knowing the power of the implanted IOL, the desired IOL power along the steep and the flat meridians are given by (4.15):

$$IOL_{SE} = IOL_S + 0.5 \times IOL_C \tag{4.14}$$

$$\begin{gathered} IOL_{steep} = IOL_S \Leftrightarrow IOL_{steep} = IOL_{SE} - 0.5 \times IOL_C \\ IOL_{flat} = IOL_{steep} + IOL_C \end{gathered} \tag{4.15}$$

5. The expected refraction (ER) for the corneal power of the steep meridian is given by (4.16) and according to III, considering 12.0 mm for the vertex distance (V), which represents the distance of the spectacle plane to the corneal plane (see Figure 4.1):

$$ER_{steep} = \frac{1336 \times (1) - IOL_{steep}(L - ACD) \times (2)}{1.336(V \times (1) + L \times r_{steep}) - 0.001IOL_{steep}(L - ACD)1.336(V \times (2) + ACD \times r_{steep})}$$
$$with : (1) = 1.336r_{steep} - 0.3333L$$
$$and : (2) = 1.336r_{steep} - 0.3333ACD \tag{4.16}$$

where the value of 1.336 corresponds to the aqueous humor refractive index, and $L = AL + T_R - t$, where $T_R = 0.2$ mm represents the retinal thickness factor, and $t = 0$ mm the IOL thickness. Likewise, the ER_{flat} is calculated by introducing the respective parameters, r_{flat} and IOL_{flat}.

6. The corresponding ER sphere, cylinder, and axis components, based on III, are given by $ER_{sph} = ER_{steep}$, $ER_{cyl} = ER_{flat} - ER_{steep}$ and $ER_{ax} = A$, referring to the PRA components: PRA_{shp}, PRA_{cyl} and PRA_{ax}.

Prediction error

The error in PRA, also referred to as EPA, was calculated by applying the Thibos *et al.* method [79] to analyze the refractive error. This method considers three power vectors: the spherical lens power, M, and two Jackson crossed cylinders, one along the 0°-180° axis (J_0) and the other along the 45° axis (J_{45}). Equations (4.17), (4.18), and (4.19) refer to each of these vectors, where α is the axis. Together, they represent the spherocylindrical power of a lens by a point in a three-dimensional dioptric profile.

$$M = S + \frac{C}{2} \tag{4.17}$$

$$J_0 = \frac{C}{2} \times \cos(2\alpha) \tag{4.18}$$

$$J_{45} = \frac{C}{2} \times \sin(2\alpha) \tag{4.19}$$

Using equations (4.17), (4.18), and (4.19), the PRA_{sph}, PRA_{cyl} and PRA_{ax} components from step 6 of the PRA calculations and the post-operative subjective refraction were decomposed into the three power vectors. The difference between the subjective refraction and PRA was calculated for each power vector, and the EPA sphere, cylinder, and axis were calculated, using equation (4.20), (4.21), and (4.22), respectively:

$$EPA_{sph} = Dif(M) - \frac{EPA_{cyl}}{2} \tag{4.20}$$

$$EPA_{cyl} = 2 \times \frac{Dif(J_{45})}{\sin(2 \times EPA_{ax})} \tag{4.21}$$

$$EPA_{ax} = \begin{cases} \frac{\arctan(F)}{2} + 180°, & if \ \frac{\arctan(F)}{2} < 0 \\ \frac{\arctan(F)}{2}, & otherwise \end{cases} \tag{4.22}$$

where in (4.22) $F = \left(\frac{Dif(J_{45})}{Dif(J_0)}\right)$, and $Dif(M)$, $Dif(J_0)$, and $Dif(J_{45})$ represent the vector differences between post-operative subjective refraction components and predicted residual refraction.

Focusing on the astigmatism, the cylindrical components of the obtained EPA were decomposed in cartesian components and represented in double-angle plots, following the Holladay *et al.* method (described in section 4.1) [73].

For 60 eyes (32 WTR, 22 ATR, and 6 Oblique) where the implanted toric IOL was known, the prediction error was also calculated with the Barrett Toric Calculator[1]. Only considered were the cases where the powers of the IOL given by the Barrett Toric Calculator matched the implanted IOL powers.

Statistical analysis

Statistical analysis was performed, using scipy.stats module in Python 3.7 (Anaconda). The Shapiro-Wilk normality test, described above (section 4.1), was performed for each EPA horizontal and vertical components and magnitude. In order to detect statistical differences between EPA horizontal and vertical components and magnitude with and without adjustment, two types of statistical tests were employed: when paired and normally distributed, the paired t-test was used; otherwise, the Wilcoxon signed-rank test was employed. A paired t-test is a parametric test, which assumes that the data follows a normal distribution, where H_0 states that the means of the two related samples are identical, or that the mean difference between the two samples is zero, and H_a that the means are different. On the other hand, the Wilcoxon signed-ranks test is a non-parametric test that does not assume the normal distribution of data, rather comparing the medians of the samples: H_0 states that the median of the differences between the samples is zero, and H_a that the median of the differences is unequal zero [75]. From the statistical point of view were considered as significant the p-values lower than 0.05.

4.2.2 Results

The mean$\pm$SD (and range) values for the pre-operative AL and ACD measurements, in mm, were, respectively, 23.91$\pm$1.54 (21.18, 30.70) and 3.08$\pm$0.40 (2.24, 4.27). According to the orientation of the measured axis, the cases were divided into subgroups: WTR (75 cases, 42.86%), ATR (85 cases, 48.57%), and Oblique (15 cases, 8.57%). The net astigmatism for the pre-operative measured KA and adjusted KA by the nomograms for the whole sample and for each subgroup are listed in Table 4.4.

[1] Barrett Toric Calculator (Version 2.0). `https://ascrs.org/tools/barrett-toric-calculator`. Accessed: 2021-10-25.

Table 4.4: Net astigmatism (D±SD @ °) for the Lenstar measured KA and adjusted by the nomograms.

Group	Measured	Generic	Specific
Total	0.12±1.46 @ 57.7	0.20±1.31 @ 17.6	0.15±1.32 @ 21.2
WTR	2.01±1.17 @ 89.6	1.61±1.05 @ 89.3	1.68±1.08 @ 89.7
ATR	1.64±0.79 @ 0.5	1.71±0.71 @ 0.7	1.65±0.71 @ 0.0
Oblique	0.12±1.01 @ 41.6	0.99±0.91 @ 35.3	1.12±1.00 @ 36.3

The net astigmatism magnitude for the WTR and ATR cases were lower and higher, respectively, when KA values were adjusted through the generic and subgroup specific nomograms. This observation was even more pronounced for the generic nomogram adjustment. Despite the low number of Oblique eyes, for this subgroup the net astigmatism magnitude increased when the KA was adjusted by the nomograms, and particularly in the specific nomogram case. Regarding the total group case, the magnitude increases when adjusted by both nomograms, which may be associated to the larger number of ATR eyes. In these cases, for the Oblique subgroup, the angle is characteristic of this subgroup.

The mean±SD values for the EPA horizontal (x) and vertical (y) components and the correspondent net astigmatism magnitude (and SD) and direction were calculated for each case with and without the generic and subgroup specific adjustments, for the whole sample and for each subgroup (Table 4.5). Furthermore, the percentages of eyes with an EPA magnitude equal or lower than 0.50, 0.75, and 1.00 D are presented. In addition, the same parameters were calculated using the Abulafia-Koch regression formulas [64].

For the total group, the horizontal EPA component decreased significantly with the KA nomogram adjustments ($p<0.001$), and even more for the generic nomogram case ($p<0.001$), that has the lowest mean value. The KA nomogram adjusted horizontal EPA components also statistically differed ($p<0.001$) from the Abulafia-Koch adjustment case, which had a negative mean value indicating a substantial WTR shift. Also for the WTR subgroup, the EPA horizontal component was significantly lower for the nomogram adjustment cases and Abulafia-Koch formula ($p<0.001$), and the generic nomogram case was statistically lower when compared to the specific nomogram case ($p=0.001$). However, both nomogram adjusted correspondent EPA horizontal components had higher mean values compared to the Abulafia-Koch formula case ($p<0.001$). For the EPA horizontal component of the ATR subgroup, the specific nomogram adjustment led to a statistically lower value compared to the case without adjustment ($p=0.0360$), and a less negative value compared to the generic adjustment case ($p<0.001$). The Abulafia-Koch adjusted ATR correspondent EPA horizontal component showed a significantly more negative mean value ($p<0.001$) in comparison to the nomogram adjustment cases and when without adjustment. Regarding the vertical components, the mean values were close to zero in the total group and the subgroups, but no statistical differences were found in the comparison between the cases.

Table 4.5: Mean±SD values for the EPA horizontal (x) and vertical (y) components, in D, and correspondent net astigmatism magnitude and direction (D @ °). Percentages of eyes with an absolute EPA equal or lower than 0.50, 0.75 and 1.00 D.

	EPA, x	**EPA,** y	**EPA, Net Astigmatism**		**% Eyes** $\leq$ **x.xx D**		
Group	Mean±SD (D)	Mean±SD (D)	Net Ast. (D@°)	SD	0.50	0.75	1.00
Total (175 eyes)							
Without	0.22*±0.64	-0.02*±0.45	0.22 @ 177.1	0.54	44.00	69.71	82.29
Generic	0.05*±0.65	-0.01*±0.38	0.05 @ 174.1	0.45	56.00	77.71	88.57
Specific	0.10*±0.56	-0.02*±0.39	0.10 @ 174.9	0.47	52.57	76.57	88.57
Abulafia-Koch	-0.17*±0.55	-0.01*±0.40	0.17 @ 91.5	0.47	51.43	73.71	86.86
WTR (75 eyes)							
Without	0.56*±0.76	0.00±0.52	0.56 @ 0.1	0.63	26.67	49.33	70.67
Generic	0.19*±0.64	0.01±0.41	0.19 @ 1.5	0.51	49.33	69.33	84.00
Specific	0.25*±0.72	0.02±0.41	0.25 @ 2.0	0.55	44.00	65.33	81.33
Abulafia-Koch	0.04*±0.62	0.03±0.43	0.05 @ 20.4	0.52	53.33	76.00	86.67
ATR (85 eyes)							
Without	-0.06±0.40	0.00*±0.38	0.06 @ 90.7	0.39	56.47	84.71	91.76
Generic	-0.08±0.41	0.00*±0.35	0.08 @ 90.2	0.38	60.00	83.53	90.59
Specific	-0.03±0.39	0.00*±0.36	0.03 @ 87.9	0.37	58.82	84.71	94.12
Abulafia-Koch	-0.39±0.42	0.00±0.36	0.39 @ 90.3	0.39	45.88	69.41	87.06
Oblique (15 eyes)							
Without	0.09±0.22	-0.27±0.46	0.28 @ 144.2	0.32	60.00	86.67	86.67
Generic	0.09±0.19	-0.17±0.38	0.19 @ 149.1	0.27	66.67	86.67	100.00
Specific	0.07±0.22	-0.30±0.39	0.31 @ 141.4	0.29	60.00	86.67	93.33
Abulafia-Koch	0.01±0.23	-0.24±0.45	0.24 @ 136.1	0.32	73.33	86.67	86.67

$\%\ Eyes\ \leq x.xx\ D =$ Percentage of eyes with an absolute error magnitude equal or lower than $x.xx$ D; *Shapiro-Wilk test with $p < 0.05$ (Non normal distribution)

When comparing the magnitude EPA values, the generic and specific adjustment cases yielded lower values than without an adjustment, with a decrease of around 0.1 D in the total case ($p<0.001$) and around 0.3 D in the WTR case ($p<0.001$). The Abulafia-Koch formula adjustment led likewise to a decrease of the magnitude EPA value: in the total case, although statistically less than the total nomogram adjustment (p=0.0007); and in the WTR case, which did not differ from the generic nomogram's adjustment (p=0.2518), but from the specific nomogram case (p=0.0225). Observing the different graphics in Figure 4.2 (b), the decrease in data spread and the WTR shift are slightly visible. The ATR subgroup cases are presented in Figure 4.2 (c), where no obvious differences are visible. For this subgroup no statistical differences were found between the EPA magnitude values adjusted by the nomograms (p=0.1821), although they were statistically lower than for the Abulafia-Koch case ($p<0.001$). The percentages of eyes with an EPA magnitude equal or lower than 0.50, 0.75, and 1.00 D increased when the nomograms were used, namely the generic nomogram, except for the ATR subgroup, where the specific nomogram led to higher percentages equal or lower than 0.75 and 1.00 D than the generic nomogram. Comparing the nomograms and Abulafia-Koch cases, for which the double-angle plots are presented in Figure B.1 in Appendix B, the percentages of eyes equal or lower than 0.50 D were similar, being slightly lower in the WTR case and higher in the ATR case. The Oblique subgroup had a small number of eyes and higher mean values for the vertical components as proper of this group, that overall did not present

differences between the EPA components and magnitude, when KA adjusted or not adjusted. In this subgroup, the percentages of eyes with an EPA equal or lower than 0.50, 0.75, and 1.00 D were higher than 60% in all cases.

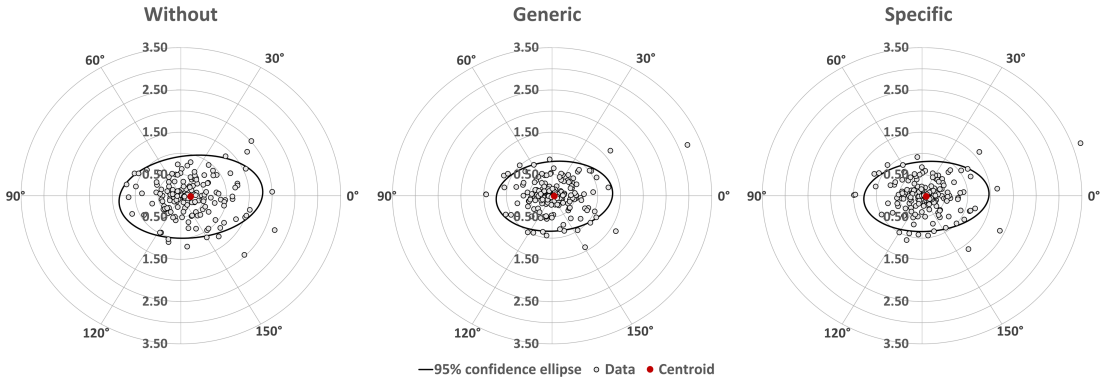

(a) Total group.

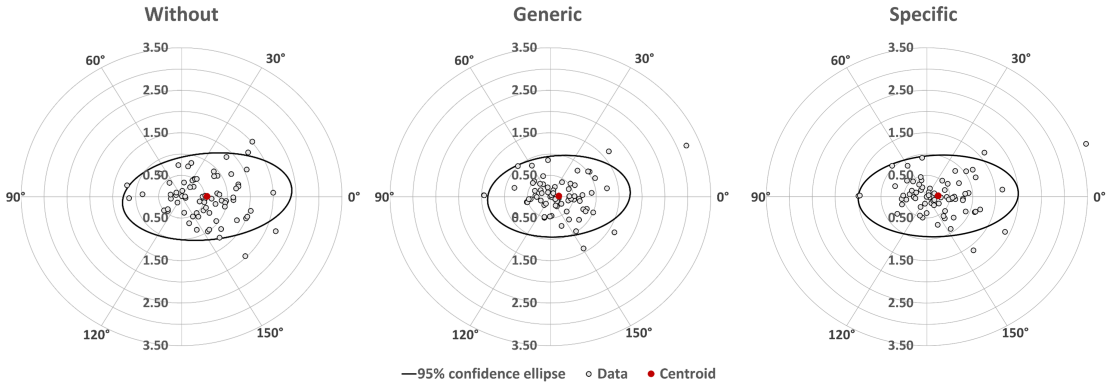

(b) WTR subgroup.

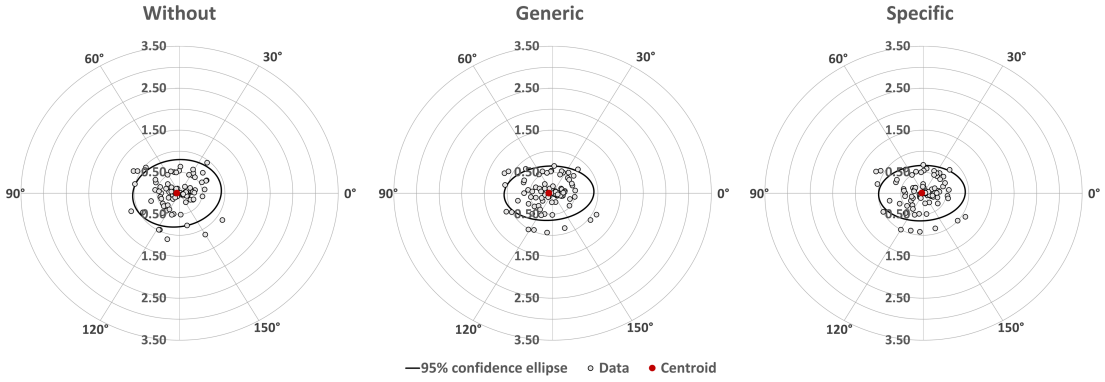

(c) ATR subgroup.

Figure 4.2: Double-angle plots of the EPA for the total group (a), and WTR (b) and ATR (c) subgroups. Each ring represents 0.50 D.

Overall, the centroid for the horizontal component decreased when KA is adjusted, with an WTR shift tendency, which can also be observed in Figure 4.2. The generic KA adjustment led not only to the largest decreases, with statistical significance, for both total and WTR cases, but led also to a lower data spread, shown as well by the narrowing of the confidence ellipses in Figure 4.2. Despite the high number of ATR cases in the test sample, no statistical differences were found, what may be related

to already low prediction errors without adjustment. When the Abulafia-Koch formula is employed the associated EPA horizontal component has a more pronounced WTR shift than the nomogram adjusted cases, specially for the ATR subgroup. So, the outcomes were better for the WTR, but worse for the ATR subgroup. The percentage of eyes with an EPA magnitude equal or lower than 0.50 D increased when the KA was adjusted, namely with the generic nomogram, and similar to the Abulafia-Koch case for the whole sample. The percentages of eyes with an EPA magnitude within 1.00 D, overall, exceeded 80% when adjusted, reaching even 90% with the nomograms' adjustment for the ATR subgroup which includes most cases.

Furthermore, for the set of eyes for which the implanted IOL was known (60 eyes), the horizontal centroid component correspondent to the case without adjustment (0.19$\pm$0.48 D) decreased for the adjustment cases with the generic (0.01$\pm$0.41 D) and specific (0.02$\pm$0.42 D) nomograms, as well as for the Barrett Calculator (0.11$\pm$0.32 D). The Abulafia-Koch Formula had a pronounced associated deviation towards WTR (-0.19$\pm$0.42 D). The magnitude and direction for the case without adjustment were 0.19 D @ 7.0°, while for the generic and specific nomograms adjustment cases these were, respectively, 0.06 D @ 40.2° and 0.05 D @ 34.2°. With the Abulafia-Koch Formula, these were 0.20 D @ 80.3° and with the Barrett Toric Calculator 0.12 D @ 175.6°. The lowest prediction error ($p<0.001$) and the highest percentage of eyes with a prediction error equal or lower than 0.50 D (88.33%) were obtained with the Barrett Toric Calculator — without adjustment the percentage was only 48.33%. Also, the nomogram adjustments led to a statistically significant decrease of the prediction error (p=0.0036 for the generic, and p=0.0018 for the specific nomogram cases) with correspondent percentages of prediction error equal or lower than 0.50 D of 56.67% and 61.67%. No statistical differences were found compared to the Abulafia-Koch Formula, which had 61.67% of eyes with a prediction error equal or lower than 0.50 D. The respective prediction error double-angle plots are presented in Figure B.2 in Appendix B.

4.3 Considerations

Relations between KA and TCA have been studied aiming the achievement of an optimum refractive result. KA measurements are still widely used with a usually high repeatability, therefore, nomograms with the purpose of accounting the PCA, for which measurements are not so easily available, but encountered in total corneal power measurements, have been developed and shown to reduce the prediction error [62–64, 72, 80]. Here, the principle employed was the linear relation between Lenstar's KA and Cassini's TCA. For both was shown a high performance regarding astigmatism, being however discouraged their interchanging [42, 45]. In a performed analysis, not presented here, relating Total Cassini and Cassini, a R^2 value of 0.97 was found between their horizontal components, while a value of 0.96 between their vertical components, indicating a high relation. The developed nomograms suggest a reduction of the WTR astigmatism (less negative horizontal component) and an increase of the ATR astigmatism (more positive horizontal component), like other adjustment methods (detailed in Chapter 3 — section 3.3), thereby, pointing to a possible reduction of the known WTR over-correction and ATR under-correction. By applying the nomograms to adjust the Lenstar's measured KA, a prediction error

reduction trend appears, as for the Abulafia-Koch regression formulas and the Barrett Toric Calculator. A decrease in the EPA horizontal component and magnitude were found overall, with a shift towards the WTR subgroup and a decrease in the spread of cases. A more pronounced improvement was found when the generic nomogram was used. The special case of Oblique eyes, usually more uncommon, showed no differences when adjusted by the nomograms and when not, what is in line with the findings of a previous study that found out that Oblique eyes do not benefit with adjustments [81]. Even though improvements were achieved with a decrease of the EPA magnitude and increase of the percentages of eyes with an EPA $\leq$ 0.50 D, they are still below 60-70% and, therefore, on the one hand, a nomogram refinement should be performed, reducing the outliers; and on the other hand, larger test samples are needed to strengthen the findings.

Chapter 5

Error in refractive astigmatism analysis

In this chapter is presented a multiple analysis of factors that influence toric IOL power calculation aiming to improve astigmatism refractive outcomes. The first section encompasses the study of variations of the rotating Scheimpflug camera TCA calculated via ray-tracing, in relation to two zones and its influence on the prediction of residual refractive astigmatism. In the second section, a retrospective study is described, in which the performed measurements according to the used modalities and the number and surgery-related acquiring stage are compared regarding the extent of their influence on the error in refractive astigmatism. Pursuing the same aim, different biometric parameters were considered in a preliminary exploratory implementation of supervised machine learning as potential improvement strategy.

5.1 Corneal astigmatism variation within 3.0- and 4.0 mm zones

5.1.1 Patients and methods

A database with pre-operative measurements from 376 patients taken with the Pentacam rotating Scheimpflug camera and provided by *Hospital da Luz Lisboa* was set up. From the total of 500 eyes, 255 were right eyes (51.00%). For the TCRP measurements from a 3.0 mm and a 4.0 mm diameter ring centered on the pupil axis, the eyes were divided into astigmatism subgroups according to the steep meridian of the 3.0 mm zone: 186 were WTR (60° to 120°), 197 ATR (0° to 30° and 150° to 180°), and 117 Oblique (31° to 59° and 121° to 149°).

From both zones, a comparison between the mean magnitude values and between the axes was performed. Whenever the difference between the two zones axes' measurements was higher than 90°, one was converted by subtracting the axis value from 180°, for example, when the measured axis in the 3.0 mm zone was 179° and 0° in the 4.0 mm zone, the first was converted to 1° (180°-179°). Using the Holladay *et al.* method [73], the astigmatism components from each zone were decomposed into

cartesian xy components, so that magnitude and direction variations were simultaneously taken into account (see Chapter 4 — section 4.1).

The differences between the 3.0- and 4.0-mm zone's astigmatism magnitude were divided into 0.25 D intervals. From the total of 500 eyes, 125 eyes (20%) were randomly chosen for astigmatism differences between zones lower than 0.50 D, since this range holds most of the cases (427 eyes), and including all eyes for differences higher than 0.50 D. For these eyes, the suggested toric IOL power for each TCRP zone values, according to the Næser-Savini Toric Calculator[1], was recorded. The predicted residual refractive astigmatism correspondent to the toric IOL power determined to be implanted with TCRP values from the 3.0 mm zone was compared to the prediction for the same toric IOL power, but with TCRP values from the 4.0 mm zone.

Statistical analysis was carried out using the scipy.stats module of Python 3.7 (Anaconda) to assess the sample's normality by the Shapiro-Wilk test and, accordingly, to compare the components based on the paired t-test or the Wilcoxon signed-rank test (see Chapter 4 — sections 4.1 and 4.2). As significant were considered p-values lower than 0.05.

5.1.2 Corneal astigmatism magnitude and axis variation

The mean corneal astigmatism values for both zones, 3.0- and 4.0 mm, are presented in Table 5.1, for the whole sample and for the specific subgroups. The indicated number of cases for each subgroup refers to the division made based on the astigmatism in the 3.0 mm zone. The three first rows show the mean values for astigmatism intervals of 1.00 D, while in the last row the astigmatism mean value is given for the case where all eyes are considered.

Table 5.1: Mean±SD, in D, values for the TCRP 3.0- and 4.0 mm zones.

	Total (n=500)		**WTR** (n=186)		**ATR** (n=197)		**Oblique** (n=117)	
Ast. (D)	3.0 mm	4.0 mm	3.0 mm	4.0 mm	3.0 mm	4.0 mm	3.0 mm	4.0 mm
$\leq$ 1.00	0.60±0.26	0.64±0.37	0.64±0.24	0.69±0.35	0.64±0.24	0.62±0.42	0.52±0.28	0.60±0.33
1.00 - 2.00	1.41±0.26	1.41±0.52	1.46±0.25	1.45±0.48	1.39±0.24	1.40±0.54	1.36±0.28	1.30±0.57
2.00 - 3.00	2.50±0.30	2.29±0.60	2.49±0.29	2.45±0.52	2.54±0.34	2.04±0.50	2.49±0.30	2.36±0.75
$>$ 3.00	3.88±0.98	3.61±0.84	3.71±0.59	3.70±0.60	4.11±1.31	3.51±1.08	3.50±0.57	3.57±0.85
All	1.15±0.83	1.14±0.84	1.23±0.80	1.25±0.84	1.19±0.88	1.12±0.84	0.96±0.76	0.99±0.79

$Ast.$ = Astigmatism interval

Observing the mean values divided into astigmatism intervals, in the cases of the whole sample (Total), WTR, and Oblique, the astigmatism values below 1.00 D are lower in the 3.0 mm zone than in the 4.0 mm zone, while for higher astigmatism intervals the opposite occurs. For the ATR subgroup, the astigmatism values below 1.00 D and above 2.00 D are, in average, higher in the 3.0 mm zone. However, for the whole astigmatism range, only for the ATR subgroup the mean astigmatism value was lower in the 4.0 mm zone when compared to the 3.0 mm zone.

[1] Næser/Savini Toric Calculator Version 1.2.4. `https://www.sedesoi.com/toric-2021/`. Accessed: 2021-10-26.

A linear regression model was fitted between the corneal astigmatism from the 3.0 mm zone, considered as reference, and the difference of astigmatism values between the 3.0- and 4.0 mm zones, shown in Figure 5.1 (a), with a 95% prediction limit. In Figure 5.1 (b) is visible the relation between the astigmatism axes in the 3.0- and 4.0 mm zones, also with a 95% prediction limit.

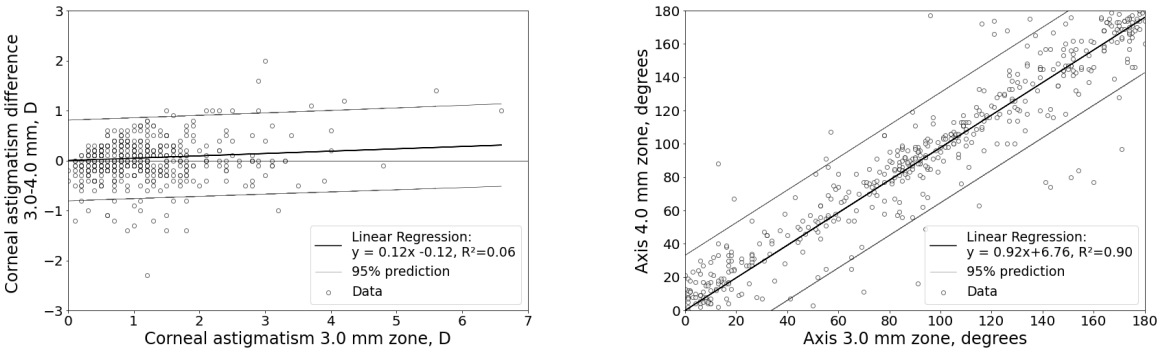

(a) Corneal astigmatism variation.

(b) Axis variation.

Figure 5.1: Linear regressions for the variations of the corneal astigmatism difference between the zones in reference to the 3.0 mm zone (a) — $y(\sigma = 0.41) = 0.12x(\sigma = 0.02) - 0.12(\sigma = 0.03)$, $R^2 = 0.06$; and for the axes variation between the 3.0- and 4.0 mm zones (b) — $y(\sigma = 16.50) = 0.92(\sigma = 0.01) + 6.76(\sigma = 0.02)$, $R^2 = 0.90$.

The astigmatism difference between the 3.0- and 4.0 mm zones has a positive value in the cases where the astigmatism is higher in the 3.0 mm zone than in the 4.0 mm zone. In Figure 5.1 (a), where most cases are below 2.00 D, the linear regression suggests that for low astigmatism values there is almost no difference between the zones. With the increase of astigmatism in the 3.0 mm zone, the astigmatism difference between zones shows a more pronounced tendency. Looking at the 95% prediction interval, the differences between zones seem to lay in a 1.00 D range. In turn, for the axis variation, there is almost no difference between the zones (Figure 5.1 (b)), with a R^2 value of 0.90.

In Figures 5.2 (a) and (b), the variations of the horizontal component difference between zones regarding the corneal astigmatism in the 3.0 mm zone are represented for the WTR and ATR subgroups, respectively. For the WTR subgroup, the linear regression line appears close to zero, suggesting no pronounced differences, while for the ATR subgroup a decreasing tendency emerges, with a slope coefficient that indicates that the horizontal component in the 3.0 mm zone is higher than in the 4.0 mm zone, being more pronounced for higher 3.0 mm astigmatism values. Performing statistical comparisons between the horizontal components for the astigmatism intervals and regarding all diopter values, differences were found in the ATR subgroup, namely: for astigmatism values below 1.00 D and in the range of 1.00-2.00 D, as well as considering the whole range, the mean value of the horizontal component is lower for the 4.0 mm zone than for the 3.0 mm zone ($p<0.001$, $p=0.005$, and $p<0.001$, respectively). Comparing the vertical components, no differences were found.

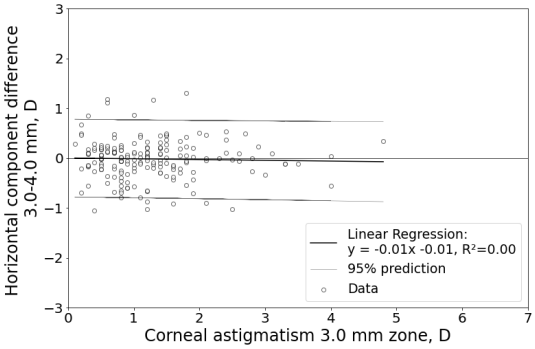

(a) WTR horizontal component variation.

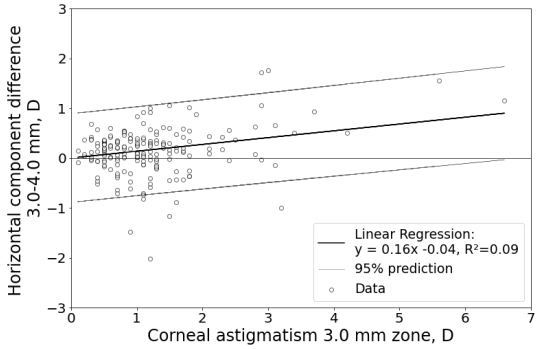

(b) ATR horizontal component variation.

Figure 5.2: Linear regressions for the variation of the horizontal component difference between zones in reference to the corneal astigmatism in the 3.0 mm zone for the WTR subgroup (a) — $y(\sigma = 0.40) = -0.01x(\sigma = 0.04) - 0.01(\sigma = 0.05)$, $R^2 = 0.00$ — and ATR subgroup (b) — $y(\sigma = 0.45) = 0.16x(\sigma = 0.04) - 0.04(\sigma = 0.05)$, $R^2 = 0.09$.

5.1.3 Prediction of residual refractive astigmatism

Comparing the suggested toric IOL to be implanted based on the TCRP values of the 3.0 mm zone to the ones of the 4.0 mm zone, the power changed in 76.80% of the eyes, whereas 52.08% of these had lower toric IOL powers in the 4.0 mm zone than in the 3.0 mm zone, while 47.92% had higher powers — Table C.1 in Appendix C. The predicted residual refractive astigmatism mean±SD values for the toric IOL power suggested, for both zones and based on the 3.0 mm TCRP, are presented in Table 5.2, as well as the calculated Mean Absolute Error (MAE), i.e., mean of the absolute differences in relation to the prediction of the 3.0 mm zone for each case.

Table 5.2: Mean±SD values, in D, for the predicted residual refractive astigmatism for both zones, considering the toric IOL for the TCRP 3.0 mm zone.

Ast. Dif. (D)	**3.0 mm** (Mean±SD)	**4.0 mm** (Mean±SD)	**MAE**
$\leq$ 0.25	0.08±0.10	0.11±0.13	0.08
0.25 - 0.50	0.11±0.09	0.37±0.28	0.26
0.50 - 0.75	0.11±0.09	0.51±0.24	0.41
0.75 - 1.00	0.21±0.37	0.86±0.39	0.75
$>$ 1.00	0.17±0.18	1.27±0.63	1.09
All	0.13±0.18	0.55±0.49	0.45

$Ast.Dif.$ = Interval of astigmatism difference between zones; MAE = Mean Absolute Error

Overall, considering the toric IOL power determined for the TCRP 3.0 mm zone, the predicted residual refractive astigmatism increases for the TCRP 4.0 mm zone, in particular for higher astigmatism difference intervals: while for differences below 0.75 D the MAE is below 0.50 D, for higher differences it increases surpassing 1.00 D for differences higher than 1.00 D. Further, except for astigmatism differences equal or lower than 0.25 D, in general, the prediction differences had values of the same order of magnitude as the correspondent interval of astigmatism differences.

5.1.4 Discussion

The most pronounced variations were found for the ATR subgroup, not only in statistical terms, when comparing the horizontal components, but also when fitting a linear regression model between the 3.0-4.0 mm horizontal component difference with respect to the 3.0 mm zone corneal astigmatism. Although the average increase for the WTR subgroup and decrease for the ATR subgroup, overall, the mean magnitude astigmatism values between the 3.0- and 4.0 mm zones are mostly similar. However, the power of the toric IOL to be implanted changed between zones, showing a decrease towards the periphery. With the increasing of astigmatism differences between zones, when considering the toric IOL power determined based on the 3.0 mm zone, the predicted residual refractive astigmatism increased in average and the prediction differences were substantial for astigmatism differences higher than 0.75 D.

In a previous study performed by Kawamorita *et al.* [57] regarding zones up to 6.0 mm, the difference of astigmatism with respect to the 3.0 mm zone was statistically significant, more pronounced for higher astigmatism values at the reference zone. In the present study, only two zones were considered, and although the similar mean astigmatism magnitude values, when analyzing the predicted residual refractive astigmatism, substantial differences were found, reinforcing the mentioned consideration of the relation between central and peripheric astigmatisms for the improvement of outcomes by Kawamorita [57].

Therefore, the astigmatism of more peripheral zones could alter the predictions and, consequently, the outcomes, and thus should be further studied with respect to its influence on the error in refractive astigmatism.

5.2 Error in refractive astigmatism

5.2.1 Patients and methods

A retrospective study was conducted at *Studio Oculistico D'Azeglio*, including 100 eyes (51 left eyes) from 79 patients undergoing cataract surgery with toric IOL implantation (Acrysof SN6ATx, Alcon Laboratories, Inc.). Pre-operatively, three consecutive measurements were performed with Pentacam (Pentacam HR, Pentacam AXL, and Pentacam AXL Wave, depending on the year of the examination — 2015 to 2021) and Aladdin. According to the corneal astigmatism measurements, the power of the IOL to be implanted was calculated. Post-operatively, namely at least one month after the surgery, three consecutive measurements were performed using the same devices; the patients' subjective refraction (spherical and cylindrical powers, and axis) was recorded; and the IOL orientation was determined using a slit-lamp aligned with the IOL indentations, as shown in Figure 5.3, and confirmed using Photopea, Online Photo Editor[2].

[2]Photopea, Online Photo Editor. `https://www.photopea.com`. Accessed: 2021-08-14.

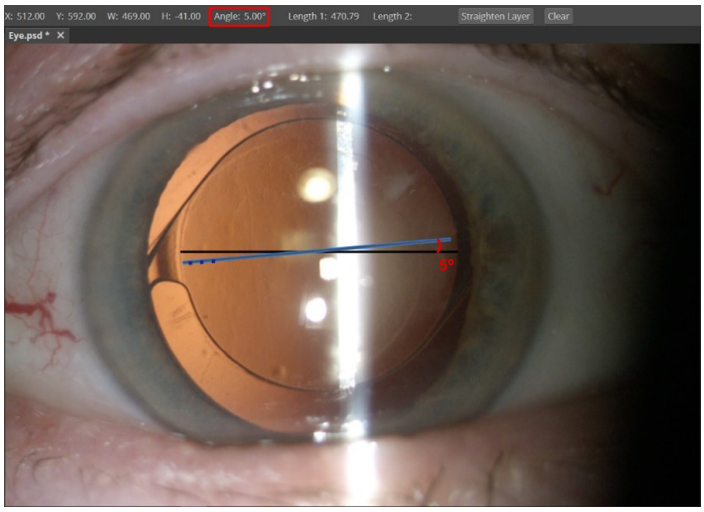

Figure 5.3: IOL orientation of 5° (red rectangle and line), determined by the angle between the flat meridian, from 0° to 180°, (black line) and the IOL indentations (blue dots and blue line).

Considering only measurements with a quality specification of "OK" for the Pentacam, the AL, ACD, and WTW parameters were recorded. Also taken into account was a parameter related to the angle kappa (angle between the visual and the pupil axes), the Chord μ, measured with Pentacam and defined as the "distance between the pupil centre and vertex normal (first Purkinje image)"[3].

Corneal astigmatism from five different measurement modalities was obtained regarding the rotating Scheimpflug camera case:

- Keratometry: calculated as the power difference between the steep and the flatt corneal meridians from keratometric measurements.
- TCRP 3.0 mm P/Z: calculates TCA centered on the pupil and covering a 3.0 mm zone.
- TCRP 3.0 mm A/Z: calculates TCA centered on the apex and covering a 3.0 mm zone.
- TCRP 4.0 mm P/Z: calculates TCA from a 4.0 mm zone and centered on the pupil.
- PCA: a negative power calculated as the power difference of the steepest and the flattest meridians.

As the Aladdin Placido disc corneal topographer only measures the keratometry, solely KA was considered. According to the first pre-operative KA measurement taken with Pentacam, the cases were divided into three subgroups based on the steep meridian: WTR (60° to 120°), ATR (0° to 30° and 150° to 180°), and Oblique (31° to 59° and 121° to 149°). 54 cases were WTR, 31 ATR, and 15 Oblique. For the corneal astigmatism modalities from both devices, except Pentacam's PCA, three sets of measurements were considered: only the first pre-operative measurement, the average of the three pre-operative measurements, and the average of the three post-operative measurements. Hereinafter, measurement modalities refer to Pentacam's KA, TCRP 3.0 mm P/Z, TCRP 3.0 mm A/Z and TCRP 4.0 mm P/Z, as well as Aladdin's KA, while measurement types refer to the average of three pre-operative measurements, only one pre-operative measurement, and the average of three post-operative measurements.

[3]Oculus: FAQ. `https://www.pentacam.com/int/faqs-1.html`. Accessed: 2021-09-20.

Error in refractive astigmatism calculation

The analysis of astigmatism power was carried out applying Næser's polar value method [20]. The astigmatism magnitude and axis (M @ α), in a plus cylinder format, were transformed into two polar components, the net meridional power along a reference meridian ϕ, by equation (5.1), and the net torsional power over the meridian ϕ, by equation (5.2).

$$\begin{aligned} Polar\ value\ along\ the\ meridian\ \phi = Net\ meridional\ power\ along\ \phi = \\ = KP(\phi) = M \times \cos(2 \times (\alpha - \phi)) \end{aligned} \tag{5.1}$$

$$\begin{aligned} Polar\ value\ along\ the\ meridian\ (\phi + 45) = Net\ torsional\ power\ over\ \phi = \\ = KP(\phi + 45) = M \times \sin(2 \times (\alpha - \phi)) \end{aligned} \tag{5.2}$$

These components can be reconverted into the net astigmatism format, by equations (5.3) and (5.4).

$$M = \sqrt{KP(\phi)^2 + KP(\phi + 45)^2} \tag{5.3}$$

$$\alpha = \arctan\left(\frac{M - KP(\phi)}{KP(\phi + 45)}\right) + \phi \tag{5.4}$$

Using equations (5.1) and (5.2), the error in refractive astigmatism (ERA) was calculated at the corneal plane following three main steps, schematically represented in Figure 5.4:

1. The target corneal astigmatism (TCAst) was calculated by vector summation of the KA or TCA and the calculated SICA. For each pre-operative astigmatism subgroup, a mean SICA value was considered, calculated as the difference between the post- and the pre-operative KA/TCA. Since this method enables the choice of a variable or fixed reference meridian, namely in SICA calculations, here a zero-reference meridian ($\phi = 0°$) was chosen, once the incisions were temporal and along the horizontal meridian [82].
2. The target refractive astigmatism (TRA) was obtained by summation of the calculated TCAst and the IOL astigmatism (IA), having as the reference meridian the steepest measured meridian. The calculation of the corresponding IOL toricity at the corneal plane was based on the relation between the AL and corneal power described by Savini [53] and the Fam's and Lim's meridional analysis [77], and considering the recorded IOL orientation.
3. The ERA was then obtained by the vector difference between the post-operative refraction astigmatism (RA) at the corneal plane and the TRA. Considering a V of 12.0 mm, the post-operative recorded manifest residual astigmatism was converted into a cross-cylinder format — with two cylinders, $C_1 = S + C$ and $C_2 = C$, where C_1 and C_2 represent the cylinders — and then transformed from the spectacle plane into the corneal plane, through the following equation:

$$REF_C = \frac{REF_V}{1 - \frac{REF_V \times V}{1000}} \tag{5.5}$$

where REF_C and REF_V are the refraction at the corneal and the vertex plane, respectively [72].

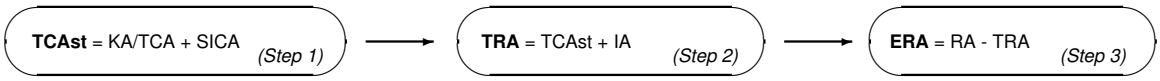

Figure 5.4: Error in refractive astigmatism calculation steps.

Statistical analysis

Statistical analysis was performed using the Python 3.7 (Anaconda) statistical functions module (spicy.stats). To assess if a sample followed a normal or Gaussian distribution, the Shapiro-Wilk statistical test was performed (see Chapter 4 — section 4.1). Two paired samples were compared regarding statistical differences, using paired t-tests when normally distributed, and Wilcoxon signed-rank test when not normally distributed (see Chapter 4 — section 4.2). When comparing three or more normal-distributed and paired samples, repeated measures analysis of variance (ANOVA) was used, and the Friedman non-parametric test for the case where the paired samples did not follow a Gaussian distribution. The ANOVA assumes that data follow a normal distribution, for which H_0 states that the means of the in-test-groups are the same, whereas H_a that these are different. The Friedman test makes no assumption regarding the data distribution, with a H_0 that the samples have the same distribution and H_a when different [75]. For all statistical tests a p-value of less than 0.05 was considered significant.

5.2.2 Measurement comparisons

For each measurement modality the mean$\pm$SD ERA meridional and torsional polar values were determined. Additionally, for the ERA net astigmatism magnitude, the MAE$\pm$SD, calculated by equation (5.3), the median, and the percentage of eyes with an ERA magnitude equal or lower than 0.50 D were obtained. The p-values for the comparison of the ERA KP(ϕ), KP(ϕ+45), and M between the different measurement types, for each modality, were also calculated. In Tables 5.3, 5.4, and 5.5, these parameters are displayed for each astigmatism subgroup: WTR, ATR and Oblique. For the three pre- and post-operative measurements, for each modality, the difference between each one of the astigmatism measurements concerning the mean value of the three measurements was calculated being organized in Table C.2 in Appendix C, section C.2, and lies between 0.10 - 0.15 D. The SICA net astigmatism values for each case of each subgroup are presented in Table C.3 in Appendix C, section C.2, being mainly between 0.10 - 0.20 D along a vertical oriented meridian.

An overall over-correction (negative ERA KP(ϕ) values) was found for the WTR, while an under-correction (positive ERA KP(ϕ) values) for the ATR case, regarding all measurements of all modalities. The Oblique subgroup also showed an over-correction, except for the one pre-operative measurement of the TCRP 3.0- and 4.0 mm P/Z modalities. Within each measurement modality, between the three different measurement types, no statistically significant differences were found regarding the ERA meridional and torsional polar values, and the ERA magnitude.

Table 5.3: ERA meridional, torsional, and magnitude components, in D, when considering SICA for the WTR subgroup. The p-values refer to the differences between measurement types.

	ERA KP(ϕ) (D)		**ERA KP(ϕ+45) (D)**		**ERA Net Astigmatism M (D)**			
WTR (n=54)	Mean±SD	p-value	Mean±SD	p-value	Median	MAE±SD	p-value	% ≤0.50 D
KA (Pentacam)								
Average 3 preop	-0.53±0.41		-0.10±0.32		0.62	0.67±0.33		33.33
1 preop	-0.54*±0.48	0.6294	-0.10±0.31	0.9375	0.58	0.67±0.41	0.7860	44.44
Average 3 postop	-0.54±0.40		-0.11±0.31		0.67	0.67±0.33		31.48
KA (Aladdin)								
Average 3 preop	-0.52±0.41		-0.15±0.33		0.57	0.64±0.39		42.59
1 preop	-0.52*±0.43	0.7860	-0.13±0.37	0.9610	0.57	0.67±0.41	0.7034	38.89
Average 3 postop	-0.52±0.34		-0.17±0.34		0.64	0.65±0.34		35.19
TCRP 3.0 mm P/Z								
Average 3 preop	-0.15*±0.42		-0.07±0.35		0.45	0.49±0.28		59.26
1 preop	-0.17*±0.46	0.4857	-0.06±0.35	0.9945	0.46	0.52±0.31	0.1145	59.26
Average 3 postop	-0.21±0.39		-0.11±0.36		0.47	0.52±0.27		57.41
TCRP 3.0 mm A/Z								
Average 3 preop	-0.36±0.40		-0.08±0.34		0.46	0.55±0.33		51.85
1 preop	-0.38±0.51	0.7953	-0.09±0.32	0.9645	0.50	0.59±0.41	0.4111	50.00
Average 3 postop	-0.39±0.36		-0.11±0.35		0.50	0.56±0.30		50.00
TCRP 4.0 mm P/Z								
Average 3 preop	-0.27*±0.36		-0.07±0.35		0.48	0.51±0.25		55.56
1 preop	-0.30±0.43	0.3231	-0.07±0.34	0.9332	0.51	0.54±0.31	0.9286	50.00
Average 3 postop	-0.32±0.38		-0.09±0.35		0.47	0.53±0.30		53.70

$A/Z =$ Apex Zone; $MAE =$ Mean Absolute Error; $P/Z =$ Pupil Zone; $\% \leq 0.50\ D =$ Percentage of eyes with an absolute error within 0.50 D; *Shapiro-Wilk test with $p < 0.05$ (Non normal distribution)

Table 5.4: ERA meridional, torsional, and magnitude components, in D, when considering SICA for the ATR subgroup. The p-values refer to the differences between measurement types.

	ERA KP(ϕ) (D)		**ERA KP(ϕ+45) (D)**		**ERA Net Astigmatism M (D)**			
ATR (n=31)	Mean±SD	p-value	Mean±SD	p-value	Median	MAE±SD	p-value	% ≤0.50 D
KA (Pentacam)								
Average 3 preop	0.32±0.31		-0.08±0.50		0.64	0.60±0.28		38.71
1 preop	0.32±0.32	0.6210	-0.10±0.54	0.9801	0.69	0.65±0.28	0.7892	29.03
Average 3 postop	0.26±0.27		-0.11±0.56		0.59	0.59±0.33		41.94
KA (Aladdin)								
Average 3 preop	0.24±0.34		-0.03*±0.49		0.52	0.55±0.32		48.39
1 preop	0.25±0.36	0.8983	-0.11*±0.49	0.066	0.54	0.57±0.34	0.6790	45.16
Average 3 postop	0.21±0.34		0.03*±0.47		0.48	0.52±0.32		51.61
TCRP 3.0 mm P/Z								
Average 3 preop	0.22±0.39		-0.04±0.48		0.59	0.59±0.27		38.71
1 preop	0.15±0.46	0.4843	-0.11±0.56	0.8766	0.66	0.65±0.34	0.4274	35.48
Average 3 postop	0.10±0.32		-0.08±0.53		0.52	0.55±0.28		48.39
TCRP 3.0 mm A/Z								
Average 3 preop	0.08±0.37		-0.05±0.48		0.52	0.55±0.25		45.16
1 preop	0.06±0.36	0.7441	-0.08±0.55	0.8202	0.55	0.60±0.27	0.7233	41.94
Average 3 postop	0.01±0.35		-0.13±0.51		0.53	0.55±0.29		45.16
TCRP 4.0 mm P/Z								
Average 3 preop	0.23±0.35		-0.03±0.48		0.54	0.57±0.27		48.39
1 preop	0.20±0.42	0.4715	-0.06±0.52	0.9719	0.66	0.61±0.32	0.6449	41.94
Average 3 postop	0.12±0.33		-0.06±0.52		0.53	0.54±0.31		48.39

$A/Z =$ Apex Zone; $MAE =$ Mean Absolute Error; $P/Z =$ Pupil Zone; $\% \leq 0.50\ D =$ Percentage of eyes with an absolute error within 0.50 D; *Shapiro-Wilk test with $p < 0.05$ (Non normal distribution)

Table 5.5: ERA meridional, torsional, and magnitude components, in D, when considering SICA for the Oblique subgroup. The p-values refer to the differences between measurement types.

	ERA KP(ϕ) (D)		**ERA KP(ϕ+45) (D)**		**ERA Net Astigmatism M (D)**			
Oblique (n=15)	Mean±SD	p-value	Mean±SD	p-value	Median	MAE±SD	p-value	% ≤0.50 D
KA (Pentacam)								
Average 3 preop	-0.15±0.44		-0.01±0.58		0.61	0.62±0.32		33.33
1 preop	-0.20±0.38	0.7971	-0.05±0.69	0.8704	0.72	0.70±0.38	0.8597	26.67
Average 3 postop	-0.09±0.50		-0.13±0.67		0.68	0.72±0.42		20.00
KA (Aladdin)								
Average 3 preop	-0.16±0.45		-0.19±0.41		0.51	0.57±0.28		46.67
1 preop	-0.23*±0.76	0.5488	-0.11±0.54	0.9190	0.53	0.75±0.58	0.2818	46.67
Average 3 postop	-0.12±0.48		-0.14±0.49		0.53	0.61±0.31		33.33
TCRP 3.0 mm P/Z								
Average 3 preop	-0.02±0.52		-0.06*±0.46		0.49	0.57±0.38		53.33
1 preop	0.05±0.44	0.6303	-0.14±0.52	0.9355	0.56	0.58±0.34	0.9848	40.00
Average 3 postop	-0.11±0.41		-0.16±0.54		0.60	0.59±0.34		46.67
TCRP 3.0 mm A/Z								
Average 3 preop	-0.24*±0.55		-0.04±0.49		0.48	0.64±0.42		53.33
1 preop	-0.23±0.41	0.6271	-0.12±0.60	0.9101	0.58	0.66±0.36	0.4203	46.67
Average 3 postop	-0.19±0.42		-0.12±0.56		0.58	0.63±0.34		33.33
TCRP 4.0 mm P/Z								
Average 3 preop	-0.04±0.45		-0.19*±0.41		0.51	0.50±0.36		46.67
1 preop	0.01±0.37	0.9216	-0.12±0.45	0.3441	0.36	0.48±0.33	0.2818	66.67
Average 3 postop	-0.05±0.38		-0.16±0.51		0.40	0.53±0.36		53.33

$A/Z =$ Apex Zone; $MAE =$ Mean Absolute Error; $P/Z =$ Pupil Zone; $\% \leq 0.50\ D =$ Percentage of eyes with an absolute error within 0.50 D; *Shapiro-Wilk test with $p < 0.05$ (Non normal distribution)

In the WTR subgroup, when comparing the five measurement modalities for each measurement type, statistical differences (p<0.001) were found, for all cases, regarding the meridional ERA component. A further modality comparison on a one-to-one level, within each measurement type, showed also statistical differences for all cases, except between the Pentacam's and Aladdin's KA. The TCRP cases had a lower mean meridional value compared to the KA cases, which can be depicted in Figure 5.5 (a) for the centroid position along the $xx-$axis compared for the Pentacam KA and TCRP 3.0 mm P/Z. By comparison of the TCRP cases, the TCRP 3.0 mm P/Z modality presented the lowest mean value for all measurement types, followed by the TCRP 4.0 mm P/Z and TCRP 3.0 mm A/Z. As regards the torsional component, no statistical differences between modalities were found for each type of measurement. The Wilcoxon signed-rank test revealed no statistical differences between the ERA magnitudes for the KA of both devices, as well as for the TCRP cases between the 3.0 mm pupil and apex centered modalities, and TCRP 3.0 mm A/Z and TCRP 4.0 mm P/Z. For the remaining cases where statistical differences were found, the mean magnitudes KA are higher than the TCRP cases. All TCRP modalities provided a higher percentage of eyes with an ERA equal or lower than 0.50 D than the KA modalities, and, in most cases, the average of three post-operative measurements had the lowest percentage associated within modalities. The highest percentage of eyes with an error equal or lower than 0.50 D was for both, the average of three and for only one pre-operative measurements, in the TCRP 3.0 mm P/Z modality (59.26%).

The ATR meridional ERA component differed statistically between all five modalities for each measurement type. When comparing this component under the five measurement modalities, the mean values of the TCRP cases covering a 3.0 mm zone were, for all three measurement types, statistically lower than the Pentacam KA — centroid position along the $xx-$axis, in Figure 5.5 (b). Also, the TCRP 3.0 mm A/Z and 4.0 mm P/Z differed, namely the first was lower than the latter one. No statistical differences were found when comparing simultaneously all five measurement modalities and when comparing these one-to-one, for the ERA torsional polar value and the ERA magnitude. In this subgroup, in general the average of three post-operative measurements had the highest percentage of eyes with an ERA equal or lower than 0.50 D, being the highest all-over achieved value (51.61%) for the Aladdin's KA.

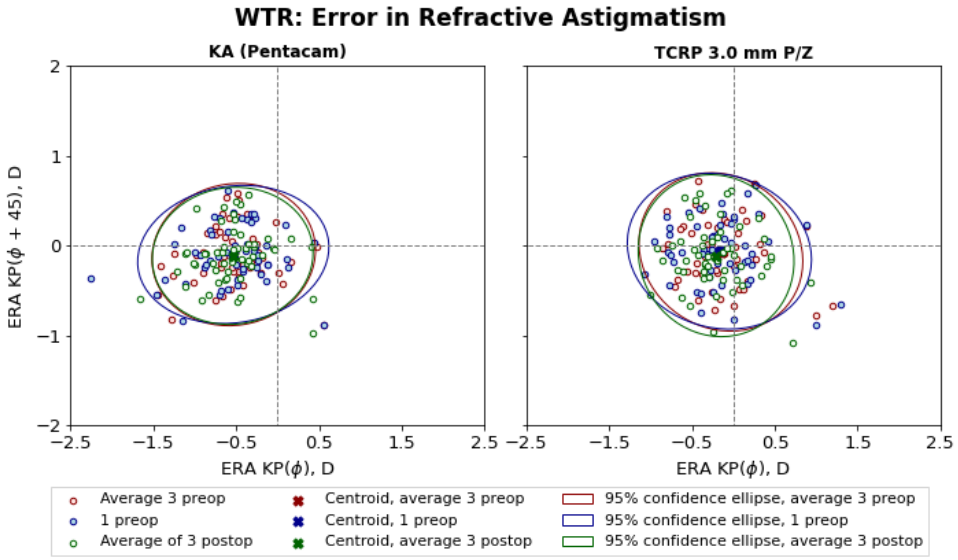

(a) Confidence ellipses for the ERA in the WTR subgroup.

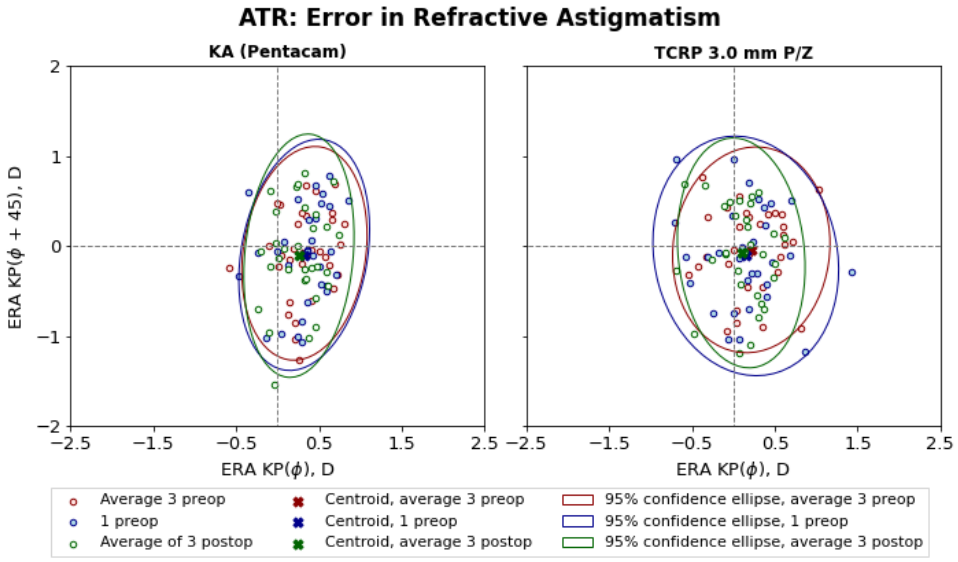

(b) Confidence ellipses for the ERA in the ATR subgroup.

Figure 5.5: Meridional and torsional ERA components displayed by 95% confidence ellipses, depending on their SDs, for the WTR and ATR subgroups regarding the Pentacam KA and TCRP 3.0 mm P/Z cases.

For the Oblique case, statistical differences within the measurement modalities were found for the average of three and for one pre-operative measurements, and none for the average of three post-operative measurements. Regarding the mean ERA torsional and magnitude components, no statistical differences were found. The TCRP cases presented a higher percentage of eyes with an ERA $\leq$0.50 D compared to the KA modalities, for which, in most cases, the lowest percentage was for the average of three post-operative measurements.

Through the observation of Figure 5.5 as well as by the analysis of the p-values higher than 0.05 for the comparison in-between measurement types for each measurement modality (Tables 5.3, 5.4 and 5.5), the post-operative measurements do not evidence any advantage compared to the pre-operative ones.

Interesting findings were made when considering the same patients and analyzing the same parameters, but excluding the SICA from the calculations for the pre-operative measurements (result tables for each astigmatism subgroup are presented in Appendix C — section C.3). The mean meridional and magnitude ERA values for the WTR subgroup were, overall, statistically lower when neglecting the SICA. However, when comparing the torsional component, no statistical differences were found for the TCRP cases. For the ATR case, the mean ERA KP(ϕ) was statistically lower without SICA than with SICA; for the ERA KP(ϕ+45) the opposite was found, i.e., when considering SICA the mean values were statistically lower. No statistical differences were found between the ERA magnitude for the TCRP cases, while statistically lower values were found for the KA cases without SICA. Moreover, for both WTR and ATR subgroups, a higher percentage of eyes regarding the ERA magnitude $\leq$0.50 D was found when neglecting SICA, for example, for the average of three pre-operative measurements of the TCRP 3.0 mm P/Z case, the percentage increased from 59.26% to 61.11% for the WTR case and from 38.71% to 58.06% in the ATR subgroup. For the Oblique subgroup, regarding all parameters, no statistical differences were observed.

Discussion

The generally observed over-correction in the WTR subgroup and under-correction in the ATR subgroup is in line with previous studies [47, 52, 65]. The Pentacam TCRP cases have a slightly higher dispersion compared to the KA cases, as shown in Figure 5.5, which is related to the reported lower repeatability of posterior corneal curvature measurements compared to anterior corneal curvature measurements [44]. However, these measurement modalities led to a decrease of the observed over- and under-correction: the centroid in the $xx-$axis is closer to zero when compared to the KA cases, what means that it is more accurate. Furthermore, this decrease is related to the posterior corneal effect of WTR KA compensation, on the one hand, and of the ATR KA adding effect, on the other [47, 49, 50]. When comparing the ERA meridional and torsional components between measurement modalities, the TCRP cases covering a 3.0 mm zone centered on the pupil provided the best outcomes for the WTR case, while the centered on the apex led to the best outcomes for the ATR case, as already found in a previous study [65]. Moreover, the median and mean ERA magnitude are lower for these cases.

Taking the SICA into account, assessing whether the average of three pre-operative measurements rather than only one pre-operative measurement improved refractive outcomes, showed no statistically significant differences even when comparing the pre-operative and post-operative measurements, suggesting no advantage in using the latter ones. Even if not statistically different, for most cases, the highest spread was observed for the one pre-operative measurement case, and the lowest percentage of eyes with an error equal or lower than 0.50 D for the average of three post-operative measurements. No previous studies comparing these measurement types within modalities were found.

Comparing the outcomes under the scope of including or excluding SICA, it was statistically shown that they were significantly better in the SICA excluding cases. Here, the SICA for each measurement type and modality had an averaged value from a patient-specific calculation, for which it is known that SICA has a large variability among patients [47]. Furthermore, for the KA cases, the better outcomes without considering the SICA — in this case with temporal located incisions that induce WTR astigmatism — may be related to the possible non-complete measurement of the posterior corneal astigmatism. Since the posterior cornea is commonly vertically orientated, with a shown reducing effect on the WTR and small ATR KA astigmatisms and increasing influence of the higher ATR KA astigmatism [47, 49, 50], if it's effect is not completely considered whilst the WTR induced astigmatism by SICA is considered, this will lead to higher WTR and small ATR KA astigmatisms, as the reduction effect of the posterior cornea is not fully encountered, while higher ATR KA astigmatisms remain unchanged. As WTR and ATR astigmatisms are mainly associated to the meridional component, they are largely influenced by this effect, whereas the influence is low on the torsional component, along the 45°/135° meridians, related to the Oblique astigmatism.

5.2.3 Optimization methods

For the optimization of the pre-operative corneal astigmatism, KA or TCA, were performed back-calculations to zero-out the meridional ERA component. The IOL toricity and SICA were subtracted from the subjective refraction. Here, the SICA was included, since it is clinically relevant. In addition, the focus was set on the one pre-operative measurement for the several modalities, that is the most feasible in a clinical environment. In a preliminary study employing the machine learning (ML) concept, different sets of parameters were studied regarding their influence on the optimization process, using different linear and non-linear estimators. Besides the measured corneal astigmatism and direction, the parameters included and their respective mean$\pm$SD (and range) values, in mm, were: AL, 24.13$\pm$1.47 (20.14, 28.30); ACD, 3.12$\pm$0.39 (2.09, 4.02); WTW, 11.68$\pm$0.41 (10.60, 12.60); and Chord μ, 0.25$\pm$0.15 (0.01, 0.72).

Machine learning has gained increasing attention in the ophthalmology field during the last decades, including IOL power calculations [83]. The ML generic idea settles on a learning problem, where data with given criteria is fed (training sample) and through analysis an underlying trend is searched, that will be used to predict and improve the outcome for new similar data (test sample). In particular, supervised learning is one of the ML-categories that aims "to predict the value of an outcome measure based on a

number of input measures". If the outcome is quantitative it is termed regression [84].

In this work, supervised learning was carried out by using estimators from the scikit-learn library in Python 3.7 (Anaconda) for the comparison of possible optimization methods. The choice of the estimators to use according to the data type and volume, and the problem in question, was based on the suggested flowchart in the scikit-learn library[4]. In this context, since the output is a quantitative prediction and, therefore, considered as a regression problem, and given the small volume of data, the chosen estimators were: Multiple Linear Regression (Linear), Linear Support Vector Regression (SVR), K-Nearest Neighbor (KNN), Random Forest (RF), and Gradient Boosting (GB). A summarized explanation of the underlying mechanism of each used estimator is as follows:

1. **Multiple Linear Regression:** it fits a linear model between the observed values, or dependent variables, y, and the features or independent variable, x, with coefficients $w = (w_1, ..., w_p)$ and intercept w_0, of the formula (5.6).The minimization criterion, (5.7), regards the residual sum of squares between the observed and the predicted values, $\widehat{y}$[5].

$$\widehat{y}(w, x) = w_0 + w_1 x_1 + ... + w_p x_p \tag{5.6}$$

$$Minimization\ Criterion : \min_{w} \|Xw - y\|_2^2 \tag{5.7}$$

2. **Linear Support Vector Regression:** it constructs a hyper-plane, that separates the points of the training vector (x) in two classes. The separation maximizes the distance to the nearest points of both classes, i.e. the margins, aiming to decrease the generalization error. The minimization concerns the coefficients, w, along possible deviations, ξ, (5.8), with the margins constrained by the maximum error, ϵ, and deviations, (5.9)[5] [84].

$$Minimization\ Criterion : \min \frac{1}{2}\|w\|^2 + C\sum_{i=1}^{n} |\xi_i| \tag{5.8}$$

$$|y_i - w_i x_i| \leq \epsilon + |\xi_i| \tag{5.9}$$

3. **K-Nearest Neighbors:** it uses feature similarity. The distance between the new value and the training points is calculated by the Eucledian distance (square-root of the sum of the quadratic differences between the points). The k nearest points are averaged, resulting in the predicted value[5] [84].

4. **Random Forest:** it uses an ensemble of individual regression Decision Trees (see Appendix C, section C.4). Out of the training sample, random samples are drawn with replacement, i.e. bootstrap samples, and separately fit with a regression Decision Tree, increasing hereby the randomness, since one point can be present in more than one sample. The outcome prediction is the average of the sum of the predictions of each Decision Tree[5] [84, 85].

5. **Gradient Boosting:** it uses a sequence of regression Decision Trees (see Appendix C, section C.4), in an additive matter, (5.10) — the latest ensemble, $F_m(x)$, is based on the new added tree,

[4]Choosing the right estimator. `https://scikit-learn.org/stable/tutorial/machine_learning_map/index.html`. Accessed: 2021-09-25.

[5]1. Supervisied learning. `https://scikit-learn.org/stable/supervised_learning.html`. Accessed: 2021-09-25.

$h_m(x)$, and the previous ensemble of trees, $F_{m-1}(x)$. The fitting of the new tree is such that it minimizes the sum of losses, that in regression usually corresponds to the Mean Squared Error (MSE, i.e., mean of the squared errors as the difference between the observed and predicted values), by taking into account the previous ensemble. The outcome prediction is the sum of the predictions of all models[5] [84, 86].

$$F_m(x) = F_{m-1}(x) + h_m(x) \tag{5.10}$$

Three other estimators were used — Ridge Regression, Polynomial Regression, and Decision Trees — that although not presented here, they are briefly described in Appendix C, section C.4.1.

Considering the whole sample, without subgroup distinction, all estimators were used in a three-step based approach: step 1, using the whole sample for both, training and testing, termed Training; step 2, a k-fold cross-validation, to predict the estimators performance when unknown data is used for testing purposes, where the sample is split into k smaller sets, for which the estimator models are fitted and the performance is evaluated, being the total performance the average of the k-fold performances, termed Cross-validation; step 3, using this sample for training and testing with another independent sample, termed Testing. The MAE and R^2 for the estimators were calculated using the metrics module of scikit-learn library. Also, the ERA was calculated for the predicted optimized corneal astigmatism, given the combination of the measured corneal astigmatism and direction with the other parameters (AL, ACD, WTW, Chord μ) and statistical analyses were performed to compare the outcomes of the different estimators (see Chapter 4 — sections 4.1 and 4.2).

Step 1: Training

Focusing on the KA (Pentacam) and TCRP 3.0 mm P/Z, clinically most often used (the remaining measurement modalities cases are presented in Appendix C, section C.4), the MAE and R^2 for each estimator and parameter combinations are listed in Tables 5.6 and 5.7, respectively.

For both cases, the MAE appears to register an overall decrease for all estimators, when taking into account more parameters than only the measured astigmatism components. This suggests that, by considering more parameters, and even when all six are considered, the difference between the predicted and observed values decreases, however, these parameters have lower values for the non-linear estimators, when compared to the linear estimators. Regarding the R^2, it has, overall, higher values for the KA case than for the TCRP case, but for both cases it increases with the number of parameters considered, and is higher for the non-linear estimators, namely the GB estimator that reaches a value of 0.994. Observable is that, on the one hand, the Linear and Linear SVR estimators have similar metrics and, on the other hand, also the RF and GB estimators. The KNN estimator is an exception, since a MAE increase and a R^2 decrease are noted for both cases, when more parameters are taken into account. The metrics are better in the KA case, which can be related to the lower spread, that was already mentioned.

Table 5.6: MAE and R^2 for each estimator and each parameter set, for the KA (Pentacam) in the Training stage.

	Estimators				
Parameters	Linear	SVR	KNN	RF	GB
CA, cos(2α)					
MAE	0.267	0.264	0.236	0.125	0.089
R^2	0.865	0.862	0.874	0.964	0.984
CA, cos(2α), AL, ACD, WTW					
MAE	0.267	0.263	0.260	0.128	0.070
R^2	0.871	0.862	0.851	0.965	0.991
CA, cos(2α), Chord μ					
MAE	0.266	0.264	0.277	0.139	0.063
R^2	0.872	0.866	0.845	0.953	0.992
All					
MAE	0.259	0.260	0.280	0.130	0.057
R^2	0.877	0.871	0.848	0.961	0.994

$CA =$ Corneal astigmatism; $GB =$ Gradient Boosting; $KNN =$ K-Nearest Neighbors; $MAE =$ Mean Absolute Error; $RF =$ Random Forest; $SVR =$ Support Vector Regression; $\alpha =$ Measured astigmatism direction

Table 5.7: MAE and R^2 for each estimator and each parameter set, for the TCRP 3.0 mm P/Z in the Training stage.

	Estimators				
Parameters	Linear	SVR	KNN	RF	GB
CA, cos(2α)					
MAE	0.340	0.338	0.291	0.146	0.122
R^2	0.767	0.766	0.833	0.955	0.968
CA, cos(2α), AL, ACD, WTW					
MAE	0.333	0.325	0.306	0.139	0.070
R^2	0.791	0.786	0.818	0.960	0.990
CA, cos(2α), Chord μ					
MAE	0.333	0.325	0.333	0.150	0.083
R^2	0.805	0.795	0.791	0.951	0.987
All					
MAE	0.331	0.324	0.321	0.139	0.062
R^2	0.811	0.802	0.818	0.956	0.992

$CA =$ Corneal astigmatism; $GB =$ Gradient Boosting; $KNN =$ K-Nearest Neighbors; $MAE =$ Mean Absolute Error; $RF =$ Random Forest; $SVR =$ Support Vector Regression; $\alpha =$ Measured astigmatism direction

The ERA optimized meridional component and resulting ERA net astigmatism magnitude, as well as the median absolute ERA and the percentage of eyes with an ERA equal or lower than 0.50 D are presented in Tables 5.8 and 5.9 for the KA and TCRP cases, respectively. It should be noted, that, here, when referring to ERA net astigmatism magnitude, it corresponds to the conversion from the mean ERA KP(ϕ) and KP(ϕ+45) by equation (5.3), with the SD referring to the total variance as the sum of the ERA KP(ϕ) and KP(ϕ+45) variances. For the non-optimized situation, the mean$\pm$SD values, in D, for the meridional, torsional, and magnitude ERA components were: for the KA case, -0.22$\pm$0.56, -0.09$\pm$0.46, 0.24$\pm$0.73; and for the TCRP case, -0.04$\pm$0.47, -0.09$\pm$0.45, 0.10$\pm$0.65. Also, it should be noted that the best achievable values in this step are limited by the back-calculated outcomes, which respects only the meridional component, namely a mean$\pm$SD zero meridional ERA and a percentage of 76% eyes with an ERA $\leq$0.50 D for both cases. The torsional ERA is not optimized by back-calculations, therefore

remaining unchanged between non-optimized and optimized. For the KA case, taking into account the Pentacam measured PCA, the net astigmatism was calculated using the Barrett Toric Calculator[6]. The correspondent mean±SD values, in D, for the ERA KP(ϕ) and KP(ϕ+45) components, and the magnitude ERA were calculated, being the results, respectively: 0.12±0.40, -0.11±0.47, and 0.16±0.61. The median absolute ERA and percentage of eyes within 0.50 D were 0.52 D and 50%.

Table 5.8: ERA meridional, torsional, and net astigmatism magnitude components, in D, for the optimized KA (Pentacam) by the several estimators for the different parameter sets, in the Training stage.

	Estimators				
Parameters	Linear	SVR	KNN	RF	GB
CA, cos(2α)					
Mean±SD: ERA KP(ϕ)	0.00±0.35	-0.04±0.35	0.01±0.34	0.01±0.18	0.00±0.12
Mean±SD: ERA M	0.09±0.58	0.10±0.58	0.09±0.57	0.09±0.49	0.09±0.47
Median ERA	0.41	0.41	0.42	0.34	0.31
% Eyes ERA M $\leq$0.50 D	59.00	61.00	64.00	71.00	75.00
CA, cos(2α), AL, ACD, WTW					
Mean±SD: ERA KP(ϕ)	0.00±0.35	-0.04±0.35	0.03±0.37	0.00±0.18	0.00±0.09
Mean±SD: ERA M	0.09±0.57	0.10±0.58	0.10±0.59	0.09±0.49	0.09±0.47
Median ERA	0.41	0.41	0.42	0.33	0.31
% Eyes $\leq$0.50 D	60.00	61.00	58.00	72.00	75.00
CA, cos(2α), Chord μ					
Mean±SD: ERA KP(ϕ)	0.00±0.34	-0.05±0.35	0.03±0.37	-0.01±0.21	0.00±0.08
Mean±SD: ERA M	0.09±0.57	0.10±0.57	0.10±0.59	0.09±0.50	0.09±0.46
Median ERA	0.41	0.44	0.45	0.34	0.31
% Eyes $\leq$0.50 D	60.00	59.00	56.00	71.00	75.00
All					
Mean±SD: ERA KP(ϕ)	0.00±0.33	-0.05±0.34	0.04±0.37	0.00±0.19	0.00±0.08
Mean±SD: ERA M	0.09±0.57	0.10±0.57	0.10±0.59	0.09±0.49	0.09±0.46
Median ERA	0.45	0.44	0.45	0.33	0.31
% Eyes $\leq$0.50 D	58.00	59.00	57.00	71.00	75.00

$CA =$ Corneal astigmatism; $GB =$ Gradient Boosting; $KNN =$ K-Nearest Neighbors; $RF =$ Random Forest; $SVR =$ Support Vector Regression; $\alpha =$ Measured astigmatism direction; $\%\ Eyes\ \leq 0.50\ D =$ Percentage of eyes with an absolute error within 0.50 D

[6]Barrett Toric Calculator (Version 2.0). `https://ascrs.org/tools/barrett-toric-calculator`. Accessed: 2021-10-25.

Table 5.9: ERA meridional, torsional, and net astigmatism magnitude components, in D, for the optimized TCRP 3.0 mm P/Z by the several estimators for the different parameter sets, in the Training stage.

	Estimators				
Parameters	Linear	SVR	KNN	RF	GB
CA, cos(2α)					
Mean±SD: ERA KP(ϕ)	0.00±0.45	0.01±0.45	0.01±0.38	-0.01±0.20	0.00±0.17
Mean±SD: ERA M	0.09±0.64	0.09±0.64	0.09±0.59	0.09±0.49	0.09±0.48
Median ERA	0.51	0.50	0.45	0.36	0.34
% Eyes $\leq$0.50 D	50.00	51.00	57.00	68.00	75.00
CA, cos(2α), AL, ACD, WTW					
Mean±SD: ERA KP(ϕ)	0.00±0.43	-0.01±0.43	0.07±0.39	-0.01±0.19	0.00±0.09
Mean±SD: ERA M	0.09±0.62	0.09±0.62	0.11±0.60	0.09±0.49	0.09±0.46
Median ERA	0.52	0.52	0.45	0.35	0.31
% Eyes $\leq$0.50 D	49.00	47.00	59.00	71.00	75.00
CA, cos(2α), Chord μ					
Mean±SD: ERA KP(ϕ)	0.00±0.41	-0.02±0.42	0.07±0.42	0.01±0.21	0.00±0.11
Mean±SD: ERA M	0.09±0.61	0.09±0.62	0.12±0.62	0.09±0.49	0.09±0.46
Median ERA	0.50	0.51	0.45	0.36	0.31
% Eyes $\leq$0.50 D	51.00	50.00	56.00	68.00	75.00
All					
Mean±SD: ERA KP(ϕ)	0.00±0.41	-0.01±0.42	0.06±0.40	-0.01±0.20	0.00±0.08
Mean±SD: ERA M	0.09±0.61	0.09±0.61	0.11±0.60	0.09±0.49	0.09±0.45
Median ERA	0.50	0.50	0.46	0.35	0.30
% Eyes $\leq$0.50 D	54.00	52.00	56.00	70.00	75.00

$CA =$ Corneal astigmatism; $GB =$ Gradient Boosting; $KNN =$ K-Nearest Neighbors; $RF =$ Random Forest; $SVR =$ Support Vector Regression; $\alpha =$ Measured astigmatism direction; $\%\ Eyes\ \leq 0.50\ D =$ Percentage of eyes with an absolute error within 0.50 D

For both KA and TCRP cases, overall, the mean meridional ERA is around zero for the considered estimators, however, the SD is lower for the tree-based estimators, decreasing when more parameters are considered. Regarding the ERA net astigmatism magnitude, a common value of 0.09 D is observable, as it is related to the mean zero meridional component with the constant torsional component. The percentages of eyes with an ERA magnitude equal or lower than 0.50 D, compared to the 76% maximum achievable, are all above 50% for the KA case, and above 47% for the TCRP case. These are higher for the tree-based estimators, remarkably for the GB estimator that achieves a percentage of 75%.

Through statistical analysis, in the KA cases the mean ERA KP(ϕ) and magnitude components were lower compared to the non-optimized case ($p<0.05$ and $p<0.001$ for the meridional and magnitude components). When comparing the optimization estimators with the Barrett Toric Calculator case, the optimized mean ERA meridional components were lower ($p<0.05$) and, overall, for the ERA magnitude no statistical differences were found for the linear estimators; however, statistically lower mean values were found for the RF and GB cases. The linear estimators had as well higher values compared to these two estimators. In general, regarding the mean meridional and magnitude ERA, no statistical differences were found when comparing the different parameter sets for the same estimator.

For the TCRP case, the mean meridional ERA values, overall, did not differ from the non-optimized ERA case, solely for the linear estimators, that had a lower mean value, when only the astigmatism measured parameters were considered. In the comparison of the mean ERA magnitude values, across all

parameter sets the optimization estimators presented lower mean values compared to the non-optimized case, with statistically lower values for the tree-based estimators, standing out the GB case. The KNN estimator was the exception, presenting a higher mean ERA meridional value, and not differing from the non-optimized case with respect to the ERA magnitude.

In Figures 5.6 and 5.7 are presented for the KA and TCRP cases, respectively, the ERA meridional and torsional components with 95% confidence ellipses for two linear estimators — Linear and Linear SVR —, the KNN estimator, and two tree-based estimators — RF and GB.

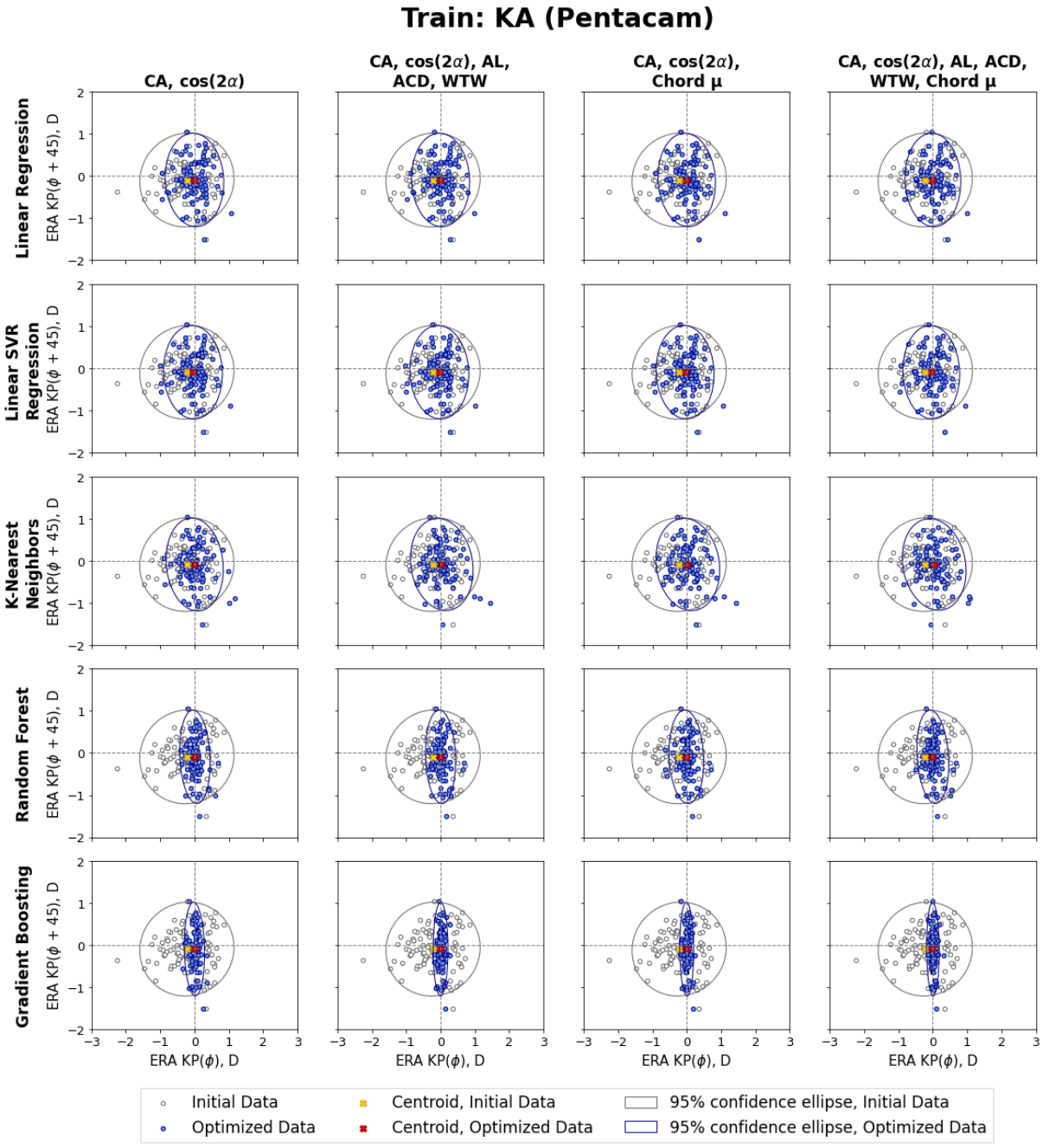

Figure 5.6: Meridional and torsional ERA components displayed by 95% confidence ellipses, for the optimized KA (Pentacam) by estimators compared to the initial data, for each set of parameters, in the Training stage.

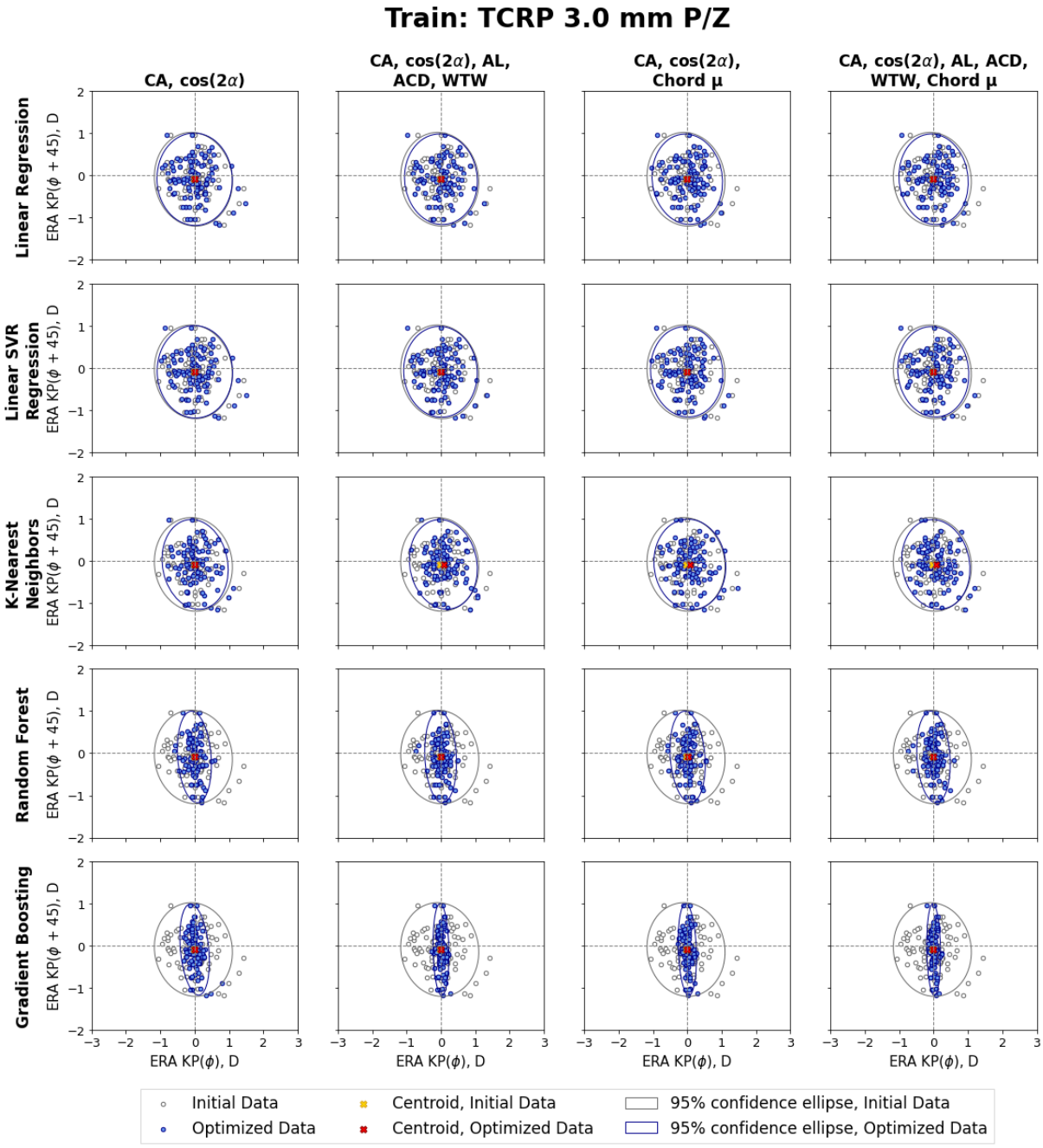

Figure 5.7: Meridional and torsional ERA components displayed by 95% confidence ellipses, for the optimized TCRP 3.0 mm P/Z by estimators compared to the initial data, for each set of parameters, in the Training stage.

The centroid is approximately zero for all cases, and the ellipses narrow towards zero along the $xx-$ axis, when considering more parameters, being less pronounced for the linear and KNN estimators. Regarding the ellipse axes along the horizontal component, they are lower for the three-based estimators, therefore showing lower variance and higher precision when compared to the linear estimators. A higher spread is visible for the TCRP case when compared to the KA case, namely for the linear estimators.

Step 2: Cross-validation

The number of splits was set to 5, thereby each fold had 80% for training and 20% for testing, randomly chosen. Tables 5.10 and 5.11 present the scores — R^2 and SD — for the several estimators regarding each set of parameters, for the KA and TCRP cases, respectively.

Table 5.10: Cross-validation estimators scores (R^2) and SD, for the KA (Pentacam).

	Estimators				
Parameters	Linear	SVR	KNN	RF	GB
CA, cos(2α)					
R^2	0.834	0.831	0.747	0.737	0.674
SD	0.038	0.046	0.144	0.105	0.255
CA, cos(2α), AL, ACD, WTW					
R^2	0.824	0.819	0.627	0.721	0.677
SD	0.049	0.055	0.349	0.139	0.263
CA, cos(2α), Chord μ					
R^2	0.833	0.836	0.631	0.732	0.715
SD	0.036	0.040	0.311	0.074	0.152
All					
R^2	0.828	0.822	0.613	0.718	0.725
SD	0.050	0.062	0.326	0.126	0.179

$CA =$ Corneal astigmatism; $GB =$ Gradient Boosting; $KNN =$ K-Nearest Neighbors; $RF =$ Random Forest; $SVR =$ Support Vector Regression; $\alpha =$ Measured astigmatism direction

Table 5.11: Cross-validation estimators scores (R^2) and SD, for the TCRP 3.0 mm P/Z.

	Estimators				
Parameters	Linear	SVR	KNN	RF	GB
CA, cos(2α)					
R^2	0.705	0.710	0.647	0.627	0.638
SD	0.104	0.103	0.167	0.142	0.147
CA, cos(2α), AL, ACD, WTW					
R^2	0.713	0.721	0.610	0.665	0.618
SD	0.096	0.080	0.230	0.124	0.210
CA, cos(2α), Chord μ					
R^2	0.737	0.731	0.598	0.655	0.665
SD	0.073	0.081	0.201	0.097	0.095
All					
R^2	0.731	0.721	0.528	0.634	0.614
SD	0.075	0.069	0.153	0.121	0.179

$CA =$ Corneal astigmatism; $GB =$ Gradient Boosting; $KNN =$ K-Nearest Neighbors; $RF =$ Random Forest; $SVR =$ Support Vector Regression; $\alpha =$ Measured astigmatism direction

The scores are overall higher in the KA case than in the TCRP case, increasing more when the Chord μ parameter is considered, rather than the AL, ACD and WTW parameters. They are higher for the linear estimators with lower SDs than for the tree-based estimators, suggesting that when using unknown data to predict optimized corneal astigmatism values, the accuracy of the first estimators will be higher and with a smaller deviation than the tree-based estimators. The KNN estimator associated score decreases considerably for the folds where more parameters are considered.

Step 3: Testing

A distinct dataset with 52 eyes (28 right eyes) from 43 patients was used for testing purposes. Besides the corneal astigmatism magnitude and direction, measurements for the following parameters were available for all cases (mean$\pm$SD and range, in mm): AL (23.68$\pm$1.61 mm; 20.03, 23.38 mm), ACD (3.18$\pm$0.46 mm; 2.25, 4.38 mm), and Chord μ (0.26$\pm$0.13 mm; 0.03, 0.60 mm). Distinguishing between astigmatism subgroups, 30 eyes were WTR and 22 ATR.

In result from the previous two steps, the KNN estimator appeared to perform worse when considering more parameters, what was also suggested by the scores in the Cross-validation. Therefore, in this step were used only the Linear and Linear SVR regressions, as well as the RF and GB estimators.

Using the previous sample with 100 eyes as training set, the KA and TCA of the test set of 52 eyes were optimized by the four estimators and the corresponding ERA components organized in Tables 5.12 and 5.13 for the KA (Pentacam) and TCRP 3.0 mm P/Z cases, respectively. These comprise the ERA meridional and net astigmatism magnitude mean$\pm$SD values, and also the median value and the percentage of eyes with an ERA magnitude equal or lower than 0.50 D.

Once again, here, when referring to ERA net astigmatism magnitude, it corresponds to the result of the conversion from the mean ERA KP(ϕ) and KP(ϕ+45) by equation (5.3), and the SD referring to the total variance. The mean$\pm$SD values for the non-optimized meridional and torsional ERA components were, for the KA case, -0.22$\pm$0.66 D and 0.12$\pm$0.53 D, while for the magnitude component, 0.25$\pm$0.85 D, with a median value of 0.71 D, and percentage of eyes within 0.50 D of 23.08%. For the TCRP 3.0 mm P/Z case, the mean$\pm$SD values for the meridional ERA were -0.13$\pm$0.52 D, for the torsional ERA component 0.12$\pm$0.51 D, and for the ERA magnitude 0.17$\pm$0.73 D, with a median value of 0.56 D and 46.15% of eyes within 0.50 D. It should be noted that the torsional component is not optimized, therefore, it remains constant.

Table 5.12: ERA meridional and net astigmatism magnitude components, in D, for the optimized KA (Pentacam) by the several estimators, in the Testing stage.

	Estimators			
Parameters	Linear	SVR	RF	GB
CA, cos(2α)				
Mean±SD: ERA KP(ϕ)	-0.06±0.41	-0.10±0.40	-0.02±0.42	-0.03±0.46
Mean±SD: ERA M	0.14±0.67	0.16±0.67	0.13±0.68	0.13±0.70
Median ERA	0.48	0.50	0.49	0.48
% Eyes ≤0.50 D	51.92	50.00	51.92	51.92
CA, cos(2α), AL, ACD				
Mean±SD: ERA KP(ϕ)	-0.05±0.40	-0.11±0.40	-0.08±0.48	-0.05±0.46
Mean±SD: ERA M	0.13±0.67	0.16±0.67	0.15±0.71	0.13±0.71
Median ERA	0.50	0.53	0.52	0.56
% Eyes ≤0.50 D	51.92	48.08	48.08	46.15
CA, cos(2α), Chord μ				
Mean±SD: ERA KP(ϕ)	-0.05±0.42	-0.09±0.41	-0.03±0.42	-0.01±0.50
Mean±SD: ERA M	0.13±0.68	0.15±0.67	0.13±0.68	0.12±0.73
Median ERA	0.51	0.52	0.51	0.53
% Eyes ≤0.50 D	50.00	48.08	50.00	44.23
All				
Mean±SD: ERA KP(ϕ)	-0.04±0.43	-0.10±0.41	-0.09±0.49	-0.03±0.49
Mean±SD: ERA M	0.13±0.68	0.16±0.67	0.15±0.72	0.13±0.72
Median ERA	0.52	0.53	0.53	0.55
% Eyes ≤0.50 D	48.08	42.31	48.08	46.15

CA = Corneal astigmatism; GB = Gradient Boosting; RF = Random Forest; SVR = Support Vector Regression; α = Measured astigmatism direction; $\%\ Eyes\ \leq 0.50\ D$ = Percentage of eyes with an absolute error within 0.50 D

Table 5.13: ERA meridional and net astigmatism magnitude components, in D, for the optimized TCRP 3.0 mm P/Z by the several estimators, in the Testing stage.

	Estimators			
Parameters	Linear	SVR	RF	GB
CA, cos(2α)				
Mean±SD: ERA KP(ϕ)	-0.11±0.47	-0.11±0.47	-0.06±0.49	-0.10±0.47
Mean±SD: ERA M	0.16±0.70	0.16±0.69	0.13±0.71	0.15±0.69
Median ERA	0.51	0.52	0.60	0.50
% Eyes ≤0.50 D	50.00	48.08	44.23	50.00
CA, cos(2α), AL, ACD				
Mean±SD: ERA KP(ϕ)	-0.09±0.48	-0.11±0.46	-0.15±0.47	-0.08±0.45
Mean±SD: ERA M	0.15±0.70	0.16±0.69	0.19±0.69	0.14±0.68
Median ERA	0.52	0.48	0.60	0.54
% Eyes ≤0.50 D	42.31	51.92	40.38	46.15
CA, cos(2α), Chord μ				
Mean±SD: ERA KP(ϕ)	-0.11±0.47	-0.13±0.45	-0.09±0.46	-0.10±0.48
Mean±SD: ERA M	0.16±0.69	0.18±0.68	0.15±0.69	0.16±0.70
Median ERA	0.53	0.52	0.56	0.50
% Eyes ≤0.50 D	46.15	48.08	40.38	50.00
All				
Mean±SD: ERA KP(ϕ)	-0.10±0.46	-0.11±0.45	-0.11±0.45	-0.08±0.42
Mean±SD: ERA M	0.15±0.69	0.16±0.68	0.16±0.68	0.14±0.66
Median ERA	0.52	0.51	0.55	0.52
% Eyes ≤0.50 D	46.15	50.00	42.31	48.08

CA = Corneal astigmatism; GB = Gradient Boosting; RF = Random Forest; SVR = Support Vector Regression; α = Measured astigmatism direction; $\%\ Eyes\ \leq 0.50\ D$ = Percentage of eyes with an absolute error within 0.50 D

For both KA and TCRP cases, the negative mean meridional ERA values indicate a general over-correction, being lower for the KA case than the TCRP. The mean values are lower for the tree-based estimators, but the SD values are lower for the linear estimators; the same results were found for the magnitude ERA case. In general, the percentage of eyes with an ERA magnitude equal or lower than 0.50 D rounds 50%. The highest percentages obtained by the estimators occur for the simple case where magnitude and direction of astigmatism were considered, whereas the percentages decrease when more parameters were included. No statistical differences were found when comparing different parameter sets for one estimator.

Statistically lower mean values were found for the KA optimized meridional ERA component compared to the non-optimized values for the first three sets of parameters, while for the last one only the linear and GB estimators had statistically lower mean values. In general, for the KA case, the SVR estimator had statistically higher mean values when compared to the other estimators. Analyzing the mean ERA magnitude, the values were statistically lower when optimized, while, overall, no differences were stated between the estimators results. In the TCRP case, no statistical differences were observed between the estimators optimized values and the non-optimized values, and when comparing the different estimators between each other. However, statistical differences were noted, when comparing the sets of parameters for the estimators: the ERA magnitude was lower when taking all parameters into account than in the case where only the corneal astigmatism and magnitude were considered for the Linear, Linear SVR, and GB estimators.

The meridional and torsional ERA components, as well as the correspondent 95% confidence ellipses for each estimator and parameter sets for the KA and TCRP cases are, respectively, shown in Figures 5.8 and 5.9. For the KA case, the optimization led to a pulling of the centroid towards zero along the $xx-$axis and an ellipse narrowing, with no pronounced differences between the linear and tree-based estimators, and parameter sets. Regarding the TCRP case, only a tender ellipse narrowing appeared when all parameters were considered and the GB estimator used.

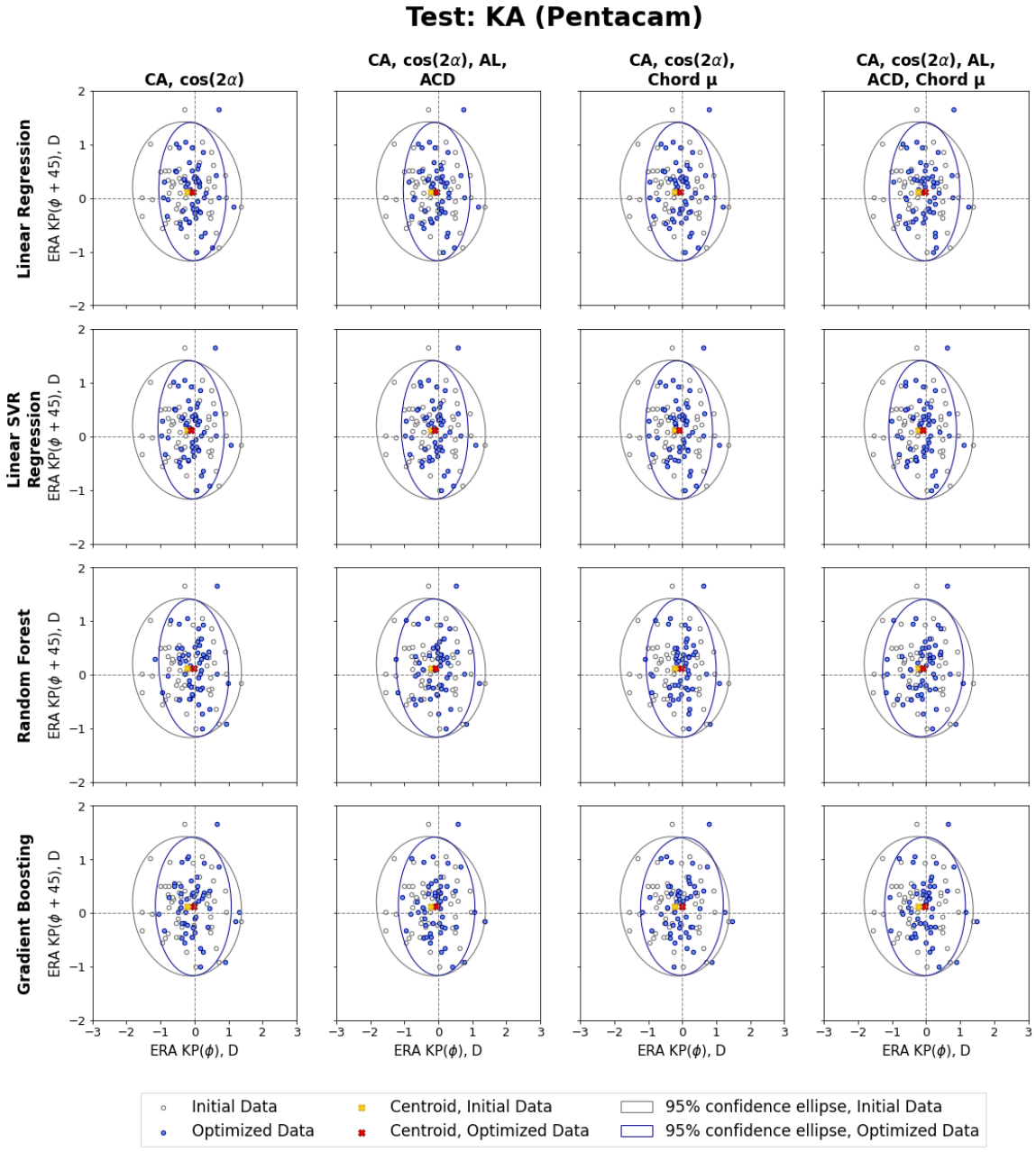

Figure 5.8: Meridional and torsional ERA components displayed by 95% confidence ellipses, for the KA (Pentacam) values optimized by estimators and compared to the initial data, given for each parameter sets, in the Testing stage.

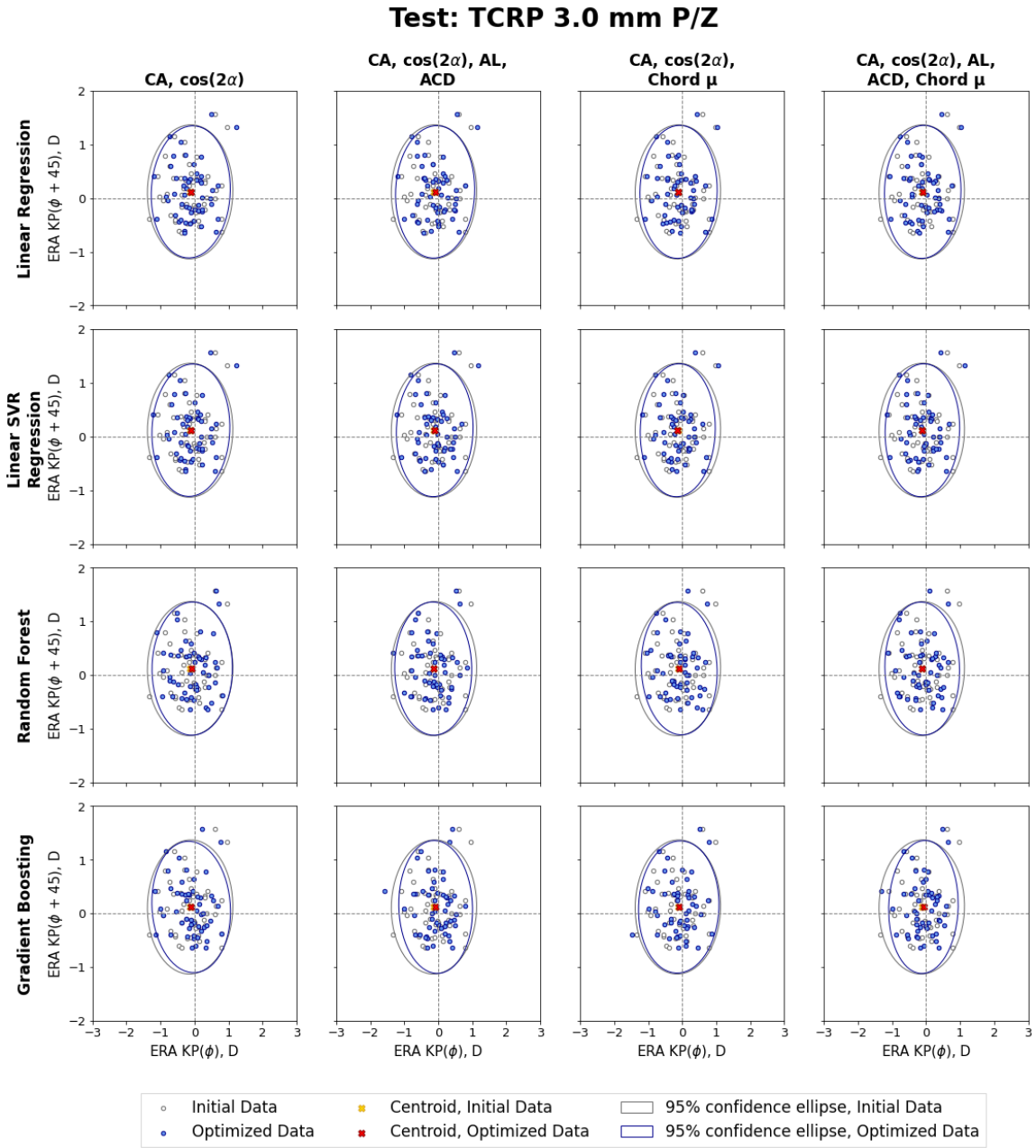

Figure 5.9: Meridional and torsional ERA components displayed by 95% confidence ellipses, for the TCRP 3.0 mm P/Z values optimized by estimators and compared to the initial data, given for each parameter sets, in the Testing stage.

5.2.4 Discussion

In this study, the implementation of the supervised machine learning concept was exploited in a three-folded exploratory analysis focused on Pentacam's KA and TCRP 3.0 mm P/Z measurement modalities. The first tryout, where the same sample was used for training and testing purposes, showed promising results, with good precision and high percentages of eyes with an ERA magnitude equal or lower than 0.50 D, attained namely with the non-linear tree-based estimators. Furthermore, the estimators' optimized values were lower than the initial ones, with a trend towards zero and reduction of the spread, namely for the TCRP cases, that is more pronounced when using the tree-based estimators. In another study performed by Savini *et al.* [65], following the same pipeline of back-calculations, but only using linear regression for optimization, was also shown a decrease in the ERA, attaining percentages of 50.79% and 45.31% for eyes with an ERA within 0.50 D, in the KA and TCRP P/Z cases, respectively. The KNN pointed out unsteady results across parameter sets, that may be related to a further need of features scaling and limitations of the number of parameters used by a model [84]. The same was observed for the 2^{nd} order Polynomial estimator, for which the analysis is not presented here, as it did not reveal good metrics, namely when considering more parameters — a percentage of 35% eyes with an ERA within 0.50 D was found for the KA (Pentacam) case, when considering all parameters in the training stage. Another estimator analyzed, but not presented as well, was the regression Decision Tree with a maximum depth of 4 (value determined by a series of simulations) that, although, presenting outcomes in the training step similar to the other tree-based estimators, had low metrics in the cross-validation step, and, overall, is the basis of the RF and GB estimators, therefore not being included. The Ridge Regression estimator, with a 0.05 constrain value, showed no differences from the Linear estimator, thus, also, not being here presented. In the testing step, four estimators, two of them linear and two tree-based, with unknown data led to improvements in the KA case in comparison to the initial state. It should be noted that the dataset used for testing purposes was made up of data collected back in 2017, however, the training set included likewise data collected between 2015 and 2017 (17 out of 100 cases), this may have influenced the outcomes due to the improvement measurement capabilities of the devices. Overall, looking at the three steps together, the KA cases, including the Aladdin case in section C.4 of Appendix C, revealed better outcomes, namely in terms of accuracy related to the confidence ellipses and spread, when compared to the TCRP cases (also TCRP 3.0 mm A/Z and TCRP 4.0 mm P/Z in Appendix C.4, section C.4), which may be due to the mentioned lower repeatabilitiy of the posterior corneal curvature measurements, in the latter cases [44].

5.3 Considerations

Multiple sources of influence on IOL power calculations have been studied in order to minimize the error in refractive astigmatism (see Chapter 3 — section 3.2). In the present study, when focusing solely on the 3.0- and 4.0 mm zones' TCRP, slight differences between mean astigmatism values were denoted, that not only showed up in power changes of the IOL suggested for implantation, but also af-

fected the predicted residual refractive astigmatism. This may be a possible interest for further analysis including more peripheric zones than solely the standard 3.0 mm zone, like it was already performed in a few studies [56, 57]. In another perspective, different KA and TCA related measurement modalities, and for the latter even different zones and centers, did not reveal differences regarding the stage (pre- or post-operatively) and number of measurements taken. In line with other studies, the TCA measurements led to better outcomes [47, 65] even for the TCRP measurement modality covering a 4.0 mm zone, for which slight differences of mean astigmatism values in relation to the 3.0 mm zone were found, namely for higher dioptric powers. Curiously, without SICA, the error in refractive astigmatism decreased, suggesting a connection to the posterior corneal curvature measurement, an important already highlighted influence factor, even though it is not clinically relevant, since for IOL power calculations the corneal astigmatism is optimized including the SICA.

In the recent years, the implementation of ML in the ophthalmology field rose considerably [83]. IOL power calculation is no exception, being the Hill-RBF Calculator[7] and the PEARL-DGS Formula [87] only two examples. Besides the linear regression model, other models, such as SVR or GB, were reported in studies showing promising results [88, 89]. These studies use large numbers of eyes (1 125 eyes in [88] and 1 450 eyes in [89]), whereas the present study could only be based on a relatively small number of eyes, being therefore this the major limitation. Even though, by analyzing different estimators for the KA case, the linear regression models — Linear and Linear SVR — showed optimistic results for different biometric parameter scales in both training and testing phases, approximating the meridional component of the centroid towards zero and optimizing the measured astigmatism. On the other hand, the tree-based estimators, namely the RF and GB, led to a pronounced decrease in the spread of cases, also approximating the meridional component of the centroid towards zero. These observations were most striking in the training phase, whereas in the test phase only smaller and less conclusive outcomes were observed, which might be related to the time when the data were collected (training between 2015 and 2017, and testing in 2017) and the subsequent improvement of measuring techniques by the used devices. Both linear and tree-based estimators appear to be potentially accurate and precise, at least for the KA case, however for the TCRP cases the differences were less pronounced, or even none, specially with respect to the spread of cases, which was more evident in the testing phase. As regards the inclusion of biometric measurements, such as the AL, ACD, and WTW, as well as the angle kappa related parameter, these are potentially important sources for the improvement of outcomes, namely in the TCRP cases. The first three parameters have been already included in toric IOL calculators, such as Barrett's and Kane's commonly used calculators (see Chapter 3 — section 3.3). Therefore, the present analysis, although in an initial state, points out the potential of regression models in a ML approach for the improvement of refractive outcomes in an toric IOL implantation cataract surgery scenario. However, future studies will be necessary including larger datasets that encompass eyes with distinct characteristics, so that the final created model will be robust even for more extreme cases, and, on the other hand, exploring the individualization of the underlying algorithms.

[7] Hill-RBF Calculator Version 3.0 - IOL Power Calculations for Cataract Surgery. `https://rbfcalculator.com/`. Accessed: 2021-10-11.

Chapter 6

Pseudophakic eye ray-tracing simulations

Using Zemax® OpticStudio along with an astigmatic pseudophakic eye model, based on the Personalized Pseudophakic Eye Model developed by Ribeiro *et al.* [11, 12], ray-tracing was exploited, namely by assessing the performance of a generic simulated toric IOL in pre- and post-operative scenarios, as well as sources of influence on the IOL spherical and cylindrical powers. In the first part of this chapter are detailed the considered patients' characteristics and the steps taken for the Zemax® implementation. The simulations of IOL power calculation using the generic simulated toric IOL are detailed in the second part of the chapter as well as the lens position and PCA influence on the IOL power.

6.1 Patients and optical model definition

Patients

For the above mentioned (Chapter 5 — section 5.2) 79 patients (100 eyes), who underwent cataract surgery at *Studio Oculistico D'Azeglio* with toric IOL implantation (Acrysof SN6ATx, Alcon Laboratories, Inc.), the data collection composed of the pre-operative measurements performed with Pentacam was cross-referenced with the one of post-operative measurements performed with MS-39, to assess the position of the implanted toric IOL. Measurements taken with both devices were recorded for 19 eyes from 16 patients — 10 WTR eyes, 6 ATR eyes, and 3 Oblique eyes. Thus, for these patients the parameters considered were: pre-operative corneal topography (radii of curvature, axis, and asphericity), AL, LT, PD, WTW, and ACD; post-operative (one month after the surgery) corneal topography and the position of the implanted IOL (ACD_{postop}) as the distance from the corneal endothelium to the anterior surface of the implanted IOL. Except corneal topography, the mean$\pm$SD and range values for the remaining parameters are organized in Table 6.1. Additionally, one month after the surgery, the subjective refraction and IOL axis of implantation were recorded.

Table 6.1: Patients' biometric parameters mean±SD, and range values, in mm.

	AL	LT	PD	WTW	ACD_{preop}	ACD_{postop}
Mean±SD	24.40±1.44	4.61±0.24	3.16±0.58	11.74±0.48	3.20±0.30	4.15±0.30
Range	22.32, 28.30	4.21, 5.08	2.03, 4.66	10.60, 12.60	2.60, 3.66	3.47, 4.62

ACD_{postop} = Post-operative anterior chamber depth; ACD_{preop} = Pre-operative anterior chamber depth

Liou-Brennan model: adaptation and Zemax® implementation

Since the Liou-Brennan model [17] is considered as anatomically and optically correct and pointed out as the currently most accurate (see Chapter 2 — section 2.1.1), it was used here as the basis for the eye modeling. The characteristic initial parameters of this model are presented in Table 6.2. The gradient indices for the lens follow equation (6.1) and are given by (6.2):

$$[Grad]\ n(w,z) = n_{00} + n_{01}z + n_{02}z^2 + n_{10}w^2 \tag{6.1}$$

$$\begin{aligned} Grad\ A &= 1.368 + 0.049057z - 0.015427z^2 - 0.001978w^2 \\ Grad\ P &= 1.407 - 0.006605z^2 - 0.001978w^2 \end{aligned} \tag{6.2}$$

where n_{00}, n_{01}, n_{02}, and n_{10} are the index coefficients, and w ($w^2 = x^2 + y^2$) is the radial distance perpendicular to the $zz-$axis, which, in turn, is along the optical axis.

Table 6.2: Liou-Brennan's eye model parameters for each surface.

♯	Surface	R (mm)	t (mm)	Q	n
1	Cornea Anterior	7.77	0.50	-0.18	1.376
2	Cornea Posterior	6.40	3.16	-0.60	1.336
3	Lens Anterior	12.40	1.59	-0.94	Grad A
4	Equator	Infinity	2.43	-	Grad P
5	Lens Posterior	-8.10	16.27	+0.96	1.336

n = Refractive index; Q = Asphericity; R = Radius; t = Thickness

Furthermore, in this model the pupil is considered as a circular aperture stop, encountering its decentration with a nasal shift of 0.50 mm in relation to the optical axis. Moreover, the Stiles-Crawford effect, related to the light brightness and the light entrance point at the pupil [14], is incorporated by pupil apodization of the form $I(w) = 10^{(\alpha/2)w^2}$, where I is the intensity, $\alpha = 0.05$, and w the radial distance, in mm, in relation to the pupil center. The photopic[1] spectral sensitivity regarding the retina receptors is, in this model, assessed by using three wavelengths — 510, 555, and 610 nm — weighting 1, 2, and 1, respectively. And the chromatic dispersion, that is considered in a way similar to scattering properties of water, defines the refractive indices according to wavelengths. A more detailed explanation can be found in [11, 12], which was also followed to modulate these characteristics in Zemax®.

[1] Photopic is the term used for high levels of illumination when the principal retinal receptors are the color sensitive cones.

Based on this model and the Personalized Pseudophakic Eye Model developed by Ribeiro *et al.* [11, 12], an astigmatic pseudophakic eye model was developed, suitable for patient-specific data incorporation, along with a generic simulated toric IOL concept developed to overcome the lack of disclosed information by manufacturers.

Statistical analysis

The Shapiro-Wilk test was performed for the assessment of the samples' distribution, and accordingly the paired t-test or the Wilcoxon signed-rank test was used for the comparison of two samples (see Chapter 4 — sections 4.1 and 4.2). These statistical analyses were carried out using the scipy.stats module of Python 3.7 (Anaconda), with p-values lower than 0.05 being considered significant.

6.2 Simulations

6.2.1 Ray-tracing intraocular lens power calculation

The generic simulated toric IOL powers were compared to the known implanted toric IOL powers, separately for the spherical and cylindrical powers. These comparisons were carried out through the optimization of the radii of curvature of the lens, converting them to power, through the thick lens equation (2.4), for each patient, considering a zero target refraction, since the desired target refraction was not known, for three models:

- Pre-operative measurements with the post-operative IOL position estimation formula obtained in the Personalized Pseudophakic Eye Model [11, 12] — $ACD_{post} = ACD_{pre} + 0.395 \times LT_{pre}$.
- Pre-operative measurements combined with the C Constant concept [68] for the post-operative IOL position estimation — $IOL_C = ACD_{pre} + C \times LT_{pre}$, with a C-value of 0.38 ("mean value in a representative sample" [68]).
- Post-operative measurements for which the IOL position was measured and recorded.

A linear regression model was fitted between the powers of the implanted IOL and the obtained powers for the pre-operative model with the PPM-based formula, Figure 6.1, for the pre-operative model with the C Constant, Figure 6.2, and for the post-operative model, Figure 6.3.

The regression parameters for the spherical cases suggest that the spherical power is higher for the generic simulated IOL than for the implanted IOL, with variations around 1.00 D. For the cylindrical powers, which are quite lower than the spherical powers, the regression parameters indicate that the generic simulated IOL power is higher for values above 2.00 D when compared to the value of the implanted IOL power, with variations around 0.50 D. For all cases the R^2 is higher than 0.8, suggesting a high correlation between the implanted and the generic simulated IOL powers, being namely the highest R^2 value for the spherical power obtained for the post-operative model, while for the cylindrical power the pre-operative measurement-based models depict higher values. It should be noted that the obtained IOL powers did not correspond to the power ranges of the commercially available IOLs.

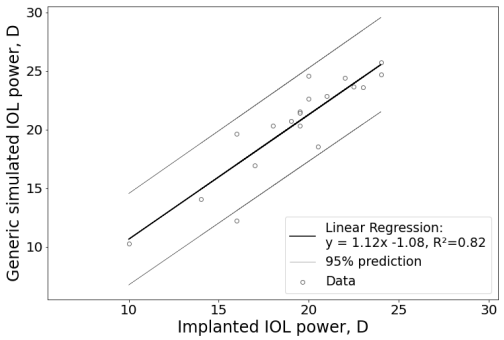

(a) Spherical power: pre-operative model with PPM formula .

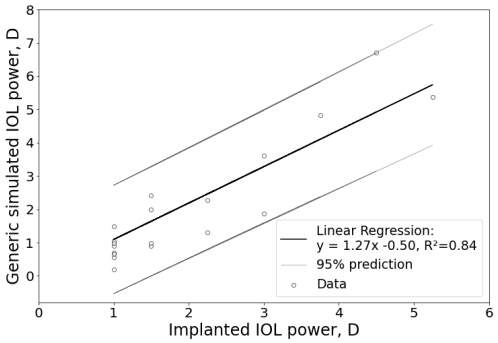

(b) Cylindrical power: pre-operative model with PPM formula.

Figure 6.1: Linear fit between the spherical powers of the implanted and the generic simulated IOLs using pre-operative measurements with the PPM-based formula (a) — $y(\sigma = 1.89) = 1.12x(\sigma = 0.13) - 1.08(\sigma = 2.46)$, $R^2 = 0.82$; and the cylindrical powers (b) — $y(\sigma = 0.74) = 1.27x(\sigma = 0.13) - 0.50(\sigma = 2.60)$, $R^2 = 0.84$.

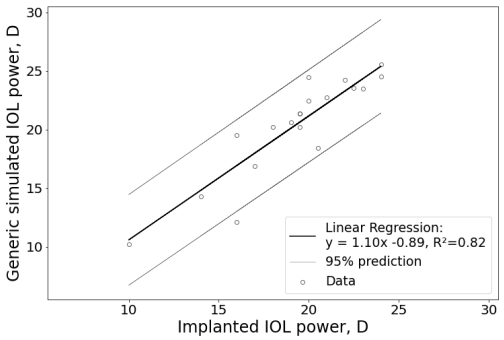

(a) Spherical power: pre-operative model with C Constant.

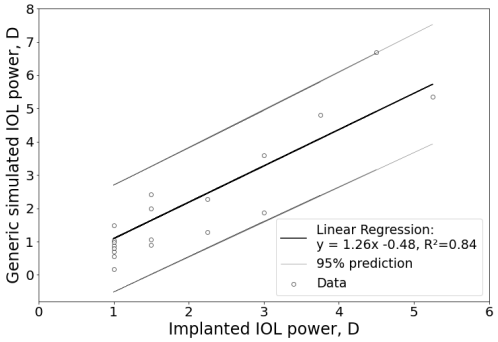

(b) Cylindrical power: pre-operative model with C Constant.

Figure 6.2: Linear fit between the spherical powers of the implanted and the generic simulated IOLs using pre-operative measurements with the C Constant (a) — $y(\sigma = 1.87) = 1.10x(\sigma = 0.13) - 0.89(\sigma = 2.45)$, $R^2 = 0.82$; and the cylindrical powers (b) — $y(\sigma = 0.73) = 1.26x(\sigma = 0.13) - 0.48(\sigma = 2.58)$, $R^2 = 0.84$.

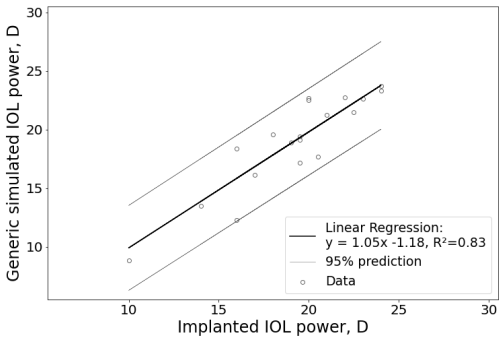

(a) Spherical power: post-operative model with IOL position.

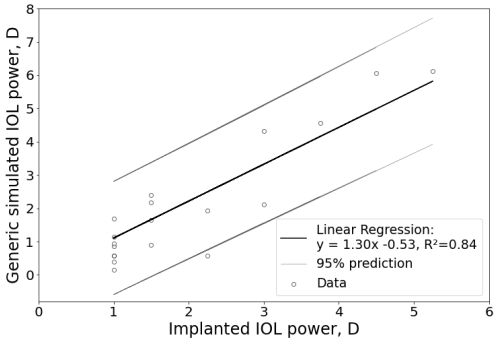

(b) Cylindrical power: post-operative model with IOL position.

Figure 6.3: Linear fit between the spherical powers of the implanted and the generic simulated IOLs using post-operative measurements (a) — $y(\sigma = 1.75) = 1.05x(\sigma = 0.12) - 1.18(\sigma = 2.28)$, $R^2 = 0.83$; and the cylindrical powers (b) — $y(\sigma = 0.77) = 1.30x(\sigma = 0.14) - 0.53(\sigma = 2.71)$, $R^2 = 0.84$.

For each model, the mean$\pm$SD and median values were calculated for the spherical and cylindrical powers, their results being depicted in Table 6.3. In addition, the MAE and the Median Absolute Error (MedAE) calculated in relation to the implanted IOL powers were determined. The p-values for the comparison in relation to the implanted IOL were obtained.

Table 6.3: Spherical and cylindrical powers, in D, for the three simulated models with respect to the implanted IOL powers. The p-values refer to the comparison to the implanted IOL powers.

Model	Mean	SD	MAE	Median	MedAE	p-values
Implanted						
Spherical	19.24	3.53	-	19.50	-	-
Cylindrical	2.00	1.31	-	1.50	-	-
Pre-operative + PPM						
Spherical	20.44	4.35	1.81	21.45	1.87	0.0071
Cylindrical	2.04	1.82	0.59	1.30	0.50	0.9530
Pre-operative + C Constant						
Spherical	20.33	4.30	1.73	21.37	1.73	0.0095
Cylindrical	2.04	1.80	0.58	1.29	0.49	0.9217
Post-operative						
Spherical	19.01	4.08	1.28	19.39	0.89	0.5750
Cylindrical	2.06	1.86	0.69	1.65	0.68	0.7381

$MAE =$ Mean Absolute Error; $MedAE =$ Median Absolute Error

The cylindrical power obtained using the three models did not statistically differ from the implanted IOL cylindrical power, and also in-between these no differences were found. However, by observation, slightly higher mean dioptric power values were obtained through simulation when compared to the implanted power. Regarding the spherical power, the mean and median values of the implanted IOL were similar to the obtained with the generic simulated IOL using the post-operative model, and statistically lower than both pre-operative models ($p<0.05$). In-between these two pre-operative models, statistical differences were also found ($p<0.001$), whereas the PPM-based model had a higher mean value. Regarding the MAE, median, and MedAE, these were higher for the pre-operative models, namely the one combined with the PPM-based formula, in comparison to the post-operative model.

Analyzing particular cases for which the absolute spherical power difference between the generic simulated and implanted IOL was higher than 1.00 D showed reasonable results. For example, a patient who had an implanted IOL with a spherical power of 20.50 D, and a post-operative subjective refraction of -2.75 D spherical power, the correspondent generic simulated IOL with the post-operative model had a lower spherical power, 17.70 D, which makes sense in myopic cases.

Considering these outcomes, the implementation of the generic simulated toric IOL was considered as valid for further simulations.

Refraction evaluation

For each of the three models, the prediction error was calculated as the difference between the recorded subjective refraction and the predicted post-operative refraction that was simulated, taking into account the biometric data and the known powers of the implanted IOL. For the post-operative model, the mean$\pm$SD difference was -0.59$\pm$0.85 D for the spherical power and -0.37$\pm$0.33 D for the cylindrical power, while regarding the pre-operative model combined with the PPM-based formula, these were -1.42$\pm$0.84 D and -0.20$\pm$0.34 D, and combined with the C Constant -1.39$\pm$0.79 D and -0.21$\pm$0.34 D. The negative mean values indicate a higher refractive power of the generic simulated IOL, for which the refraction spherical power is higher for the pre-operative models, pointing out the influence of the effective IOL position. For the cylindrical power, the variation is small between models, i.e., below 0.50 D, and a percentage of 63.16% was attained for a prediction error equal or lower than 0.50 D, for all models.

In turn, calculating the differences between the refraction of the post-operative model and the pre-operative model combined with the PPM-based formula, the respective mean$\pm$SD values were -0.83$\pm$0.47 D for the spherical power and 0.17$\pm$0.05 D for the cylindrical power, while combined with the C Constant formula they were -0.80$\pm$0.41 D and 0.16$\pm$0.05 D. The differences were similar for both models, showing that the refraction spherical power is in average higher for the pre-operative models and lower for the refraction cylindrical power, when compared to the post-operative model.

Lens position

Since it is known that the lens position influences specially the spherical power, the mean$\pm$SD values for the estimated ACD for the pre-operative models, as well as the post-operative measured ACD were calculated and are presented in Table 6.4. The MAE in relation to the post-operative ACD was calculated as well, and the Pearson coefficient was determined to assess the relation between the different models' ACD and other ocular parameters — WTW, LT, PD, and AL.

Table 6.4: Mean$\pm$SD and MAE values, in mm, for the models' ACD. Pearson coefficient for the relation of the ACD with the WTW, LT, PD, and AL biometric parameters.

	ACD (mm)		**Pearson coefficient**			
Model	Mean$\pm$SD	MAE	WTW	LT	PD	AL
Pre-operative + PPM	5.02$\pm$0.31	0.87	0.5990	0.2455	-0.1325	0.1986
Pre-operative + C Constant	4.95$\pm$0.31	0.80	0.5971	0.2346	-0.1298	0.2008
Post-operative	4.15$\pm$0.30	-	0.5842	0.2607	-0.0143	0.1802

$MAE =$ Mean Absolute Error

The pre-operative model-estimated IOL positions are higher than the post-operative effective measured ACD, namely the PPM estimation, that also has a higher MAE. As regards the ACD of each model, the highest Pearson coefficient is observed for the WTW parameter, suggesting a significantly positive correlation between these two parameters. The remaining parameters have lower Pearson coefficients, and while for the LT and AL a positive relation is suggested, indicating that with an ACD increase these increase as well; the contrary is observed for the PD by the negative Pearson coefficients.

6.2.2 Posterior cornea and intraocular lens power

Aiming to assess the influence of not considering posterior corneal measurements, and therefore real PCA measurements, as in keratometry, Zemax® simulations were performed keeping the posterior corneal surface parameters constant with the respective Liou-Brennan's model values of Table 6.2. Also, the refractive index of the anterior corneal surface was considered as 1.3375 (standard keratometric index) rather than 1.336. Once again, the spherical and cylindrical powers for the generic toric IOL were determined by converting the optimized curvature radii into power. The mean$\pm$SD values for these powers for the three models are presented in Table 6.5, when considering the posterior corneal surface and when not. In the two first columns, all eyes are considered, and in the remaining, the specific eyes were considered separately according to their classification into WTR and ATR astigmatism subgroups.

Overall, the spherical power is higher when considering the posterior cornea for the pre-operative models than when neglecting the posterior cornea, in all astigmatism groups. On the other hand, the cylindrical power is higher for the post-operative model, in the total and WTR cases. The spherical power always decreases without considering the posterior corneal surface, and in a quite pronounced way for the post-operative model. As regards the cylindrical power, when considering all eyes, the power increases when not encountering the PCA, which is related to the higher number of WTR eyes, where this tendency is also evident. On the contrary, the power decreases for the ATR subgroup.

Table 6.5: Mean$\pm$SD values, in D, for the spherical and cylindrical powers of the three simulated models when and when not considering the posterior corneal astigmatism, for the whole sample, and the WTR and ATR subgroups.

	Total (19 eyes)		**WTR** (10 eyes)		**ATR** (6 eyes)	
	Spherical	Cylindrical	Spherical	Cylindrical	Spherical	Cylindrical
With PCA						
Preop + PPM	20.44$\pm$4.35	2.04$\pm$1.82	20.88$\pm$4.05	2.65$\pm$2.01	20.20$\pm$5.15	0.97$\pm$0.59
Preop + C Constant	20.33$\pm$4.30	2.04$\pm$1.80	20.75$\pm$4.02	2.64$\pm$2.00	20.08$\pm$5.12	0.97$\pm$0.59
Postop	19.01$\pm$4.08	2.06$\pm$1.86	19.81$\pm$3.61	2.84$\pm$1.95	18.14$\pm$5.06	0.85$\pm$0.69
Without PCA						
Preop + PPM	19.10$\pm$4.34	2.12$\pm$1.96	19.69$\pm$3.98	2.91$\pm$2.07	18.61$\pm$5.17	0.71$\pm$0.53
Preop + C Constant	19.08$\pm$4.28	2.11$\pm$1.88	19.56$\pm$3.95	2.89$\pm$2.06	18.81$\pm$5.14	0.81$\pm$0.54
Postop	17.70$\pm$4.05	2.16$\pm$1.96	18.58$\pm$3.53	3.03$\pm$2.01	16.65$\pm$5.01	0.72$\pm$0.60

$Postop =$ Post-operative; $Preop =$ Pre-operative

6.3 Considerations

Exact ray-tracing enables precise calculations independently of previous patient-specific data, with the exception of the post-operative position of the IOL that, pre-operatively, is always a population-based estimation. Therefore, the accuracy of this method is limited by the precision of the incorporated patients' biometric measurements and by the pre-operative estimation of the IOL position. The possibility of IOL power calculations using ray-tracing was already assessed [69, 70]. Adapting eye models, such as the anatomically correct Liou-Brennan model, for the context of pseudophakia and designing them so that patient-specific data can be incorporated, was shown to be suitable for IOL power calculations even in more challenging situations, as after corneal refractive surgery, for example LASIK [11, 12]. Conversely, the AS-OCT MS-39 measuring device employs this technique for IOL power calculation, using IOL specificities along with AL and PD biometric parameters, and was shown to be potentially accurate even for eyes with more uncommon inherent characteristics, e.g. as long eyes with formula adjustments [71].

In this study, the PPM model developed by Ribeiro *et al.* [11, 12] based on the Liou-Brennan model, was adapted to an astigmatic pseudophakic eye model for Zemax® ray-tracing simulations. However, to overcome the lack of IOL characteristics, a generic simulated toric IOL was created, showing similar spherical and cylindrical powers when compared to the implanted IOL powers for pre- and post-operative measurements based models, even though the desired target refraction was not known.

The pre-operative models combined with the PPM-based formula and the C Constant concept designated for ray-tracing implementation dependent on the same pre-operative biometric measurements, had higher spherical IOL powers compared to the post-operative model and the implanted IOL. Further, the difference between the subjective refraction and the simulated refraction, regarding the spherical power, for the post-operative model was lower than for the pre-operative models. These observations are in accordance with the highlighted major impact of the prediction of the post-operative ACD on the refractive error [30], even identified as 76.8% for pseudophakic eyes [11, 54]. Bearing in mind the improvement of the ACD estimation, potentially with ray-tracing implementation, this parameter was related with other biometric parameters showing a significant correlation with the WTW parameter, underlying its possible inclusion in future studies for the improvement in refractive outcomes.

Despite the low number of eyes considered in these optical ray-tracing simulations, the implementation of the generic simulated toric IOL led to outcomes in line with the implanted IOL, showing the potential of this concept to be exploited in further studies employing the ray-tracing method for IOL power calculations and their improvement. Along with the employed astigmatic pseudophakic eye model and resorting to Zemax®, the obtained spherical and cylindrical IOL powers were patient-specific, however not correspondent to the power ranges of the commercially available IOLs. Even though, an effect of the ACD post-operative prediction on the IOL spherical power was found, as well as the posterior corneal influence on the IOL cylindrical power. Therefore, this study yielded to point out the ray-tracing potential regarding the combination of the astigmatic pseudophakic eye model, suitable for the incorporation of patient-specific data, and the generic simulated toric IOL, as the basis for further studies, encountering

a much larger number of eyes, improving the optimization methods, and providing the necessary model adjustments.

Chapter 7

Conclusions

As achieving optimum refractive outcomes following cataract surgery turns out to be more and more important, IOL power calculation is a constantly evolving field that aims to reduce the prediction error and identify influence factors that need to be taken into account. In this work, mainly three different approaches were studied as strategies for the improvement of the refractive astigmatism prediction error associated to cataract surgery with toric IOL implantation.

Given the overly known importance of encountering the PCA and the fact that a device measuring TCA is not everywhere available, regression nomograms have been developed that relate the KA measured by the Lenstar optical biometer with the TCA measured by the Cassini color-LED topographer. The results of the KA nomogram adjustment reflected a significant reduction of the prediction error in residual astigmatism, increasing the percentage of eyes with a prediction error within 0.50 D from 44% to 56% when adjusted by the generic nomogram. An overall shift towards WTR was depicted, in line with other adjustment methods. Nevertheless, an enhancement of the developed nomograms may be necessary for the reduction of outlier cases and for the increase of the correlation coefficient between the measured KA and TCA.

Focusing on further possible factors that should be considered, the present study about TCA from a 4.0 mm zone compared to the 3.0 mm zone pointed out that at least slight variations existed between them, namely for the ATR subgroup. Higher variations were in line with an increase of the predicted residual refractive astigmatism difference between zones, which may produce an impact on refractive outcomes. Conversely, it was shown that by considering the average of three pre-operative measurements or solely one pre-operative measurement did not reflect differences in the error in refractive astigmatism across different measurement modalities, even when compared to the average of three post-operative measurements.

The exploratory study about the employment of linear and non-linear machine learning estimators for the optimization of the pre-operative KA and TCA highlighted their potential to reduce the error in refractive astigmatism, in particular of the Linear and Linear SVR estimators, as well as the Random Forest and Gradient Boosting, attaining percentages of eyes with an error in refractive astigmatism equal or lower than 0.50 D as high as 75%, when the same sample was used for training and testing.

Beyond including a vast number of estimators, this study encountered various biometric parameters, which showed to be relevant for the improvement of outcomes, namely for the TCRP measurement modalities. However, more recent datasets should be used in future studies to test the estimators combined with several other biometric parameters and also the possibility of adaptation of the machine learning algorithms.

The developed astigmatic pseudophakic eye model along with the generic simulated toric IOL for ray-tracing power calculations, necessarily created to overcome the lack of lens specificities, provided the major advantages for being suitable for patient-specific data incorporation, from corneal topography to AL, ACD, PD, and LT, and moreover they do not depend on previous population data for IOL power calculations. The model's limitations are the unavoidable pre-operative lens position estimation and the inherent biometric measurements accuracy. The implementation of this model for IOL power ray-tracing calculations striked the potential not only of the model and toric IOL concept, but also of the method for the improvement of refractive outcomes, highlighting their versatility for the study of several scenarios regarding the challenging issue of post-operative IOL physical position estimations and the cylindrical power relation to the posterior cornea encountering. More simulations, including more eyes, with the generic simulated toric IOL should be performed to give strength to this concept and point out the adaptations needed. Alternative optimization methods need to be further studied as well as methods for the assessment of the refraction to determine more accurately the prediction error.

In essence, the main contributions of the conducted studies rely on the distinct improvement strategies to overcome some of the highlighted sources of error and exploit other possible factors to be taken into account for the improvement of refractive outcomes, pointing out that future studies require mainly a global inclusion of larger numbers of eyes to sustain the found results and enable more robust conclusions.

Based on the work carried out during the internship at *Studio Oculistico D'Azeglio*, the preliminary results of the retrospective study with respect to the number of measurements and surgery-related acquiring stage were presented at the IOL Power Club 16^{th} Annual Scientific Session. Furthermore is in sight a paper publication about the same subject. Already submitted for publication was a paper about ray-tracing IOL power calculation after corneal refractive surgery, in which the author participated. More recently for the European Society of Cataract and Refractive Surgeons (ESCRS) 2022 Winter meeting were submitted three abstracts, one about the developed regression nomograms, another about the performed analysis of center and peripheric zones total corneal astigmatism variation, and the third about ray-tracing IOL power simulations with the developed eye model and lens concept. In view are further paper publications with respect to these issues.

Bibliography

[1] W. Haigis. Challenges and approaches in modern biometry and IOL calculation. *Saudi Journal of Ophthalmology*, 26(1):7–12, January 2012. doi: 10.1016/j.sjopt.2011.11.007.

[2] Y.-C. Liu, M. Wilkins, T. Kim, B. Malyugin, and J. S. Mehta. Cataracts. *Lancet*, 390(10094):600–612, August 2017. doi: 10.1016/S0140-6736(17)30544-5.

[3] M. Lundström, M. Dickman, Y. Henry, S. Manning, P. Rosen, M.-J. Tassignon, D. Young, and U. Stenevi. Risk factors for refractive error after cataract surgery: Analysis of 282 811 cataract extractions reported to the European Registry of Quality Outcomes for cataract and refractive surgery. *Journal of Cataract and Refractive Surgery*, 44(4):447–452, April 2018. doi: 10.1016/j.jcrs.2018.01.031.

[4] P. C. Hoffmann and W. W. Hütz. Analysis of biometry and prevalence data for corneal astigmatism in 23,239 eyes. *Journal of Cataract and Refractive Surgery*, 36(49):1479–1485, September 2010. doi: 10.1016/j.jcrs.2010.02.025.

[5] T. Ferrer-Blasco, R. Montés-Micó, S. C. P. de Matos, J. M. González-Méijome, and A. Cerviño. Prevalence of corneal astigmatism before cataract surgery. *Journal of Cataract and Refractive Surgery*, 35(1):70–75, January 2009. doi: 10.1016/j.jcrs.2008.09.027.

[6] E. A. Villegas, E. Alcón, and P. Artal. Minimum amount of astigmatism that should be corrected. *Journal of Cataract and Refractive Surgery*, 40(1):13–19, January 2014. doi: 10.1016/j.jcrs.2013.09.010.

[7] R. B. Melles, J. T. Holladay, and W. J. Chang. Accuracy of Intraocular Lens Calculation Formulas. *Ophthalmology*, 125(2):169–178, February 2018. doi: 10.1016/j.ophtha.2017.08.027.

[8] G. Savini, M. D. Maita, K. J. Hoffer, K. Næser, D. Schiano-Lomoriello, A. Vagge, L. D. Cello, and C. E. Traverso. Comparison of 13 formulas for IOL power calculation with measurements from partial coherence interferometry. *The British Journal of Ophthalmology*, 105(4):484–489, April 2021. doi: 10.1136/bjophthalmol-2020-316193.

[9] J. X. Kane and B. Connell. A Comparison of the Accuracy of 6 Modern Toric Intraocular Lens Formulas. *Ophthalmology*, 127(11):1472–1486, November 2020. doi: 10.1016/j.ophtha.2020.04.039.

[10] T. B. Ferreira, P. Ribeiro, F. J. Ribeiro, and J. G. O'Neill. Comparison of Methodologies Using Estimated or Measured Values of Total Corneal Astigmatism for Toric Intraocular Lens Power Calculation. *Journal of Refractive Surgery*, 33(12):794–800, December 2017. doi: 10.3928/1081597X-20171004-03.

[11] M. F. J. Ribeiro. *Personalized Pseudophakic Model*. PhD thesis, Instituto Superior Técnico, 2014.

[12] F. J. Ribeiro, A. Castanheira-Dinis, and J. M. Dias. Personalized Pseudophakic Model for Refractive Assessment. *PLoS One*, 7(10):e46780, October 2012. doi: 10.1371/journal.pone.0046780.

[13] K. Irsch and D. L. Guyton. Anatomy of Eyes. In S. Z. Li and A. Jain, editors, *Encyclopedia of Biometrics*, pages 11–16. Springer US, Boston, MA, 2009. doi: 10.1007/978-0-387-73003-5_253.

[14] D. A. Atchison and G. Smith. *Optics of the Human Eye*. Butterworth-Heinemann, 2000. ISBN:978-0-7506-3775-6.

[15] E. Hecht. *Optics*. Addison-Wesley, fourth edition, 2001.

[16] R. C. Bakaraju, K. Ehrmann, E. Papas, and A. Ho. Finite schematic eye models and their accuracy to *in-vivo* data. *Vision Research*, 48(16):1681–1694, 2008. doi: 10.1016/j.visres.2008.04.009.

[17] H.-L. Liou and N. A. Brennan. Anatomically accurate, finite model eye for optical modeling. *Journal of the Optical Society of America A*, 14(8):1684–1695, August 1997. doi: 10.1364/JOSAA.14.001684.

[18] D. W. DelMonte and T. Kim. Anatomy and physiology of the cornea. *Journal of Cataract and Refractive Surgery*, 37(3):588–598, March 2011. doi: 10.1016/j.jcrs.2010.12.037.

[19] W. J. Smith. *Modern Optical Engineering*. McGraw-Hill, 2000. ISBN:978-0819438386.

[20] K. Næser. Assessment and Statistics of Surgically Induced Astigmatism. *Acta ophthalmologica*, 86:349, June 2008. doi: 10.1111/j.1755-3768.2008.01287.x. Thesis.

[21] N. R. C. U. C. on Vision. CONTRAST SENSITIVITY FUNCTION. In *Emergent Techniques for Assessment of Visual Performance*. Washington (DC): National Academies Press (US), 1985.

[22] C. McAlinden, M. McCartney, and J. Moore. Mathematics of Zernike polynomials: a review. *Clinical and Experimental Ophthalmology*, 39(8):820–827, November 2011. doi: 10.1111/j.1442-9071.2011.02562.x.

[23] M. Aaron, W. A. Solley, and G. Broocker. General Eye Examination. In *Primary Care Ophthalmology*, chapter 1, pages 1–23. Mosby, second edition, 2005. doi: 10.1016/B978-032303316-9.50007-3.

[24] T. L. C. B. Ferreira. *Improving strategies on toric intraocular lens power calculation*. PhD thesis, NOVA Medical School | Faculdade de Ciências Médicas, 2019.

[25] S. Marcos, M. Velasco-Ocana, C. Dorronsoro, L. Sawides, M. Hernandez, and G. Marin. Impact of astigmatism and high-order aberrations on subjective best focus. *Journal of Vision*, 15:4, August 2015. doi: 10.1167/15.11.4.

[26] International Council of Ophthalmology 1984. Visual Acuity Measurements Standard. *Italian Journal of Ophthalmology*, II/I:1–15, 1988.

[27] F. L. Ferris and I. Bailey. Standardizing the measurement of visual acuity for clinical research studies: Guidelines from the Eye Care Technology Forum. *Ophthalmology*, 103(1):181–182, January 1996. doi: 10.1016/s0161-6420(96)30742-2.

[28] D. B. Elliott and J. Flanagan. Assessment of Visual Function. In *Clinical Procedures in Primary Eye Care*, chapter 3, pages 29–81. Butterworth-Heinemann, third edition, 2007. doi: 10.1016/B978-0-7506-8896-3.50007-9.

[29] E. J. Linebarger, D. R. Hardten, G. K. Shah, and R. L. Lindstrom. Phacoemulsification and Modern Cataract Surgery. *Survey of Ophthalmology*, 44(2):123–147, September-October 1999. doi: 10.1016/S0039-6257(99)00085-5.

[30] S. Norrby. Sources of error in intraocular lens power calculation. *Journal of Cataract and Refractive Surgery*, 34(3):368–376, March 2008. doi: 10.1016/j.jcrs.2007.10.031.

[31] R. Belluci. An Introduction to Intraocular Lenses: Material, Optics, Haptics, Design and Aberration. *Cataract*, pages 38–55, August 2013. doi: 10.1159/000350902.

[32] M. A. Lawless and C. Hodge. Wavefront's role in corneal refractive surgery. *Clinical and Experimental Ophthalmology*, 33(2):199–209, April 2005. doi: 10.1111/j.1442-9071.2005.00994.x.

[33] M. Lombardo and G. Lombardo. Wave aberration of human eyes and new descriptors of image optical quality and visual performance. *Journal of Cataract and Refractive Surgery*, 36(2):313–331, February 2010. doi: 10.1016/j.jcrs.2009.09.026.

[34] N. Visser, R. Ruíz-Mesa, F. Pastor, N. J. C. Bauer, R. M. Nuijts, and R. Montés-Micó. Cataract surgery with toric intraocular lens implantation in patients with high corneal astigmatism. *Journal of Cataract and Refractive Surgery*, 37(8):1403–1410, August 2011. doi: 10.1016/j.jcrs.2011.03.034.

[35] M. Corbett, N. Maycock, E. Rosen, and D. O'Brart. *Corneal Topography*. Springer International Publishing, second edition, 2019. doi: 10.1007/978-3-030-10696-6.

[36] R. Fan, T. C. Y. Chan, G. Prakash, and V. Jhanji. Applications of corneal topography and tomography: a review. *Clinical and Experimental Ophthalmology*, 46:133–146, 2018. doi: 10.1111/ceo.13136.

[37] G. Savini, K. J. Hoffer, P. Barboni, N. Balducci, D. Schiano-Lomoriello, and P. Ducoli. Accuracy of optical biometry combined with Placido disc corneal topography for intraocular lens power calculation. *PLoS One*, 12(2):e0172634, February 2017. doi: 10.1371/journal.pone.0172634.

[38] W. Hill, R. Osher, D. Cooke, K. Solomon, H. Sandoval, R. Salas-Cervantes, and R. Potvin. Simulation of toric intraocular lens results: manual keratometry versus dual-zone automated keratometry from an integrated biometer. *Journal of Cataract and Refractive Surgery*, 37(12):2181–2187, December 2011. doi: 10.1016/j.jcrs.2011.06.028.

[39] M. Mohammadpour. *Diagnostics in Ocular Imaging*. Springer International Publishing, first edition, 2021. doi: 10.1007/978-3-030-54863-6.

[40] G. Savini, D. Schiano-Lomoriello, and K. J. Hoffer. Repeatability of automatic measurements by a new anterior segment optical coherence tomographer combined with Placido topography and agreement with 2 Scheimpflug cameras. *Journal of Cataract and Refractive Surgery*, 44(4):471–478, April 2018. doi: 10.1016/j.jcrs.2018.02.015.

[41] J. Huang, G. Savini, F. Wu, X. Yu, J. Yang, A. Yu, Y. Yu, and Q. Wang. Repeatability and reproducibility of ocular biometry using a new noncontact optical low-coherence interferometer. *Journal of Cataract and Refractive Surgery*, 41(10):2233–2241, October 2015. doi: 10.1016/j.jcrs.2015.10.062.

[42] B. V. Ventura, Z. Al-Mohtaseb, L. Wang, D. D. Koch, and M. P. Weikert. Repeatability and comparability of corneal power and corneal astigmatism obtained from a point-source color light-emitting diode topographer, a Placido-based corneal topographer, and a low-coherence reflectometer. *Journal of Cataract and Refractive Surgery*, 41(10):2242–2250, October 2015. doi: 10.1016/j.jcrs.2015.11.003.

[43] M. Mohamed, M. Khan, A. Kanakamedala, I. Gupta, L. Wang, D. Koch, and Z. Al-Mohtaseb. Repeatability and comparability of the Galilei-G4 and Cassini in measuring corneal power and astigmatism in normal and post-refractive surgery eyes. *Scientific Reports*, 11(1):16141, August 2021. doi: 10.1038/s41598-021-94319-w.

[44] J. Aramberri, L. Araiz, A. Garcia, I. Illarramendi, J. Olmos, I. Oyanarte, A. Romay, and I. Vigara. Dual versus single Scheimpflug camera for anterior segment analysis: Precision and agreement. *Journal of Cataract and Refractive Surgery*, 38(11):1934–1949, November 2012. doi: 10.1016/j.jcrs.2012.06.049.

[45] T. B. Ferreira and F. J. Ribeiro. Comparability and repeatability of different methods of corneal astigmatism assessment. *Clinical Ophthalmology*, 20(12):29–34, December 2017. doi: 10.2147/OPTH.S146730.

[46] D. P. Piñero, A. Molina-Martín, V. J. Camps, D. de Fez, and M. T. Caballero. Validation of corneal topographic and aberrometric measurements obtained by color light-emitting diode reflection topography in healthy eyes. *Graefe's Archive for Clinical and Experimental Ophthalmology*, 257(11):2437–2447, November 2019. doi: 10.1007/s00417-019-04453-5.

[47] G. Savini and K. Næser. An Analysis of the Factors Influencing the Residual Refractive Astigmatism After Cataract Surgery With Toric Intraocular Lenses. *Investigate Ophthalmology & Visual Science*, 56(2):827–835, February 2015. doi: 10.1167/iovs.14-15903.

[48] J.-D. Ho, C.-Y. Tsai, and S.-W. Liou. Accuracy of Corneal Astigmatism Estimation by Neglecting the Posterior Corneal Surface Measurement. *American Journal of Ophthalmology*, 147(5):788–795, February 2009. doi: 10.1016/j.ajo.2008.12.020.

[49] G. Savini, F. Versaci, G. Vestri, P. Ducoli, and K. Næser. Influence of posterior corneal astigmatism on total corneal astigmatism in eyes with moderate to high astigmatism. *Journal of Cataract and Refractive Surgery*, 40:1645–1653, October 2014. doi: 10.1016/j.jcrs.2014.01.046.

[50] D. D. Koch, S. F. Ali, M. P. Weikert, M. Shirayama, R. Jenkins, and L. Wang. Contribution of posterior corneal astigmatism to total corneal astigmatism. *Journal of Cataract and Refractive Surgery*, 38: 2080–2087, December 2012. doi: 10.1016/j.jcrs.2012.08.036.

[51] K. Hayashi, T. Sato, H. Sasaki, A. Hirata, and K. Yoshimura. Sex-related differences in corneal astigmatism and shape with age. *Journal of Cataract and Refractive Surgery*, 44:1130–1139, September 2018. doi: 10.1016/j.jcrs.2018.06.020.

[52] M. Goggin, S. Moore, and A. Esterman. Outcome of toric intraocular lens implantation after adjusting for anterior chamber depth and intraocular lens sphere equivalent power effects. *Archives of Ophthalmology*, 129(8):998–1003, August 2011. doi: 10.1001/archophthalmol.2011.188.

[53] G. Savini, K. J. Hoffer, M. Carbonelli, P. Ducoli, and P. Barboni. Influence of axial length and corneal power on the astigmatic power of toric intraocular lenses. *Journal of Cataract and Refractive Surgery*, 39(12):1900–1903, August 2013. doi: 10.1016/j.jcrs.2013.04.047.

[54] F. Ribeiro, A. Castanheira-Dinis, and J. M. Dias. Refractive Error Assessment: Influence of Different Optical Elements and Current Limits of Biometric Techniques. *Journal of Refractive Surgery*, 29(3): 206–212, March 2013. doi: 10.3928/1081597X-20130129-07.

[55] T. Zheng, Z. Chen, and Y. Lu. Influence factors of estimation errors for total corneal astigmatism using keratometric astigmatism in patients before cataract surgery. *Journal of Cataract and Refractive Surgery*, 42:84–94, January 2016. doi: 10.1016/j.jcrs.2015.07.037.

[56] S. A. Read, M. J. Collins, L. G. Carney, and R. J. Franklin. The Topography of the Central and Peripheral Cornea. *Investigate Ophthalmology & Visual Science*, 47(4):1404–1415, April 2006. doi: 10.1167/iovs.05-1181.

[57] T. Kawamorita, K. Shimizu, R. Hoshikawa, K. Kamiya, and N. Shoji. Relationship between central and peripheral corneal astigmatism in elderly patients. *Optical Review*, 25:336–339, March 2018. doi: 10.1007/s10043-018-0427-2.

[58] K. J. Hoffer and G. Savini. Effect of Gender and Race on Ocular Biometry. *International Ophthalmology Clinics*, 57(3):137–142, April 2017. doi: 10.1097/IIO.0000000000000180.

[59] T. B. Ferreira, K. J. Hoffer, F. Ribeiro, P. Ribeiro, and J. G. O'Neill. Ocular biometric measurements in cataract surgery candidates in Portugal. *PLoS One*, 12:e0184837, October 2017. doi: 10.1371/journal.pone.0184837.

[60] N. Visser, N. J. C. Bauer, and R. M. M. A. Nuijts. Toric intraocular lenses: historical overview, patient selection, IOL calculation, surgical techniques, clinical outcomes, and complications. *Journal of Cataract and Refractive Surgery*, 39(4):624–637, April 2013. doi: 10.1016/j.jcrs.2013.02.020.

[61] M. P. Weikert, A. Golla, and L. Wang. Astigmatism induced by intraocular lens tilt evaluated via ray tracing. *Journal of Cataract and Refractive Surgery*, 44(6):745–749, June 2018. doi: 10.1016/j.jcrs.2018.04.035.

[62] D. D. Koch, R. B. Jenkins, M. P. Weikert, E. Yeu, and L. Wang. Correcting astigmatism with toric intraocular lenses: effect of posterior corneal astigmatism. *Journal of Cataract and Refractive Surgery*, 39(12):1803–1809, December 2013. doi: 10.1016/j.jcrs.2013.06.027.

[63] M. Goggin, K. Zamora-Alejo, A. Esterman, and L. van Zyl. Adjustment of anterior corneal astigmatism values to incorporate the likely effect of posterior corneal curvature for toric intraocular lens calculation. *Journal of Refractive Surgery*, 31(2):98–102, February 2015. doi: 10.3928/1081597X-20150122-04.

[64] A. Abulafia, D. D. Koch, L. Wang, W. E. Hill, E. I. Assia, M. Franchina, and G. D. Barrett. New regression formula for toric intraocular lens calculations. *Journal of Cataract and Refractive Surgery*, 42(5):663–671, May 2016. doi: 10.1016/j.jcrs.2016.02.038.

[65] G. Savini, K. Næser, D. Schiano-Lomoriello, and P. Ducoli. Optimized keratometry and total corneal astigmatism for toric intraocular lens calculation. *Journal of Cataract and Refractive Surgery*, 43 (9):1140–1148, September 2017. doi: 10.1016/j.jcrs.2017.06.040.

[66] C. Canovas, A. Alarcon, R. Rosén, S. Kasthurirangan, J. J. K. Ma, D. D. Koch, and P. Piers. New algorithm for toric intraocular lens power calculation considering the posterior corneal astigmatism. *Journal of Cataract and Refractive Surgery*, 44(2):168–174, February 2018. doi: 10.1016/j.jcrs.2017.11.008.

[67] P.-R. Preussner. Ray Tracing for IOL Power Calculations. *Cataract Refractive Surgery Today*, pages 46–48, May 2012.

[68] T. Olsen and P. Hoffmann. C constant: New concept for ray tracing-assisted intraocular lens power calculation. *Journal of Cataract and Refractive Surgery*, 40(5):764–773, May 2014. doi: 10.1016/j.jcrs.2013.10.037.

[69] P.-R. Preussner, J. Wahl, H. Lahdo, B. Dick, and O. Findl. Ray tracing for intraocular lens calculation. *Journal of Cataract and Refractive Surgery*, 28(8):1412–1419, August 2002. doi: 10.1016/s0886-3350(01)01346-3.

[70] T. Olsen and M. Funding. Ray-tracing analysis of intraocular lens power in situ. *Journal of Cataract and Refractive Surgery*, 38(4):641–647, April 2012. doi: 10.1016/j.jcrs.2011.10.035.

[71] G. Savini, K. J. Hoffer, F. J. Ribeiro, J. M. Dias, C. P. Coutinho, P. Barboni, and D. S. Lomoriello. IOL power calculation with ray tracing based on anterior segment OCT and adjusted axial length after myopic excimer laser surgery. 2021. Submitted for publication.

[72] T. B. Ferreira, P. Ribeiro, F. J. Ribeiro, and J. G. O'Neill. Comparison of astigmatic prediction errors associated with new calculation methods for toric intraocular lenses. *Journal of Cataract and Refractive Surgery*, 43(3):340–347, March 2017. doi: 10.1016/j.jcrs.2016.12.031.

[73] J. T. Holladay, J. R. Moran, and G. M. Kezirian. Analysis of aggregate surgically induced refractive change, prediction error, and intraocular astigmatism. *Journal of Cataract and Refractive Surgery*, 27(1):61–79, January 2001. doi: 10.1016/s0886-3350(00)00796-3.

[74] J. R. Taylor. *An Introduction to Error Analysis*. University Science Books, second edition, 1997. ISBN:978-0935702750.

[75] R. H. Riffenburgh. *Statistics in Medicine*. Academic Press, second edition, 2006. ISBN: 978-0-12-088770-5.

[76] J. T. Holladay, T. C. Prager, T. Y. Chandler, K. H. Musgrove, J. W. Lewis, and R. S. Ruiz. A three-part system for refining intraocular lens power calculations. *Journal of Cataract and Refractive Surgery*, 14(1):17–24, January 1988. doi: 10.1016/s0886-3350(88)80059-2.

[77] H. B. Fam and K. L. Lim. Meridional analysis for calculating the expected spherocylindrical refraction in eyes with toric intraocular lenses. *Journal of Cataract and Refractive Surgery*, 33(12):2072–2076, December 2007. doi: 10.1016/j.jcrs.2007.07.034.

[78] L. Wang, M. Shirayama, X. J. Ma, T. Kohnen, and D. D. Koch. Optimizing intraocular lens power calculations in eyes with axial lengths above 25.0 mm. *Journal of Cataract and Refractive Surgery*, 37(11):2018–2027, November 2011. doi: 10.1016/j.jcrs.2011.05.042.

[79] L. N. Thibos, W. Wheeler, and D. Horner. Power vectors: an application of Fourier analysis to the description and statistical analysis of refractive error. *Optometry and Vision Science*, 74(6): 367–375, June 1997. doi: 10.1097/00006324-199706000-00019.

[80] O. Reitblat, A. Levy, G. Kleinmann, A. Abulafia, and E. I. Assia. Effect of posterior corneal astigmatism on power calculation and alignment of toric intraocular lenses: Comparison of methodologies. *Journal of Cataract and Refractive Surgery*, 42(2):217–225, February 2016. doi: 10.1016/j.jcrs.2015.11.036.

[81] S. S. Ophir, B. LaHood, and M. Goggin. Refractive outcome of toric intraocular lens calculation in cases of oblique anterior corneal astigmatism. *Journal of Cataract and Refractive Surgery*, 46(5): 688–693, May 2020. doi: 10.1097/j.jcrs.0000000000000162.

[82] K. Næser. Surgically induced astigmatism made easy: calculating the surgically induced change in sphere and cylinder for corneal incisional, corneal laser, and intraocular lens–based surgery. *Journal of Cataract and Refractive Surgery*, 47(1):118–122, January 2021. doi: 10.1097/j.jcrs.0000000000000518.

[83] A. Lee, P. Taylor, , J. Kalpathy-Cramer, and A. Tufail. Machine Learning Has Arrived! *American Academy of Ophthalmology*, 124(12):1726–1728, December 2017. doi: 10.1016/j.ophtha.2017.08.046.

[84] T. Hastie, R. Tibshirani, and J. Friedman. *The Elements of Statistical Learning*. Springer, second edition, 2009. ISBN:978-0387848570.

[85] A. Cutler, D. R. Cutler, and J. R. Stevens. Random Forests. In C. Zhang and Y. Ma, editors, *Ensemble Machine Learning*, pages 157–176. Springer-Verlag, New York, 2012. doi: 10.1007/978-1-4419-9326-7_5.

[86] A. J. Ferreira and M. T. Figueiredo. Boosting Algorithms: A Review of Methods, Theory, and Applications. In C. Zhang and Y. Ma, editors, *Ensemble Machine Learning*, pages 35–85. Springer-Verlag, New York, 2012. doi: 10.1007/978-1-4419-9326-7_2.

[87] G. Debellemanière, M. Dubois, M. Gauvin, A. Wallerstein, L. F. Brenner, R. Rampat, A. Saad, and D. Gatinel. The PEARL-DGS Formula: The Development of an Open-source Machine Learning-based Thick IOL Calculation Formula. *American Journal of Ophthalmology*, 13:58–69, May 2021. doi: 10.1016/j.ajo.2021.05.004.

[88] T. Fukuda, N. Kamiura, A. Saitoh, T. Isokawa, N. Matsui, and H. Tabuchi. Formula selection for intraocular power calculation using support vector machines and self-organizing maps. In *2011 IEEE International Conference on Systems, Man, and Cybernetics*, pages 1111–1116, 2011. doi: 10.1109/ICSMC.2011.6083823.

[89] L. Wei, Y. Song, W. He, X. Chen, B. Ma, Y. Lu, and X. Zhu. Accuracy Improvement of IOL Power Prediction for Highly Myopic Eyes With an XGBoost Machine Learning-Based Calculator. *Frontiers in Medicine (Lausanne)*, 7(592663), December 2020. doi: 10.3389/fmed.2020.592663.

[90] R. Martin. Cornea and anterior eye assessment with placido-disc keratoscopy, slit scanning evaluation topography and scheimpflug imaging tomography. *Indian Journal of Ophthalmology*, 66(3):360–366, March 2018. doi: 10.4103/ijo.IJO_850_17.

[91] S. A. Klein. Axial Curvature and the Skew Ray Error in Corneal Topography. *Optometry and Vision Science*, 74(11):931–944, November 1997. doi: 10.1097/00006324-199711000-00027.

[92] P. Kanclerz, R. Khoramnia, and X. Wang. Current Developments in Corneal Topography and Tomography. *Diagnostics (Basel, Switzerland)*, 11(8):1466, August 2021. doi: 10.3390/diagnostics11081466.

[93] J. J. Snellenburg, B. Braaf, E. A. Hermans, R. G. van der Heijde, and V. A. D. P. Sicam. Forward ray tracing for image projection prediction and surface reconstruction in the evaluation of corneal topography systems. *Optics Express*, 18(18):19324–19338, August 2010. doi: 10.1364/OE.18.019324.

[94] R. Jain and S. Grewal. Pentacam: Principle and Clinical Applications. *Journal of Current Glaucoma Practice*, 3(2):20–32, May 2009. doi: 10.5005/jp-journals-10008-1012.

[95] J. G. Fujimoto, C. Pitris, S. A. Boppart, and M. E. Brezinski. Optical coherence tomography: an emerging technology for biomedical imaging and optical biopsy, journal = Neoplasia. 2(1-2):9–25, January-April 2000. doi: 10.1038/sj.neo.7900071.

Appendix A

Device measurement technologies: descriptions

A.1 Placido disc-based technology

Placido disc technology[1] is used in keratoscopic-based instruments, covering a wider zone than keratometers [90]. An illuminated circular target is projected on the anterior cornea with a series of alternating concentric dark and light rings (Figure A.1) and a central aperture with a convex lens to assess the light reflections. According to the type of Placido discs, the devices using this technology can be classified into small-cone or large-cone Placido disc systems. The first ones include a larger number of rings and, thus, a larger coverage of the cornea including information of the periphery, however, the working distance decreases. Large-cone systems, in turn, project less rings on the cornea, therefore, fewer points and information, although having a longer working distance [35, 39].

A camera captures the reflected rings, that are then qualitatively and quantitatively analyzed by an incorporated software, evaluating the corneal shape and calculating its curvature and power from information of thousands of points of the anterior corneal surface. The shape of the cornea is characterized according to the light reflections: a regular-shaped cornea presents equally spaced reflections with an image of a series of circular concentric rings; otherwise, the image contains non-circular rings with irregular bends, indicating abnormal corneal shapes, as, for example, astigmatism represented on the right side of Figure A.1 [35].

Placido disc-based systems enable a fast acquisition, the major drawback being the absence of posterior corneal surface information, along with the potential inaccurate characterization in highly irregular corneas, or abrupt elevation changes, and skew ray error [35, 91, 92].

[1] Called after the Portuguese ophthalmologist and microbiologist António Plácido da Costa (1848-1915).

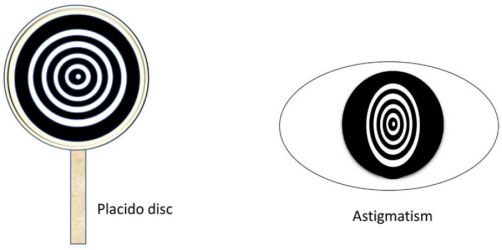

Figure A.1: Schematic representation of the Placido disc technology (left) and an astigmatism respective pattern (right) [36].

A.2 Point-source color light-emitting diode technology

In point-source LED technology, reflections of point sources of the corneal surface are captured and a correspondence of one-to-one is made between image and source points. For the reconstruction of the surface, an algorithm based on forward ray-tracing is used, i.e., propagation is traced from the source to the image points, rather than back ray-tracing, where propagation is traced from image to source.

In Figure A.2 is represented a diagram of the forward ray-tracing model. The source points (x_s, y_s, z_s) correspond to the LED source and are traced to the corneal surface intersection points (x_c, y_c, z_c). Afterwards, the ray reflected by the corneal surface is traced to the image points (x_i, y_i, z_i) that are captured by the camera, and has necessarily to pass through the camera lens nodal point $(0, 0, 0)$, since only chief rays[2] are considered. This model can be adapted from simulating the image points via source point tracing through a known surface, to corneal surface reconstruction, when the source and image points are known. Describing the corneal surface by a set of Zernike coefficients and relating the known LED source and image points by vectors, a step by step and iterative process can be employed for the determination of the Zernike coefficients to model the corneal surface. No assumptions of rotationally symmetric surfaces are made. A one-to-one correspondence between source and image points is performed, thus being encountered different light reflections by the cornea and skew rays, as well as irregular or distorted corneal surfaces [93].

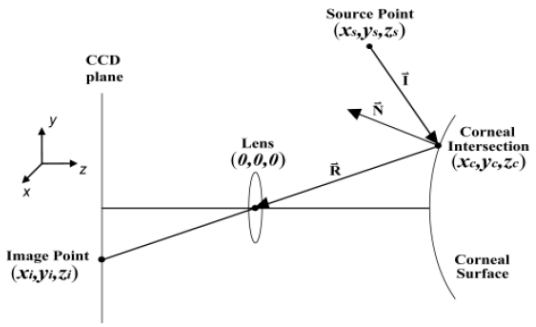

Figure A.2: Schematic representation of the forward ray-tracing procedure [93].

[2] A chief ray comes from an off-axis object.

A.3 Scheimpflug imaging-based technology

In an ideal case, the planes of object, image, and lens are parallel, and a sharp focused image will emerge on the focus plane, which is parallel to the lens plane, Figure A.3 (a). When some parts of the object are not parallel to the image plane, the image is not focused entirely along the focal plane, Figure A.3 (b). The Scheimpflug principle[3] is a geometric rule used for the latter case to describe the orientation of the focus plane of an optical system. To obtain the focused image, the lens and the image planes are manipulated using this principle by drawing an oblique tangent from the lens and the image planes that intersect at the point of focus, the so called Scheimpflug intersection — Figure A.3 (c). Thereby, applying this principle, an image without distortion can be obtained with an enhanced depth of focus [35, 94].

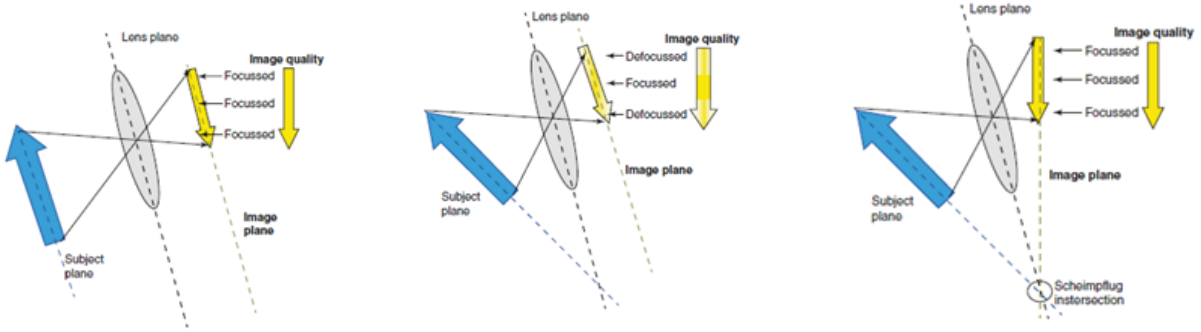

(a) Parallel object, lens and image planes.

(b) Non-parallel object, lens and image planes.

(c) Scheimpflug intersection.

Figure A.3: Schematic representation of three object, lens and image planes orientations and Scheimpflug principle [35].

A.4 Coherence-based technology

LCI uses an interferometer to measure the time delay and intensity of backscattered light by comparing it to light that traveled through a reference path. A light source directs the emitted light to a beam splitter, that sends one component to a reference mirror through a reference path, and the second to the sample through the sample path. The light reflected by the reference mirror and the light backscattered by the sample are recombined in the beam splitter, originating an interference pattern, captured afterwards by the detector — Figure A.4. The interference output is demodulated and correlated with the reference path length, thereby measuring the time delay and the intensity of the light backscattered by different sites of the sample [95]. By displacing the light source across the sample, an image can be constructed combining cross-section (B-scans) of several axial scans (A-scans) with the intensity of the backscattered light as a function of depth. In particular, the dimensions of the eye structures can be determined through the measurement of the echo time delay of the backscattered light at various axial distances[4].

[3]Named after the Austrian naval officer and geodetic engineer Theodor Scheimpflug (1865-1911).

[4]NovAcam: How low-coherence interferometry (LCI) works. `https://www.novacam.com/technology/how-lci-works/`. Accessed: 2021-09-04.

OCT employs the LCI principle to measure the depth of the reflected light from different tissue layers of the eye, being sensitive to the difference in refractive indices. Typically, infrared light is used, that penetrates the ocular media with minimal scattering, leading to high resolution tomographic images. Two-dimensional images represent the backscatterring profile through a cross-section plane of the tissue in a logarithmic grayscale of time delay and intensity, enabling a clear distinction of optical structures. A three-dimensional image represents a cross-sectional volume of the tissue [39, 95]. OCT systems can be divided mainly into time-domain (TD-OCT) and spectral-domain (SD-OCT) [39].

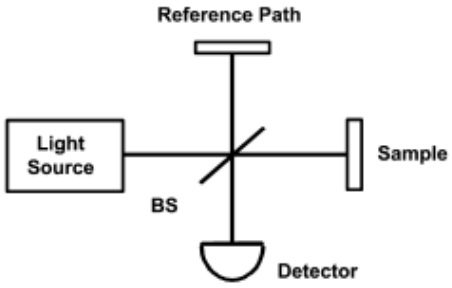

Figure A.4: Michelson type interferometer representation, where BS stands for beam splitter [95].

Appendix B

Prediction error in residual astigmatism: double-angle plots

B.1 Prediction error with Abulafia-Koch formula

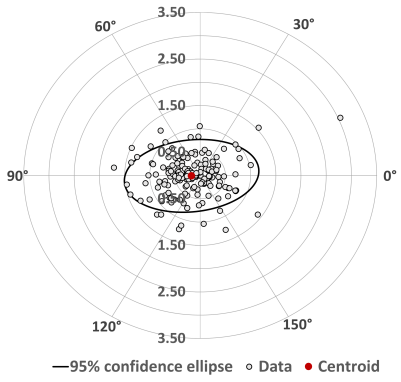

(a) Total group.

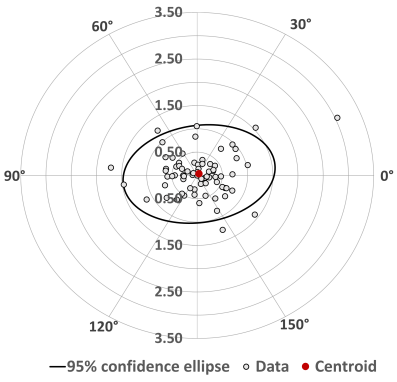

(b) WTR subgroup.

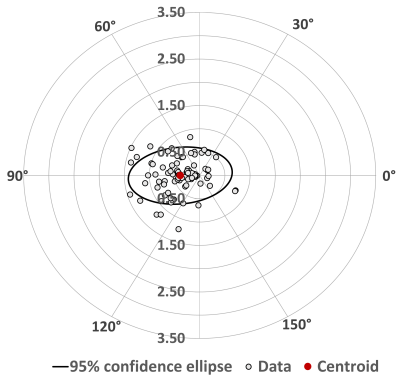

(c) ATR subgroup.

Figure B.1: Double-angle plots of the EPA for the total group (a), and WTR (b) and ATR (c) subgroups, for the adjustment with the Abulafia-Koch formula. Each ring represents 0.50 D.

B.2 Prediction error with three adjustment methods

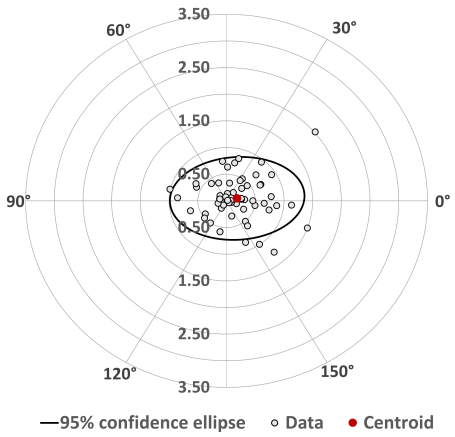

(a) Without adjustment.

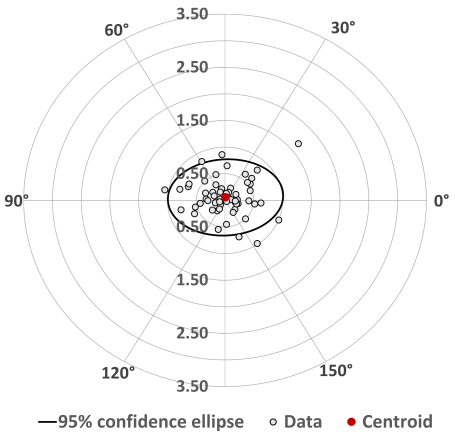

(b) Generic nomogram adjustment.

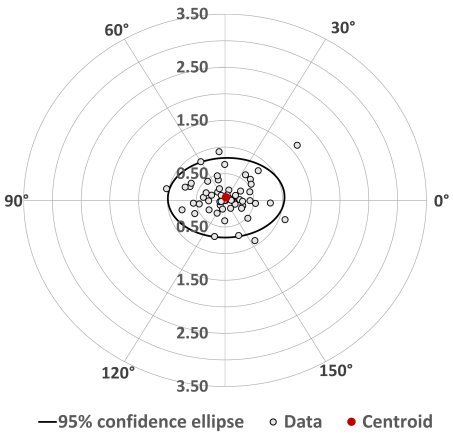

(c) Specific nomogram adjustment.

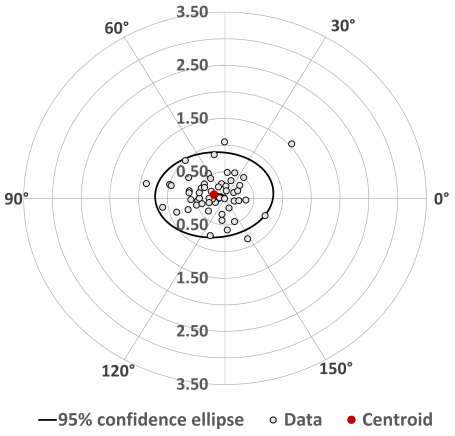

(d) Abulafia-Koch Formula.

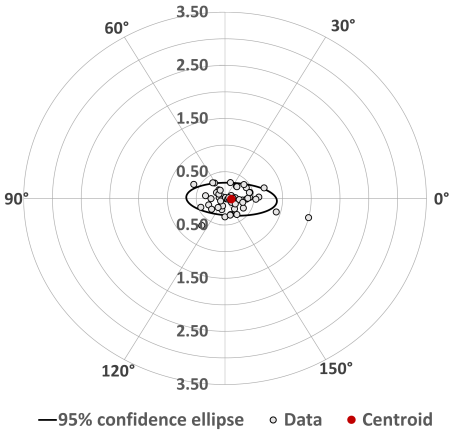

(e) Barrett Toric Calculator.

Figure B.2: Double-angle plots of the EPA for 60 eyes without adjustment (a); with the generic (b) and specific (c) nomogram adjustments; with the Abulafia-Koch Formula (d); and with the Barrett Toric Calculator (e). Each ring represents 0.50 D.

Appendix C

Error in refractive analysis: descriptions, tables and graphics

C.1 Predicted residual refractive astigmatism: IOL power change within zones

In Table C.1 is represented the number of cases for each IOL power change between the 3.0- and 4.0 mm zones based on the TCRP measurements. The values in the diagonal correspond to the cases, where the power did not change between zones (29 cases); below the diagonal, the cases, where the power decreased according to the 3.0 mm zone compared to the 4.0 mm zone (50 cases); and above the diagonal, the cases, where the power increased (46 cases).

Table C.1: Number of cases for the change of power of the IOL suggested for implantation according to the TCRP of the 3.0 mm and 4.0 mm zones.

		4.0 mm								
		-	**T2**	**T3**	**T4**	**T5**	**T6**	**T7**	**T8**	**T9**
3.0 mm	**-**	**9**	8	3	1	0	0	0	0	0
	T2	9	**10**	9	5	1	0	0	0	0
	T3	5	13	**4**	4	4	1	1	0	0
	T4	0	3	3	**3**	4	0	1	0	0
	T5	0	1	3	3	**1**	1	0	0	0
	T6	0	1	1	1	3	**1**	2	1	0
	T7	0	0	0	0	1	0	**0**	0	0
	T8	0	0	0	0	0	1	1	**0**	0
	T9	0	0	0	0	0	0	0	1	**1**

– = No suggestion for toric IOL implantation

C.2 Measurement comparisons

Table C.2: Mean±SD, in D, for the difference between the first, second, and third astigmatism measurements compared to the mean value of the three, for both three pre- and post-operative measurement types regarding each measurement modality.

	3 preop			**3 postop**		
	1º	2º	3º	1º	2º	3º
KA (Pentacam)	0.10±0.13	0.11±0.13	0.13±0.24	0.11±0.17	0.10±0.15	0.10±0.15
KA (Aladdin)	0.13±0.18	0.12±0.15	0.18±0.28	0.12±0.10	0.15±0.21	0.13±0.21
TCRP 3.0 mm P/Z	0.15±0.14	0.16±0.20	0.16±0.20	0.16±0.19	0.14±0.15	0.15±0.13
TCRP 3.0 mm A/Z	0.17±0.17	0.19±0.24	0.19±0.25	0.16±0.19	0.14±0.13	0.14±0.14
TCRP 4.0 mm P/Z	0.11±0.11	0.13±0.14	0.13±0.20	0.12±0.14	0.10±0.11	0.10±0.09

1º/2º/3º = First/Second/Third measurement performed; $3\,preop =$ Average of three pre-operative measurements; $3\,postop =$ Average of three post-operative measurements

Table C.3: SICA net values in a net astigmatism format, M @ α (D @ $^\circ$), in D, for the WTR, ATR, and Oblique astigmatism subgroups.

	WTR		**ATR**		**Oblique**	
	3 preop	1 preop	3 preop	1 preop	3 preop	1 preop
KA (Pentacam)	0.15 @ 86.0	0.17 @ 89.6	0.24 @ 95.5	0.27 @ 97.5	0.14 @ 55.0	0.15 @ 86.9
KA (Aladdin)	0.13 @ 103.2	0.11 @ 98.9	0.20 @ 111.1	0.17 @ 108.5	0.12 @ 88.6	0.24 @ 90.2
TCRP 3.0 mm P/Z	0.18 @ 92.2	0.19 @ 90.1	0.23 @ 104.9	0.24 @ 102.9	0.10 @ 77.8	0.17 @ 82.6
TCRP 3.0 mm A/Z	0.17 @ 87.6	0.19 @ 89.7	0.27 @ 100.2	0.33 @ 98.8	0.12 @ 65.7	0.17 @ 83.2
TCRP 4.0 mm P/Z	0.20 @ 91.4	0.21 @ 92.2	0.24 @ 101.0	0.26 @ 102.4	0.12 @ 80.6	0.12 @ 89.4

$1\,preop =$ One pre-operative measurement; $3\,preop =$ Average of three pre-operative measurements

C.3 Error in refractive astigmatism when neglecting SICA

Table C.4: ERA meridional, torsional, and magnitude components, in D, when neglecting SICA for the WTR subgroup. The p-values refer to the differences between measurement types.

	ERA KP(ϕ)		ERA KP(ϕ+45)		ERA Net Astigmatism M			
WTR (n=54)	Mean±SD	p-value	Mean±SD	p-value	Median	MAE±SD	p-value	% ≤0.50 D
KA (Pentacam)								
Average 3 preop	-0.42±0.40		-0.13±0.32		0.54	0.59±0.32		46.30
1 preop	-0.43*±0.47	0.0006	-0.14±0.31	0.9159	0.52	0.60±0.40	0.0173	48.15
Average 3 postop	-0.54±0.40		-0.11±0.31		0.67	0.67±0.33		31.48
KA (Aladdin)								
Average 3 preop	-0.43±0.40		-0.12*±0.34		0.48	0.58±0.39		53.70
1 preop	-0.47±0.43	0.5103	-0.13*±0.37	0.7408	0.55	0.63±0.41	0.2588	46.30
Average 3 postop	-0.52±0.34		-0.17±0.34		0.64	0.65±0.34		35.19
TCRP 3.0 mm P/Z								
Average 3 preop	0.02*±0.42		-0.09±0.36		0.45	0.46±0.31		61.11
1 preop	-0.01*±0.46	0.0006	-0.10±0.36	0.9653	0.46	0.50±0.32	0.0952	57.14
Average 3 postop	-0.21±0.39		-0.11±0.36		0.47	0.52±0.27		57.41
TCRP 3.0 mm A/Z								
Average 3 preop	-0.25±0.40		-0.13±0.35		0.47	0.51±0.31		57.41
1 preop	-0.28±0.51	0.2224	-0.13±0.33	0.9212	0.48	0.55±0.39	0.3480	53.70
Average 3 postop	-0.39±0.36		-0.11±0.35		0.50	0.56±0.30		50.00
TCRP 4.0 mm P/Z								
Average 3 preop	-0.09*±0.36		-0.08±0.35		0.37	0.45±0.25		66.67
1 preop	-0.10±0.43	<0.001	-0.09±0.34	0.9959	0.41	0.47±0.30	0.0147	66.67
Average 3 postop	-0.32±0.38		-0.09±0.35		0.47	0.53±0.30		53.70

A/Z = Apex Zone; MAE = Mean Absolute Error; P/Z = Pupil Zone; $\% \leq 0.50\ D$ = Percentage of eyes with an absolute error within 0.50 D; *Shapiro-Wilk test with $p < 0.05$ (Non normal distribution)

Table C.5: ERA meridional, torsional, and magnitude components, in D, when neglecting SICA for the ATR subgroup. The p-values refer to the differences between measurement types.

	ERA KP(ϕ)		ERA KP(ϕ+45)		ERA Net Astigmatism M			
ATR (n=31)	Mean±SD	p-value	Mean±SD	p-value	Median	MAE±SD	p-value	% ≤0.5 D
KA (Pentacam)								
Average 3 preop	0.12±0.32		-0.12±0.43		0.52	0.51±0.23		48.39
1 preop	0.10±0.33	0.0904	-0.15±0.45	0.9263	0.50	0.52±0.25	0.4235	54.84
Average 3 postop	0.26±0.27		-0.11±0.56		0.59	0.59±0.33		41.94
KA (Aladdin)								
Average 3 preop	0.12±0.35		-0.14*±0.46		0.49	0.51±0.31		54.84
1 preop	0.13±0.35	0.5304	-0.19*±0.46	0.0142	0.52	0.52±0.35	0.8569	48.39
Average 3 postop	0.21±0.34		0.03*±0.47		0.48	0.52±0.32		51.61
TCRP 3.0 mm P/Z								
Average 3 preop	0.04±0.40		-0.14±0.43		0.48	0.54±0.26		58.06
1 preop	-0.04±0.46	0.4208	-0.19±0.49	0.6415	0.50	0.61±0.32	0.5920	51.61
Average 3 postop	0.10±0.32		-0.08±0.53		0.52	0.55±0.28		48.39
TCRP 3.0 mm A/Z								
Average 3 preop	-0.15±0.39		-0.13±0.42		0.43	0.52±0.29		51.61
1 preop	-0.22±0.38	0.0509	-0.16±0.46	0.9594	0.52	0.56±0.33	0.6790	48.39
Average 3 postop	0.01±0.35		-0.13±0.51		0.53	0.55±0.29		45.16
TCRP 4.0 mm P/Z								
Average 3 preop	0.03±0.37		-0.12±0.44		0.45	0.51±0.26		61.29
1 preop	0.00±0.44	0.4261	-0.15±0.45	0.7530	0.48	0.57±0.29	0.3679	61.29
Average 3 postop	0.12±0.33		-0.06±0.52		0.53	0.54±0.31		48.39

A/Z = Apex Zone; MAE = Mean Absolute Error; P/Z = Pupil Zone; $\% \leq 0.50\ D$ = Percentage of eyes with an absolute error within 0.50 D; *Shapiro-Wilk test with $p < 0.05$ (Non normal distribution)

Table C.6: ERA meridional, torsional, and magnitude components, in D, when neglecting SICA for the Oblique subgroup. The p-values refer to the differences between measurement types.

	ERA KP(ϕ)		ERA KP(ϕ+45)		ERA Net Astigmatism M			
Oblique (n=15)	Mean±SD	p-value	Mean±SD	p-value	Median	MAE±SD	p-value	% ±0.50 D
KA (Pentacam)								
Average 3 preop	-0.18±0.44		-0.03±0.56		0.66	0.65±0.30		26.67
1 preop	-0.19±0.37	0.7786	-0.10±0.62	0.9110	0.50	0.65±0.34	0.8450	26.67
Average 3 postop	-0.09±0.50		-0.13±0.67		0.68	0.72±0.42		20.00
KA (Aladdin)								
Average 3 preop	-0.16±0.442		-0.22±0.35		0.55	0.53±0.28		46.67
1 preop	-0.24*±0.78	0.8187	-0.17±0.42	0.8883	0.46	0.66±0.64	0.6271	53.33
Average 3 postop	-0.12±0.48		-0.14±0.49		0.53	0.61±0.31		33.33
TCRP 3.0 mm P/Z								
Average 3 preop	-0.03±0.52		-0.08*±0.46		0.55	0.57±0.38		46.67
1 preop	0.02±0.45	0.7559	-0.18±0.50	0.5488	0.49	0.59±0.33	0.9737	53.33
Average 3 postop	-0.11±0.41		-0.16±0.54		0.60	0.59±0.34		46.67
TCRP 3.0 mm A/Z								
Average 3 preop	-0.27*±0.55		-0.06±0.49		0.50	0.64±0.44		53.33
1 preop	-0.26±0.42	0.4204	-0.16±0.58	0.8739	0.61	0.67±0.36	0.9383	40.00
Average 3 postop	-0.19±0.42		-0.12±0.56		0.58	0.63±0.34		33.33
TCRP 4.0 mm P/Z								
Average 3 preop	-0.06±0.43		-0.09*±0.44		0.47	0.52±0.33		60.00
1 preop	-0.01±0.36	0.9264	-0.15*±0.44	0.9899	0.36	0.48±0.31	0.8187	66.67
Average 3 postop	-0.05±0.38		-0.16±0.51		0.40	0.53±0.36		53.33

$A/Z =$ Apex Zone; $MAE =$ Mean Absolute Error; $P/Z =$ Pupil Zone; $\% \leq 0.50\ D =$ Percentage of eyes with an absolute error within 0.50 D; *Shapiro-Wilk test with $p < 0.05$ (Non normal distribution)

C.4 Optimization methods

C.4.1 Estimators description

Ridge Regression: it also fits a linear model between the independent and dependent variables as in equation (C.1) , but adds a penalization term, α, to regulate the sizes of the coefficients and thereby minimizes a penalized residual sum of squares under the form (C.2)[1].

$$\widehat{y}(w, x) = w_0 + w_1 x_1 + ... + w_p x_p \tag{C.1}$$

$$Minimization\ Criterion : \min_{w} \|Xw - y\|_2^2 + \alpha \|w\|_2^2 \tag{C.2}$$

Polynomial Regression: it is a linear n-th order relation, here 2nd order, between the features and the expected values, following the format of equation (C.1)[1] [74].

Regression Decision Tree: it predicts a new value based on decision rules established according to the features of the training set. The feature space is recursively split into regions, so that similar features are grouped together, according to the feature, j, and a threshold, t_m, where m denotes the node ($\theta = (j, t_m)$). Each partition leads to two subsets, $Q_m^{left}(\theta)$ and $Q_m^{right}(\theta)$, where Q_m denotes the data at node m with an N_m number of samples, according to (C.3). The choice of the split parameters

[1] 1. Supervisied learning. `https://scikit-learn.org/stable/supervised_learning.html`. Accessed: 2021-09-25.

settles on the minimization of the loss function (C.4), in this case the MSE, for the two subsets, according to equation (C.5). For each subset, the prediction is modeled as a constant, here by the mean value $\bar{y}_m$[1] [84].

$$\begin{aligned} Q_m^{left}(\theta) &= \{(x,y)|x_j <= t_m\} \\ Q_m^{right}(\theta) &= Q_m \setminus Q_m^{left}(\theta) \end{aligned} \tag{C.3}$$

$$H(Q_m) = \frac{1}{N_m} \sum_{y \in Q_m} (y - \bar{y}_m)^2 \text{ , } where\ \bar{y}_m = \frac{1}{N_m} \sum_{y \in Q_m} y \tag{C.4}$$

$$Minimization\ Criterion : \min_{\theta} \left[\frac{N_m^{left}}{N_m} H(Q_m^{left}(\theta)) + \frac{N_m^{right}}{N_m} H(Q_m^{right}(\theta)) \right] \tag{C.5}$$

C.4.2 Step 1: Training

Estimators metrics

Table C.7: MAE and R^2 for each estimator and each parameter set, for the KA (Aladdin) in the Training stage.

	Estimators				
Parameters	Linear	SVR	KNN	RF	GB
CA, cos(2α)					
MAE	0.298	0.296	0.251	0.134	0.098
R^2	0.811	0.810	0.874	0.952	0.982
CA, cos(2α), AL, ACD, WTW					
MAE	0.299	0.297	0.261	0.134	0.066
R^2	0.814	0.810	0.840	0.954	0.992

$CA =$ Corneal astigmatism; $GB =$ Gradient Boosting; $KNN =$ K-Nearest Neighbors; $MAE =$ Mean Absolute Error; $RF =$ Random Forest; $SVR =$ Support Vector Regression; $\alpha =$ Measured astigmatism direction

Table C.8: MAE and R^2 for each estimator and each parameter set, for the TCRP 3.0 mm A/Z in the Training stage.

	Estimators				
Parameters	Linear	SVR	KNN	RF	GB
CA, cos(2α)					
MAE	0.312	0.306	0.262	0.157	0.117
R^2	0.820	0.816	0.860	0.947	0.973
CA, cos(2α), AL, ACD, WTW					
MAE	0.312	0.306	0.293	0.153	0.081
R^2	0.821	0.815	0.843	0.947	0.987
CA, cos(2α), Chord μ					
MAE	0.309	0.305	0.280	0.139	0.089
R^2	0.824	0.819	0.849	0.962	0.985
All					
MAE	0.306	0.302	0.292	0.148	0.077
R^2	0.827	0.822	0.836	0.951	0.989

$CA =$ Corneal astigmatism; $GB =$ Gradient Boosting; $KNN =$ K-Nearest Neighbors; $MAE =$ Mean Absolute Error; $RF =$ Random Forest; $SVR =$ Support Vector Regression; $\alpha =$ Measured astigmatism direction

Table C.9: MAE and R^2 for each estimator and each parameter set, for the TCRP 4.0 mm P/Z in the Training stage.

	Estimators				
Parameters	Linear	SVR	KNN	RF	GB
CA, cos(2α)					
MAE	0.316	0.315	0.261	0.131	0.139
R^2	0.818	0.817	0.868	0.960	0.975
CA, cos(2α), AL, ACD, WTW					
MAE	0.294	0.292	0.280	0.130	0.068
R^2	0.839	0.836	0.854	0.963	0.991
CA, cos(2α), Chord μ					
MAE	0.311	0.304	0.283	0.138	0.077
R^2	0.829	0.821	0.851	0.957	0.987
All					
MAE	0.295	0.293	0.308	0.133	0.055
R^2	0.841	0.835	0.826	0.965	0.994

$CA =$ Corneal astigmatism; $GB =$ Gradient Boosting; $KNN =$ K-Nearest Neighbors; $MAE =$ Mean Absolute Error; $RF =$ Random Forest; $SVR =$ Support Vector Regression; $\alpha =$ Measured astigmatism direction

Estimators associated ERA

Table C.10: ERA meridional, torsional, and net astigmatism magnitude components, in D, for the optimized KA (Aladdin) by the several estimators for the different parameter sets, in the Training stage.

	Estimators				
Parameters	Linear	SVR	KNN	RF	GB
CA, cos(2α)					
Mean$\pm$SD: ERA KP(ϕ)	0.00$\pm$0.41	-0.02$\pm$0.41	-0.01$\pm$0.33	-0.01$\pm$0.20	0.00$\pm$0.13
Mean$\pm$SD: ERA M	0.12$\pm$0.59	0.12$\pm$0.59	0.12$\pm$0.54	0.12$\pm$0.48	0.12$\pm$0.45
Median ERA	0.41	0.42	0.39	0.33	0.30
% Eyes $\leq$0.50 D	66.00	66.00	69.00	78.00	79.00
CA, cos(2α), AL, ACD, WTW					
Mean$\pm$SD: ERA KP(ϕ)	0.00$\pm$0.40	-0.03$\pm$0.41	0.03$\pm$0.37	-0.01$\pm$0.20	0.00$\pm$0.08
Mean$\pm$SD: ERA M	0.12$\pm$0.59	0.13$\pm$0.59	0.13$\pm$0.57	0.12$\pm$0.48	0.12$\pm$0.44
Median ERA	0.43	0.43	0.41	0.33	0.28
% Eyes $\leq$0.50 D	64.00	66.00	67.00	78.00	80.00

$CA =$ Corneal astigmatism; $GB =$ Gradient Boosting; $KNN =$ K-Nearest Neighbors; $RF =$ Random Forest; $SVR =$ Support Vector Regression; $\alpha =$ Measured astigmatism direction; $\%\ Eyes\ \leq 0.50\ D =$ Percentage of eyes with an absolute error within 0.50 D

Table C.11: ERA meridional, torsional, and net astigmatism magnitude components, in D, for the optimized TCRP 3.0 mm A/Z by the several estimators for the different parameter sets, in the Training stage.

	Estimators				
Parameters	Linear	SVR	KNN	RF	GB
CA, cos(2α)					
Mean±SD: ERA KP(ϕ)	0.00±0.40	-0.05±0.40	0.02±0.35	0.01±0.22	0.00±0.15
Mean±SD: ERA M	0.09±0.60	0.10±0.60	0.09±0.57	0.09±0.50	0.09±0.47
Median ERA	0.49	0.49	0.44	0.35	0.34
% Eyes ≤0.50 D	51.00	53.00	58.00	69.00	74.00
CA, cos(2α), AL, ACD, WTW					
Mean±SD: ERA KP(ϕ)	0.00±0.40	-0.05±0.40	0.02±0.37	0.02±0.22	0.00±0.11
Mean±SD: ERA M	0.09±0.60	0.09±0.62	0.09±0.58	0.09±0.50	0.09±0.46
Median ERA	0.49	0.52	0.47	0.37	0.31
% Eyes ≤0.50 D	52.00	52.00	54.00	69.00	75.00
CA, cos(2α), Chord μ					
Mean±SD: ERA KP(ϕ)	0.00±0.40	-0.04±0.40	0.04±0.36	0.01±0.18	0.00±0.11
Mean±SD: ERA M	0.09±0.60	0.10±0.60	0.10±0.58	0.09±0.48	0.09±0.46
Median ERA	0.50	0.49	0.44	0.36	0.33
% Eyes ≤0.50 D	50.00	52.00	62.00	72.00	75.00
All					
Mean±SD: ERA KP(ϕ)	0.00±0.39	-0.05±0.40	0.04±0.38	0.00±0.21	0.00±0.10
Mean±SD: ERA M	0.09±0.60	0.10±0.60	0.10±0.59	0.09±0.49	0.09±0.46
Median ERA	0.51	0.48	0.44	0.38	0.32
% Eyes ≤0.50 D	51.00	53.00	60.00	69.00	76.00

$CA =$ Corneal astigmatism; $GB =$ Gradient Boosting; $KNN =$ K-Nearest Neighbors; $RF =$ Random Forest; $SVR =$ Support Vector Regression; $\alpha =$ Measured astigmatism direction; $\%\ Eyes\ \leq 0.50\ D =$ Percentage of eyes with an absolute error within 0.50 D

Table C.12: ERA meridional, torsional, and net astigmatism magnitude components, in D, for the optimized TCRP 4.0 mm P/Z by the several estimators for the different parameter sets, in the Training stage.

	Estimators				
Parameters	Linear	SVR	KNN	RF	GB
CA, cos(2α)					
Mean±SD: ERA KP(ϕ)	0.00±0.40	-0.01±0.40	0.02±0.34	-0.02±0.19	0.00±0.15
Mean±SD: ERA M	0.07±0.58	0.07±0.58	0.07±0.54	0.07±0.46	0.07±0.44
Median ERA	0.48	0.47	0.41	0.33	0.30
% Eyes ≤0.50 D	56.00	60.00	62.00	75.00	77.00
CA, cos(2α), AL, ACD, WTW					
Mean±SD: ERA KP(ϕ)	0.00±0.38	-0.02±0.38	0.04±0.36	-0.02±0.18	0.00±0.09
Mean±SD: ERA M	0.07±0.56	0.07±0.56	0.08±0.55	0.07±0.45	0.07±0.42
Median ERA	0.48	0.48	0.40	0.33	0.28
% Eyes ≤0.50 D	56.00	58.00	65.00	76.00	79.00
CA, cos(2α), Chord μ					
Mean±SD: ERA KP(ϕ)	0.00±0.39	-0.04±0.40	0.03±0.36	0.00±0.19	0.00±0.11
Mean±SD: ERA M	0.07±0.57	0.08±0.57	0.08±0.55	0.07±0.46	0.09±0.46
Median ERA	0.45	0.46	0.44	0.33	0.29
% Eyes ≤0.50 D	56.00	60.00	58.00	75.00	79.00
All					
Mean±SD: ERA KP(ϕ)	0.00±0.38	-0.04±0.38	0.05±0.39	-0.01±0.18	0.00±0.07
Mean±SD: ERA M	0.07±0.56	0.08±0.56	0.09±0.57	0.07±0.45	0.07±0.42
Median ERA	0.46	0.48	0.45	0.34	0.28
% Eyes ≤0.50 D	57.00	60.00	59.00	77.00	79.00

$CA =$ Corneal astigmatism; $GB =$ Gradient Boosting; $KNN =$ K-Nearest Neighbors; $RF =$ Random Forest; $SVR =$ Support Vector Regression; $\alpha =$ Measured astigmatism direction; $\%\ Eyes\ \leq 0.50\ D =$ Percentage of eyes with an absolute error within 0.50 D

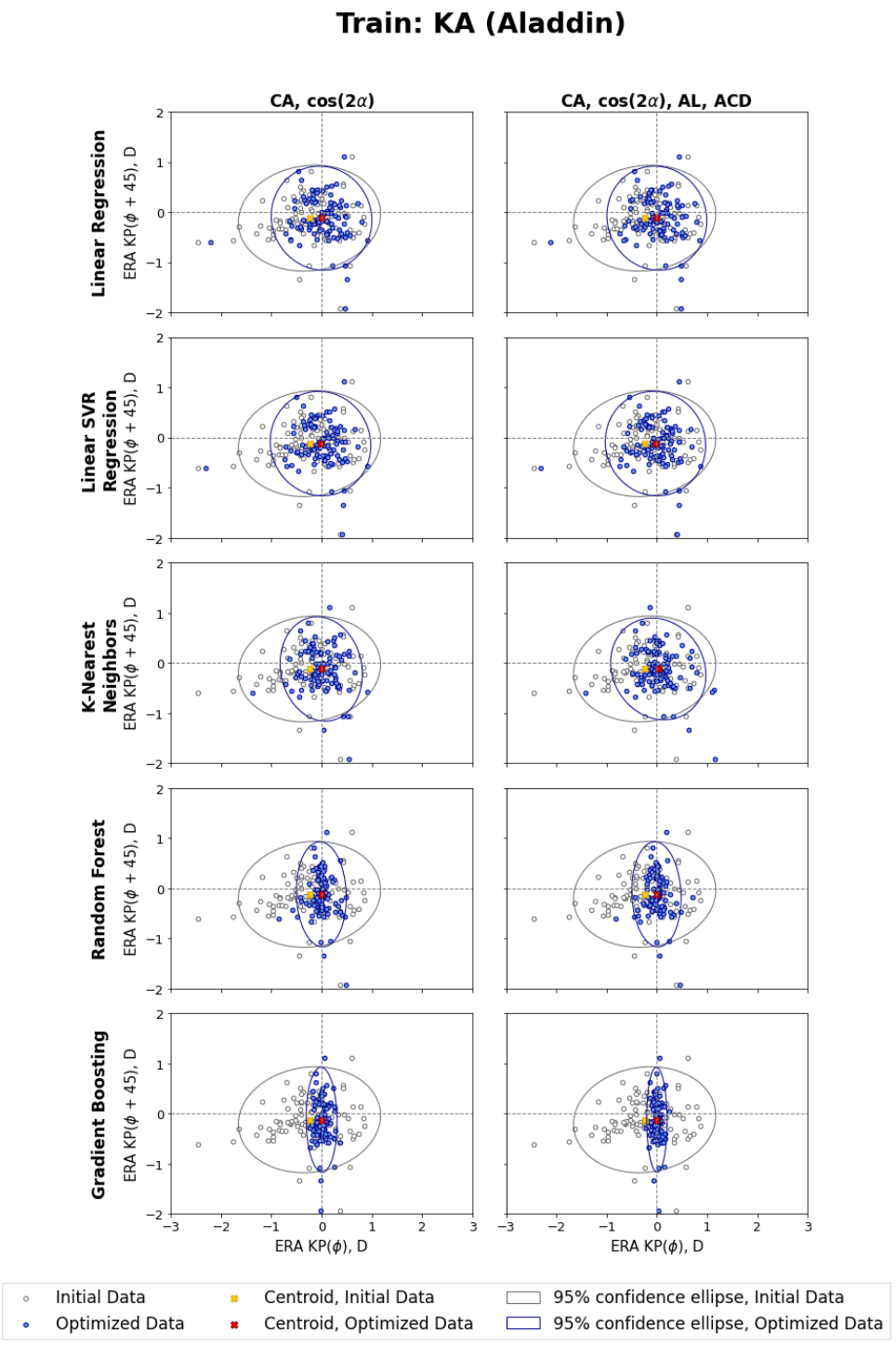

Figure C.1: Meridional and torsional ERA components displayed by 95% confidence ellipses, for the optimized KA (Aladdin) by estimators compared to the initial data, for each set of parameters, in the Training stage.

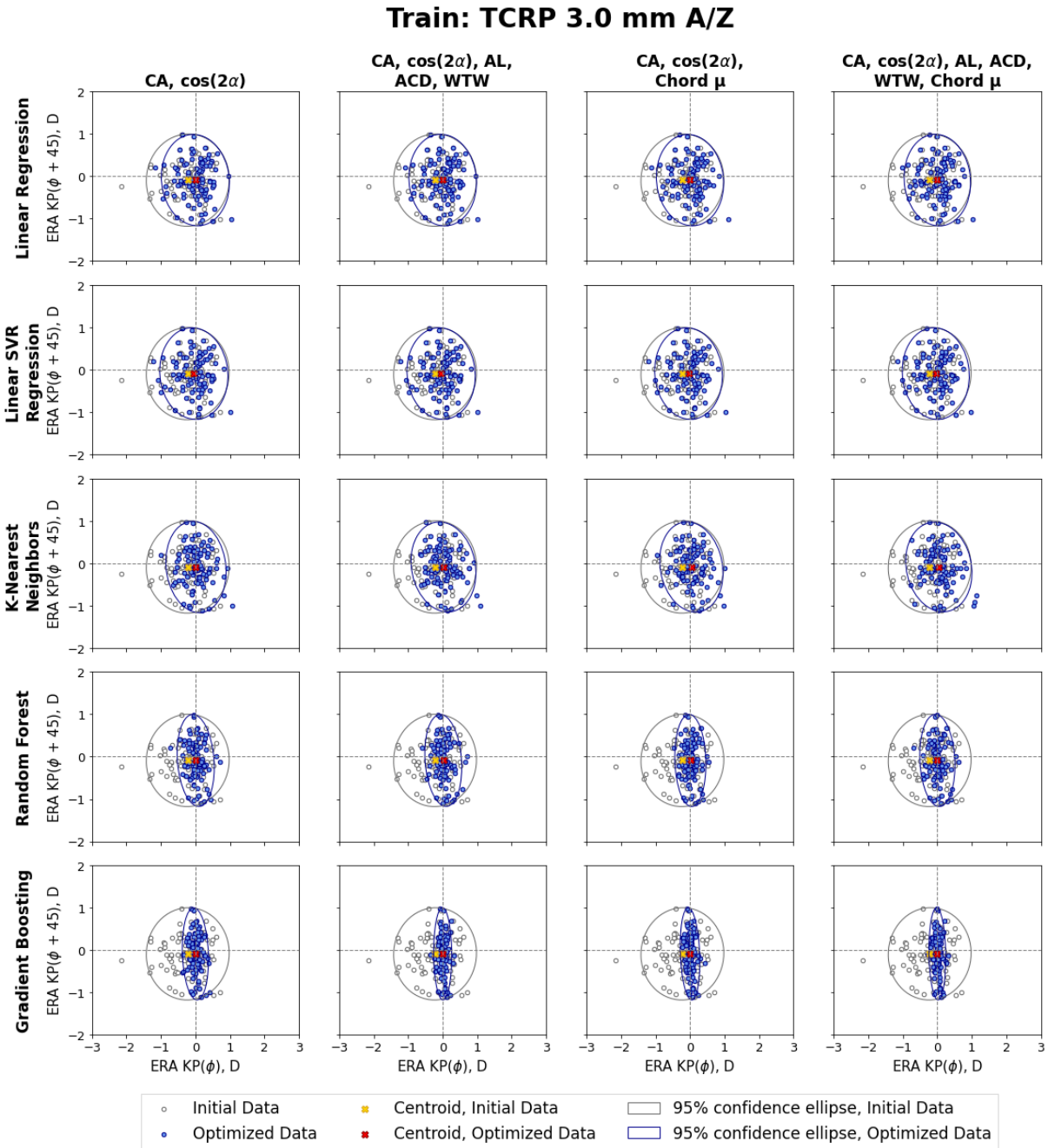

Figure C.2: Meridional and torsional ERA components displayed by 95% confidence ellipses, for the optimized TCRP 3.0 mm A/Z by estimators compared to the initial data, for each set of parameters, in the Training stage.

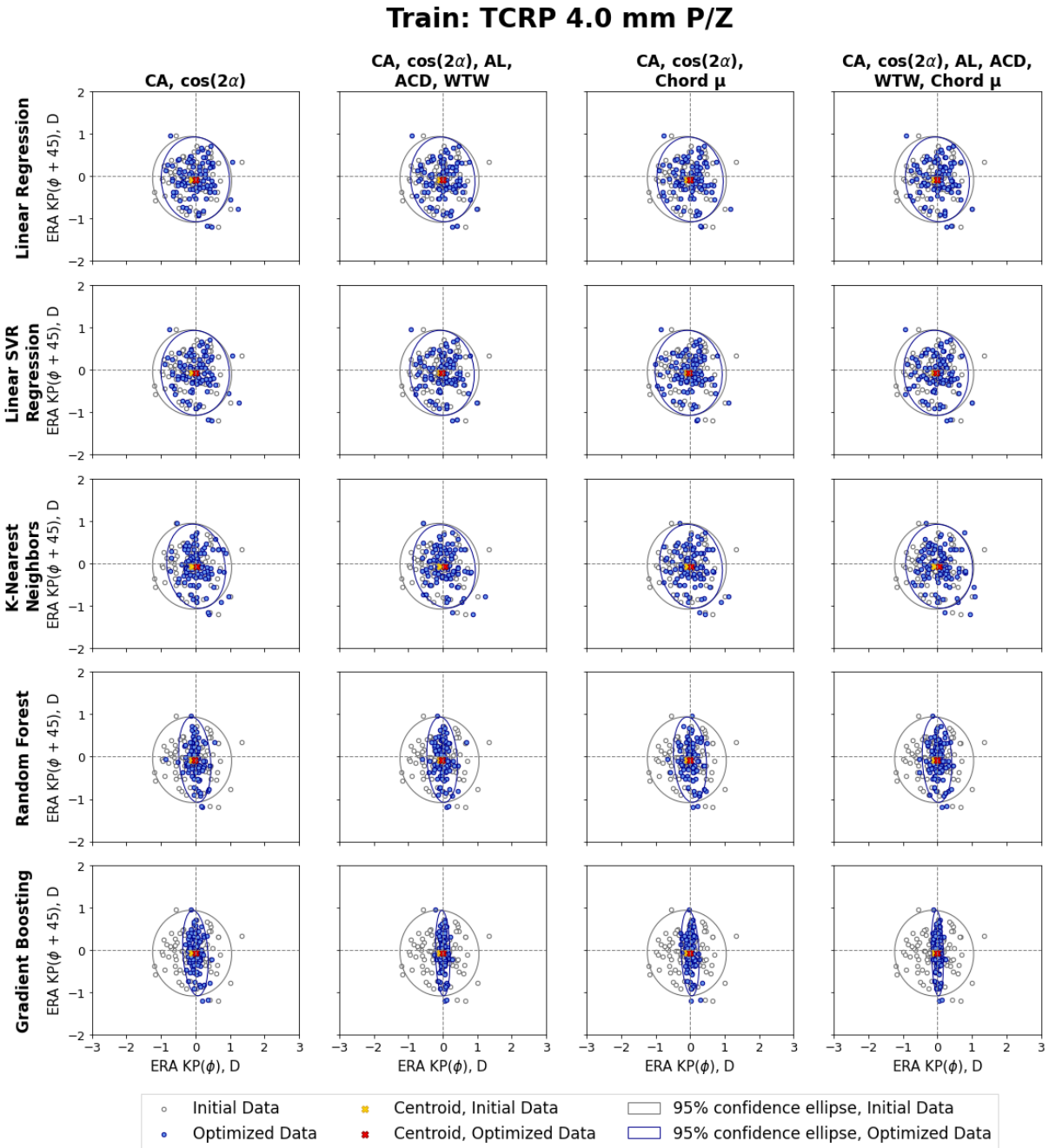

Figure C.3: Meridional and torsional ERA components displayed by 95% confidence ellipses, for the optimized TCRP 4.0 mm P/Z by estimators compared to the initial data, for each set of parameters, in the Training stage.

C.4.3 Step 2: Cross-validation

Table C.13: Cross-validation estimators scores (R^2) and SD, for the KA (Aladdin).

	Estimators				
Parameters	Linear	SVR	KNN	RF	GB
CA, cos(2α)					
R^2	0.711	0.720	0.719	0.668	0.651
SD	0.199	0.190	0.234	0.216	0.173
CA, cos(2α), AL, ACD, WTW					
R^2	0.703	0.720	0.573	0.607	0.602
SD	0.202	0.181	0.399	0.293	0.238

$CA =$ Corneal astigmatism; $GB =$ Gradient Boosting; $KNN =$ K-Nearest Neighbors; $RF =$ Random Forest; $SVR =$ Support Vector Regression; $\alpha =$ Measured astigmatism direction

Table C.14: Cross-validation estimators scores (R^2) and SD, for the TCRP 3.0 mm A/Z.

	Estimators				
Parameters	Linear	SVR	KNN	RF	GB
CA, cos(2α)					
R^2	0.767	0.777	0.698	0.667	0.612
SD	0.071	0.062	0.180	0.141	0.166
CA, cos(2α), AL, ACD, WTW					
R^2	0.761	0.765	0.617	0.715	0.614
SD	0.070	0.071	0.316	0.097	0.222
CA, cos(2α), Chord μ					
R^2	0.765	0.772	0.649	0.702	0.700
SD	0.063	0.066	0.290	0.129	0.102
All					
R^2	0.766	0.763	0.638	0.667	0.665
SD	0.062	0.068	0.237	0.169	0.150

$CA =$ Corneal astigmatism; $GB =$ Gradient Boosting; $KNN =$ K-Nearest Neighbors; $RF =$ Random Forest; $SVR =$ Support Vector Regression; $\alpha =$ Measured astigmatism direction

Table C.15: Cross-validation estimators scores (R^2) and SD, for the TCRP 4.0 mm P/Z.

	Estimators				
Parameters	Linear	SVR	KNN	RF	GB
CA, cos(2α)					
R^2	0.763	0.768	0.646	0.675	0.666
SD	0.060	0.061	0.230	0.213	0.244
CA, cos(2α), AL, ACD, WTW					
R^2	0.752	0.764	0.595	0.661	0.673
SD	0.089	0.069	0.298	0.276	0.265
CA, cos(2α), Chord μ					
R^2	0.771	0.764	0.655	0.716	0.718
SD	0.045	0.058	0.190	0.142	0.143
All					
R^2	0.756	0.769	0.563	0.684	0.668
SD	0.079	0.057	0.203	0.202	0.263

$CA =$ Corneal astigmatism; $GB =$ Gradient Boosting; $KNN =$ K-Nearest Neighbors; $RF =$ Random Forest; $SVR =$ Support Vector Regression; $\alpha =$ Measured astigmatism direction

C.4.4 Step 3: Testing

Table C.16: ERA meridional, torsional, and net astigmatism magnitude components, in D, for the optimized TCRP 3.0 mm A/Z by the several estimators, in the Testing stage.

	Estimators			
Parameters	Linear	SVR	RF	GB
CA, cos(2α)				
Mean$\pm$SD: ERA KP(ϕ)	-0.05$\pm$0.47	-0.09$\pm$0.47	-0.09$\pm$0.56	-0.06$\pm$0.52
Mean$\pm$SD: ERA M	0.12$\pm$0.70	0.15$\pm$0.70	0.14$\pm$0.76	0.13$\pm$0.73
Median ERA	0.50	0.50	0.51	0.56
% Eyes $\leq$0.50 D	51.92	51.92	48.08	46.15
CA, cos(2α), AL, ACD				
Mean$\pm$SD: ERA KP(ϕ)	-0.04$\pm$0.46	-0.09$\pm$0.47	-0.10$\pm$0.52	-0.02$\pm$0.46
Mean$\pm$SD: ERA M	0.12$\pm$0.69	0.14$\pm$0.70	0.15$\pm$0.73	0.11$\pm$0.69
Median ERA	0.49	0.50	0.47	0.50
% Eyes $\leq$0.50 D	51.92	51.92	51.92	52.91
CA, cos(2α), Chord μ				
Mean$\pm$SD: ERA KP(ϕ)	-0.05$\pm$0.48	-0.09$\pm$0.47	-0.06$\pm$0.52	-0.06$\pm$0.52
Mean$\pm$SD: ERA M	0.12$\pm$0.71	0.14$\pm$0.70	0.13$\pm$0.73	0.13$\pm$0.73
Median ERA	0.48	0.50	0.48	0.48
% Eyes $\leq$0.50 D	55.77	50.00	51.92	55.77
All				
Mean$\pm$SD: ERA KP(ϕ)	-0.04$\pm$0.48	-0.09$\pm$0.47	-0.09$\pm$0.52	-0.03$\pm$0.47
Mean$\pm$SD: ERA M	0.12$\pm$0.70	0.14$\pm$0.70	0.14$\pm$0.73	0.11$\pm$0.70
Median ERA	0.49	0.50	0.51	0.50
% Eyes $\leq$0.50 D	51.92	51.92	50.00	51.92

CA = Corneal astigmatism; GB = Gradient Boosting; RF = Random Forest; SVR = Support Vector Regression; α = Measured astigmatism direction; $\%\ Eyes\ \leq 0.50\ D$ = Percentage of eyes with an absolute error within 0.50 D

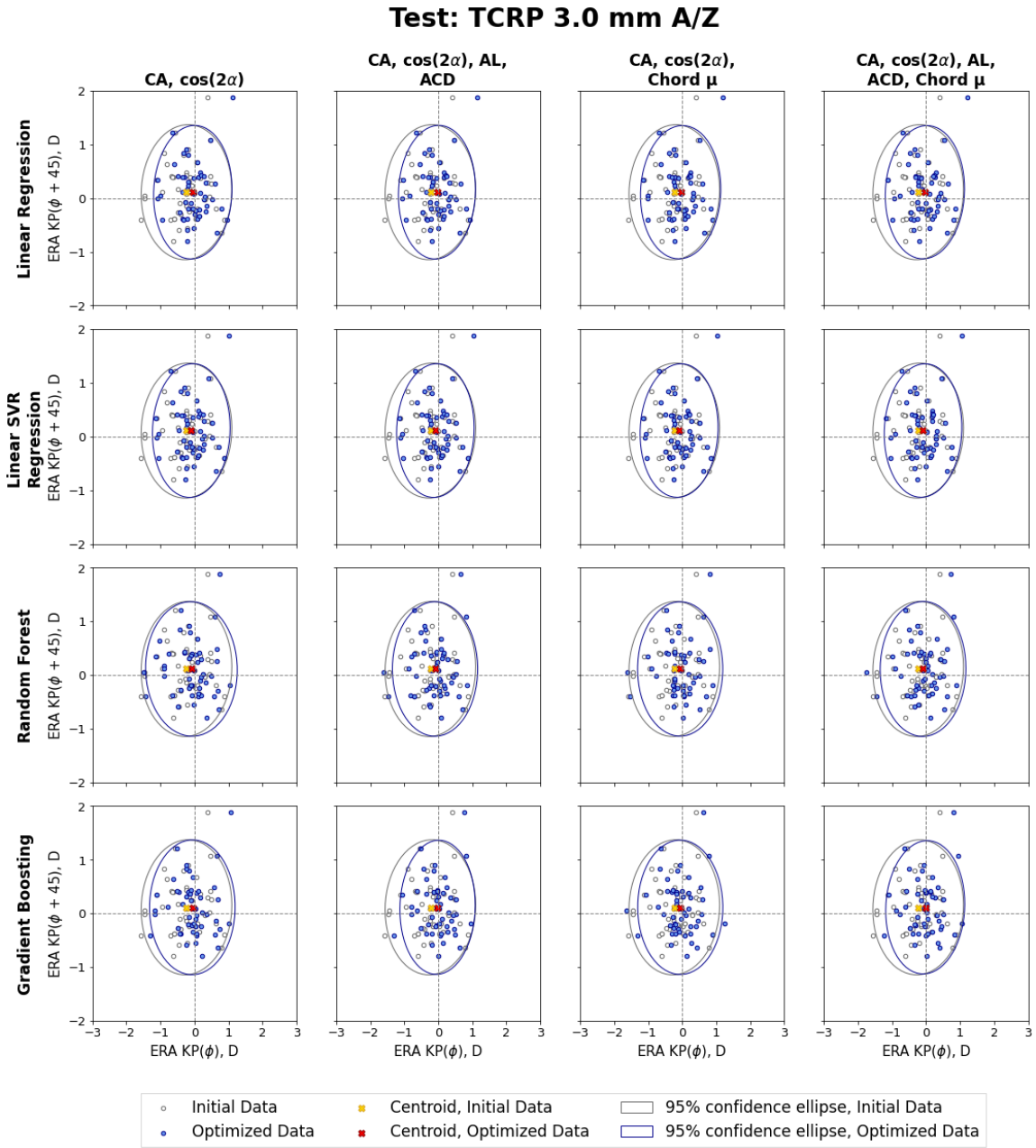

Figure C.4: Meridional and torsional ERA components displayed by 95% confidence ellipses, for the TCRP 3.0 mm A/Z values optimized by estimators and compared to the initial data, given for each parameter sets, in the Testing stage.